

Cancer –
From Mechanisms of Invasion to Targeted Therapy

Inauguraldissertation

Zur Erlangung der Würde eines Doktors der Philosophie
vorgelegt der
Philosophisch-Naturwissenschaftlichen Fakultät der
Universität Basel

von
Andreas Christian Wicki
Basel (BS) und Romoos (LU)

Basel, 2007

Genehmigt von der Philosophisch-Naturwissenschaftlichen Fakultät
auf Antrag von:

Referent: Prof. Dr. Gerhard M. Christofori

Co-Referent: Prof. Dr. Curzio Rüegg

Fakultätsverantwortlicher: Prof. Dr. Urs A. Meyer

Basel, den 24.04.2007

DER DEKAN

PROF. DR. HANS-PETER HAURI

Table of contents

List of figures	5
List of tables	8
Zusammenfassung	9
Summary	10
Preface	11
PART I: Mechanisms of Tumor Invasion – Cancer Progression through EMT- and Non-EMT Mediated Pathways	13
1. Introduction	14
1.1 Mechanisms of tumor invasion	
1.2 Tumor progression and signaling	
1.3 Signaling in EMT-mediated and EMT-independent tumor invasion	
1.4 Models used for studying morphological patterns and molecular pathways present in tumor invasion	
1.5 Aim of the study (part I)	
2. Materials & Methods	25
2.1 Transgenic and knock-out mice	
2.2 Histopathological analysis	
2.3 MCF7 and A549 cell transfection and induction experiments	
2.4 Immunoblotting of total cell lysates	
2.5 Isolation and preparation of pancreatic islets	
2.6 Immunofluorescence of cultured cells	
2.7 Cell migration and invasion assays	
2.8 Induction of podoplanin expression with stromal factors	
2.9 MTT cell proliferation assay	
2.10 <i>In vitro</i> wounding assay	
2.11 Cell spreading assay	
2.12 RhoA, Cdc42 and Rac activity assay	
2.13 Xenograft assays with MCF7 and A549 cells	
2.14 Statistical analysis	
3. Results and Discussion	32
3.1 Tumor invasion in the absence of EMT: podoplanin-induced remodeling of the actin cytoskeleton	
3.2 Tumor invasion in the presence of EMT: the role of E-cadherin in early carcinogenesis,	

microinvasion and metastasis

4.	Conclusions	59
PART II: Molecular Imaging and Targeted Therapy of Insulinoma		64
5.	Introduction	65
5.1	Targets in anti-cancer therapy	
5.2	Radiolabelling of antibodies or small peptide ligands for imaging and therapy	
5.3	The glucagon-like peptide-1 receptor (GLP-1R) as a drug target in human insulinoma	
5.4	Aim of the study (part II)	
6.	Materials & Methods	71
6.1	Reagents and instrumentation	
6.2	Peptide synthesis and radiolabeling	
6.3	Mice	
6.4	In vitro GLP-1 receptor autoradiography	
6.5	Cell culture, radioligand internalization, externalization, and peptide stability studies	
6.6	Biodistribution in Rip1Tag2 mice	
6.7	GLP-1 receptor imaging with multipinhole SPECT/MRI	
6.8	GLP-1 receptor imaging with SPECT/CT	
6.9	Dosimetry	
6.10	Histological analysis	
6.11	Immunofluorescent stainings	
6.12	Electron microscopy	
6.13	Light microscopy	
6.14	Statistical analysis	
7.	Results and Discussion	77
7.1	[Lys ⁴⁰ (Ahx-DTPA- ¹¹¹ In)NH ₂]-Exendin-4, a promising ligand for glucagon-like peptide-1 (GLP-1) receptor targeting	
7.2	A new therapeutic approach to insulinoma: [Lys ⁴⁰ (Ahx-DTPA- ¹¹¹ In)NH ₂]-Exendin-4 is a highly efficient radiotherapeutic for glucagon-like peptide-1 (GLP-1) receptor targeted therapy	
8.	Conclusions	96
References		98
Acknowledgments		107
Publication list		108

List of figures

PART I

- 1.1 **Single and collective cell invasion**
Wicki A, Christofori G (2007) The Potential Role of Podoplanin in Tumour Invasion. Br J Cancer 96(1):1-5
- 1.2 **Stages of tumor progression**
Courtesy of Prof. G Christofori
- 1.3 **Multistep carcinogenesis is recapitulated in the Rip1Tag2 tumor mouse**
Courtesy of Prof. G Christofori
- 3.1 **Expression of podoplanin in β -cells of Rip1Tag2 mice**
Wicki A, Lehenbre F, Wick N, et al. (2006) Tumor invasion in the absence of epithelial-mesenchymal transition: Podoplanin-mediated remodeling of the actin cytoskeleton. Cancer Cell 9(4): 261-72
- 3.2 **Tumor progression in podoplanin-overexpressing and control mice**
Wicki A, Lehenbre F, Wick N, et al. (2006) Tumor invasion in the absence of epithelial-mesenchymal transition: Podoplanin-mediated remodeling of the actin cytoskeleton. Cancer Cell 9(4): 261-72
- 3.3 **Apoptosis, proliferation, blood vessel and lymphatic vessel density**
Wicki A, Lehenbre F, Wick N, et al. (2006) Tumor invasion in the absence of epithelial-mesenchymal transition: Podoplanin-mediated remodeling of the actin cytoskeleton. Cancer Cell 9(4): 261-72
- 3.4 **Podoplanin induces tumor invasion without loss of E-cadherin expression**
Wicki A, Lehenbre F, Wick N, et al. (2006) Tumor invasion in the absence of epithelial-mesenchymal transition: Podoplanin-mediated remodeling of the actin cytoskeleton. Cancer Cell 9(4): 261-72
- 3.5 **Maintenance of epithelial markers in podoplanin-expressing tumor cells**
Wicki A, Lehenbre F, Wick N, et al. (2006) Tumor invasion in the absence of epithelial-mesenchymal transition: Podoplanin-mediated remodeling of the actin cytoskeleton. Cancer Cell 9(4): 261-72
- 3.6 **Expression of the tight-junctions protein ZO-1 is not lost upon podoplanin-mediated tumor invasion**
Wicki A, Lehenbre F, Wick N, et al. (2006) Tumor invasion in the absence of epithelial-mesenchymal transition: Podoplanin-mediated remodeling of the actin cytoskeleton. Cancer Cell 9(4): 261-72
- 3.7 **Podoplanin-mediated tumor cell invasion does not involve a cadherin switch**
Wicki A, Lehenbre F, Wick N, et al. (2006) Tumor invasion in the absence of epithelial-mesenchymal transition: Podoplanin-mediated remodeling of the actin cytoskeleton. Cancer Cell 9(4): 261-72
- 3.8 **Ezrin and actin filaments are re-localized by podoplanin**
Wicki A, Lehenbre F, Wick N, et al. (2006) Tumor invasion in the absence of epithelial-mesenchymal transition: Podoplanin-mediated remodeling of the actin cytoskeleton. Cancer Cell 9(4): 261-72
- 3.9 **Podoplanin does not induce EMT in MCF7 cells. The expression of podoplanin can be induced upon stimulation with stromal factors**
Wicki A, Lehenbre F, Wick N, et al. (2006) Tumor invasion in the absence of epithelial-mesenchymal transition: Podoplanin-mediated remodeling of the actin cytoskeleton. Cancer Cell 9(4): 261-72
- 3.10 **Podoplanin induces a migratory phenotype in MCF7 cells**
Wicki A, Lehenbre F, Wick N, et al. (2006) Tumor invasion in the absence of epithelial-mesenchymal transition: Podoplanin-mediated remodeling of the actin cytoskeleton. Cancer Cell 9(4): 261-72
- 3.11 **Podoplanin induces spreading, migration and invasion of MCF7 cells**
Wicki A, Lehenbre F, Wick N, et al. (2006) Tumor invasion in the absence of epithelial-mesenchymal transition: Podoplanin-mediated remodeling of the actin cytoskeleton. Cancer Cell 9(4): 261-72

- 3.12 **Scratch wound assay**
Wicki A, Lehembre F, Wick N, et al. (2006) Tumor invasion in the absence of epithelial-mesenchymal transition: Podoplanin-mediated remodeling of the actin cytoskeleton. *Cancer Cell* 9(4): 261-72
- 3.13 **Podoplanin downregulates RhoA, Cdc42 and Rac activity**
Wicki A, Lehembre F, Wick N, et al. (2006) Tumor invasion in the absence of epithelial-mesenchymal transition: Podoplanin-mediated remodeling of the actin cytoskeleton. *Cancer Cell* 9(4): 261-72
- 3.14 **Morphology of MCF7 cells after migration through a matrigel-coated membrane**
Wicki A, Lehembre F, Wick N, et al. (2006) Tumor invasion in the absence of epithelial-mesenchymal transition: Podoplanin-mediated remodeling of the actin cytoskeleton. *Cancer Cell* 9(4): 261-72
- 3.15 **Subcutaneously grafted A549 or MCF7 cells transfected with podoplanin or empty vector**
Wicki A, unpublished result
- 3.16 **Podoplanin and E-cadherin are co-expressed in the invasive front of human cancers**
Wicki A, Lehembre F, Wick N, et al. (2006) Tumor invasion in the absence of epithelial-mesenchymal transition: Podoplanin-mediated remodeling of the actin cytoskeleton. *Cancer Cell* 9(4): 261-72
- 3.17 **Knock-out of E-cadherin has a profound impact on the adhesive apparatus of β -cells**
Wicki A, manuscript in preparation
- 3.18 **Knock-out of E-cadherin promotes microinvasion**
Wicki A, manuscript in preparation
- 3.19 **Knock-out of E-cadherin induces metastasis**
Wicki A, manuscript in preparation
- 4.1 **Mechanisms of tumor invasion**
Wicki A, Christofori G (2007) The Potential Role of Podoplanin in Tumour Invasion. *Br J Cancer* 96(1):1-5

PART II

- 5.1 **Monoclonal antibodies**
Wicki A, illustration
- 5.2 **Targeted therapy in nuclear medicine**
Wicki A, illustration
- 7.1 **Receptor autoradiography for GLP-1R**
 Wild D, Béhé M, Wicki A, et al. (2006) Preclinical Evaluation of [Lys⁴⁰(Ahx-DTPA-¹¹¹In)NH₂]-Exendin-4, a very promising ligand for glucagon-like-peptide-1 (GLP-1) receptor targeting. *J Nucl Med.* 47(12):2025-2033
- 7.2 **Internalization and peptide stability**
 Wild D, Béhé M, Wicki A, et al. (2006) Preclinical Evaluation of [Lys⁴⁰(Ahx-DTPA-¹¹¹In)NH₂]-Exendin-4, a very promising ligand for glucagon-like-peptide-1 (GLP-1) receptor targeting. *J Nucl Med.* 47(12):2025-2033
- 7.3 **Biodistribution of [Lys⁴⁰(Ahx-DTPA-¹¹¹In)NH₂]-Exendin-4 in Rip1Tag2 and wt mice**
 Wild D, Béhé M, Wicki A, et al. (2006) Preclinical Evaluation [Lys⁴⁰(Ahx-DTPA-¹¹¹In)NH₂]-Exendin-4, a very promising ligand for glucagon-like-peptide-1 (GLP-1) receptor targeting. *J Nucl Med.* 47(12):2025-2033
- 7.4 **Molecular imaging of GLP-1R expression by multipinhole SPECT/MRI and conventional SPECT/CT**
 Wild D, Béhé M, Wicki A, et al. (2006) Preclinical Evaluation of [Lys⁴⁰(Ahx-DTPA-¹¹¹In)NH₂]-Exendin-4, a very promising ligand for glucagon-like-peptide-1 (GLP-1) receptor targeting. *J Nucl Med.* 47(12):2025-2033
- 7.5 **Uptake and therapeutic effect of [Lys⁴⁰(Ahx-DTPA-¹¹¹In)NH₂]-Exendin-4**

- Wicki A, Wild D, Storch D, et al. (2007) [Lys⁴⁰(Ahx-DTPA-¹¹¹In)NH₂]-Exendin-4 is a highly efficient radiotherapeutic for glucagon-like peptide-1 receptor targeted therapy for insulinoma. Clin Cancer Res. 13(12):3696-3705.
- 7.6 **[Lys⁴⁰(Ahx-DTPA-¹¹¹In)NH₂]-Exendin-4 reduces tumor cell proliferation**
Wicki A, Wild D, Storch D, et al. (2007) [Lys⁴⁰(Ahx-DTPA-¹¹¹In)NH₂]-Exendin-4 is a highly efficient radiotherapeutic for glucagon-like peptide-1 receptor targeted therapy for insulinoma. Clin Cancer Res. 13(12):3696-3705.
- 7.7 **Tumor cell death induced by [Lys⁴⁰(Ahx-DTPA-¹¹¹In)NH₂]-Exendin-4 occurs by both apoptosis and necrosis**
Wicki A, Wild D, Storch D, et al. (2007) [Lys⁴⁰(Ahx-DTPA-¹¹¹In)NH₂]-Exendin-4 is a highly efficient radiotherapeutic for glucagon-like peptide-1 receptor targeted therapy for insulinoma. Clin Cancer Res. 13(12):3696-3705.
- 7.8 **Infiltration of tumors by immune cells after treatment of mice with [Lys⁴⁰(Ahx-DTPA-¹¹¹In)NH₂]-Exendin-4**
Wicki A, Wild D, Storch D, et al. (2007) [Lys⁴⁰(Ahx-DTPA-¹¹¹In)NH₂]-Exendin-4 is a highly efficient radiotherapeutic for glucagon-like peptide-1 receptor targeted therapy for insulinoma. Clin Cancer Res. 13(12):3696-3705.
- 7.9 **Blood glucose levels, body weight and organ toxicity after treatment with [Lys⁴⁰(Ahx-DTPA-¹¹¹In)NH₂]-Exendin-4**
Wicki A, Wild D, Storch D, et al. (2007) [Lys⁴⁰(Ahx-DTPA-¹¹¹In)NH₂]-Exendin-4 is a highly efficient radiotherapeutic for glucagon-like peptide-1 receptor targeted therapy for insulinoma. Clin Cancer Res. 13(12):3696-3705.
- 7.10 **Light (LM) and electron (EM) microscopy images of mouse kidneys 180 days after injection of 28 MBq of [Lys⁴⁰(Ahx-DTPA-¹¹¹In)NH₂]-Exendin-4. Chronic radiation damage of the glomeruli**
Wicki A, Wild D, Storch D, et al. (2007) [Lys⁴⁰(Ahx-DTPA-¹¹¹In)NH₂]-Exendin-4 is a highly efficient radiotherapeutic for glucagon-like peptide-1 receptor targeted therapy for insulinoma. Clin Cancer Res. 13(12):3696-3705.
- 7.11 **Electron (EM) microscopy images of mouse kidneys 180 days after injection of 28 MBq of [Lys⁴⁰(Ahx-DTPA-¹¹¹In)NH₂]-Exendin-4. Chronic radiation damage of the tubuli**
Wicki A, Wild D, Storch D, et al. (2007) [Lys⁴⁰(Ahx-DTPA-¹¹¹In)NH₂]-Exendin-4 is a highly efficient radiotherapeutic for glucagon-like peptide-1 receptor targeted therapy for insulinoma. Clin Cancer Res. 13(12):3696-3705.
- 8.1 **Molecular imaging, predictive imaging and therapy of insulinoma**
Wicki A, illustration

List of tables

PART I

- 1.1 **Invasion pattern of malignant human tumors**
Modified after Friedl P & Wolf K, 2003, Nat Rev Cancer
- 1.2 **Summary of mouse models used for studying tumor invasion**
Wicki A, illustration
- 3.1 **Engraftment and exulceration of A549 and MCF7 xenografts in nude-mice**
Wicki A, unpublished results
- 4.1 **Progression of β -cell carcinomas in β -EcadKO;Rip1Tag2, Rip1Tag2 and Rip1Podo;Rip1Tag2 mice**
Wicki A, unpublished results

PART II

- 5.1 **Targeted agents (antibodies) against cancer, FDA-approved as at 2006**
Modified after Imai K and Takaoka A, 2006, Nat Rev Cancer
- 5.2 **Targeted agents (small molecule inhibitors) against cancer, FDA-approved as at 2006**
Modified after Imai K and Takaoka A, 2006, Nat Rev Cancer
- 7.1 **Biodistribution and tissue radioactivity ratio in tumor-bearing Rip1Tag2 mice at 4, 24 and 48 hours after injection of 2 pmol [Lys⁴⁰(Ahx-DTPA-¹¹¹In)NH₂]-Exendin-4**
Wild D, Béhé M, Wicki A, et al. (2006) Preclinical Evaluation of [Lys⁴⁰(Ahx-DTPA-¹¹¹In)NH₂]-Exendin-4, a very promising ligand for glucagon-like-peptide-1 (GLP-1) receptor targeting. J Nucl Med. 47(12):2025-2033
- 7.2 **Absorbed dose per Megabecquerel (MBq) injected activity and tumor-to-normal tissue absorbed dose of [Lys⁴⁰(Ahx-DTPA-¹¹¹In)NH₂]-Exendin-4 in tumor bearing Rip1Tag2 mice**
Wicki A, Wild D, Storch D, et al. (2007) [Lys⁴⁰(Ahx-DTPA-¹¹¹In)NH₂]-Exendin-4 is a highly efficient radiotherapeutic for glucagon-like peptide-1 (GLP-1) receptor targeted therapy for insulinoma. Clin Cancer Res. 13(12):3696-3705.

Zusammenfassung

Krebs ist eine der grossen Herausforderungen der modernen Medizin. Das Krankheitsbild ist vielseitig und die Ätiologie vieler Krebsformen nach wie vor nur bruchstückhaft bekannt. Um die Krankheit wirklich zu begreifen, muss der gesamte molekularbiologische Apparat der Zelle erkundet, muss das komplizierte Netzwerk der Signaltransduktion bis in seine feinsten Verästelungen erfasst werden.

Die Erforschung der Tumorinvasion ist eine Subspezialität der Krebsforschung. Sie beschäftigt sich mit intra- und extrazelluläre Mechanismen, die dazu führen, dass eine Zelle zu wandern beginnt und auf zerstörerische Weise ins umgebende Gewebe eindringt. In einem gesunden Gewebe sind die Zellen durch Zell-Zell-Kontakte miteinander verbunden. Geht diese Gewebeskohäsion verloren, können einzelne Zellen aus dem Verband auswandern und andere Gewebe infiltrieren. Der Verlust der Adhäsion ist eingebettet in ein umfassenderes Phänomen, welches "epithelial-mesenchymal transition" (EMT) genannt wird. Dabei verlieren epitheliale Zellen die Zeichen ihres epithelialen Ursprungs und verwandeln sich in mesenchymale Zellen. Dazu benutzen sie zelluläre Programme, die in ähnlicher Form bei der Embryonalentwicklung aktiv sind.

Alternativ können Zellen aber auch ihre Kontakte mit den Nachbarn beibehalten und als Zellverband in ein gesundes Gewebe einwandern. Bei dieser Form der Invasion besitzen die äussersten, invadierenden Zellen unter Umständen andere Charakteristiken als Zellen im Inneren des Verbandes. Diese Form der Invasion ist i.d.R. unabhängig von einer EMT.

In dieser Studie haben wir sowohl Einzelzellinvasion nach EMT als auch kollektive Invasion ohne EMT untersucht. Wir zeigen, dass der Verlust des Zelladhäsionsmoleküles E-cadherin zu Einzelzellinvasion führt. Diese Invasionsform ist begleitet von einer Hochregulation eines Adaptormoleküls namens p120-Catenin sowie der Überexpression des cytoplasmatischen Fragments von N-cadherin, eines anderen Zelladhäsionsmoleküls. Dagegen führt die Expression von Podoplanin, eines kleinen mucinösen Membranproteins, zu kollektiver Invasion. Diese ist gekennzeichnet durch die Beibehaltung von E-cadherin, der Phosphorylierung von Ezrin, einem anderen Adaptorprotein, und der Hemmung von RhoA, Rac und Cdc42, einer Familie von kleinen GTPasen.

Ein zweites grosses Untergebiet der Krebsforschung ist die Krebstherapie. Dabei werden Medikamente entwickelt, die selektiv Krebszellen angreifen, ohne gesunde Zellen zu Schädigen. Voraussetzung dafür ist entweder ein spezifischer Marker, der es erlaubt, gezielt Medikament in eine Krebszelle zu bringen, oder aber eine Substanz, die ausschliesslich Krebszellen schädigt und keinen Einfluss auf gesunde Zellen hat.

Im zweiten Teil dieser Studie zeigen wir, dass der Glucagon-like-peptide-1 receptor (GLP1-R) spezifisch auf entarteten β -Zellen des Pankreas exprimiert wird. Mit einem spezifischen Liganden des GLP1 Rezeptors können Radionuclide in die Krebszellen eingeschleust werden. Wir haben den Liganden mit 111 Indium markiert, einem γ - und Auger-Emitter. Mit der γ -Komponente haben wir Single Photon Emission Computed Tomography (SPECT) Aufnahmen gemacht, und mit gleichzeitigen Computed Tomography (CT) und Magnetic Resonance Imaging (MRI) Bildern verglichen. Mit dieser Methode können Tumoren mit einem Durchmesser von einem Millimeter nachgewiesen werden. Die Auger-Komponente wirkt therapeutisch und kann, in einer Dosierung von 28 MBq, die Tumormasse in einem Insulinom-Mausmodell um mehr als 94% reduzieren. Der limitierende Faktor bei dieser Therapie ist die Nierentoxizität.

Summary

Cancer is one of the big challenges of modern medicine. The manifestations of cancer are manifold, and the knowledge of the etiology of cancer is still fragmentary. In order to understand the disease, the complete molecular apparatus and the whole signal transduction network of the cell must be analysed.

Tumor invasion is one specific topic in the vast field of cancer research. It investigates the intra- and extracellular mechanisms that define the migratory properties of a cancer cell and lead to invasion and destruction of the surrounding tissue. In a healthy human tissue, cells are connected one to another by adhesive molecules. Loss of the adhesion results in the migration of single cells and the infiltration of neighboring tissues. This is part of a larger phenomenon known as epithelial-mesenchymal transition (EMT), during which cells lose their epithelial markers and start to act as if they were mesenchymal cells. The cellular program that determines this transition is similar to that active during developmental processes such as gastrulation or neurulation.

Alternatively, cells can maintain contact with their neighbors and invade as a cell sheet. This so-called collective cell invasion is characterized by a specialization of the cells of the invasive margin. This invasion pattern usually is independent from EMT.

In this study, we investigated both EMT-dependent single cell invasion and EMT-independent collective cell invasion. We show that the loss of the adhesion molecule E-cadherin induces single cell invasion, which is accompanied by the upregulation of p120-catenin, an adaptor molecule, and the C-terminal fragment of N-cadherin, another cell adhesion molecule. In contrast, the expression of podoplanin, a small mucin-like transmembrane protein, promotes collective cell invasion. E-cadherin is maintained at the cell membrane, and ezrin, another adaptor protein, is phosphorylated. In addition, members of the small GTPase family, including RhoA, Rac and Cdc42, are downregulated.

A second major topic in cancer research is the therapy of cancer. The aim is to develop drugs that selectively target cancer cells. This is either done by targeting drugs to a specific marker that is only expressed on cancer and not on healthy cells, or by developing compounds that selectively inhibit molecular pathways active in cancer cells.

In the second part of this study we show that the glucagon-like-peptide-1 (GLP1) receptor is selectively upregulated by malignant β -cells of the Langerhans islets. With the help of a specific ligand, radionuclides can be targeted to the transformed β -cells. We labeled the ligand with $^{111}\text{Indium}$, a γ - and Auger-emitter. Using the γ -component, we performed single photon emission computed tomography (SPECT), combined with conventional computed tomography (CT) or magnetic resonance (MR) imaging. Through this technique, we could detect tumors of 1mm in diameter. The Auger-component has a therapeutic effect, and after the injection of 28 MBq in a mouse model of human insulinoma, the tumor mass was reduced by more than 94%. The dose-limiting factor of this therapy is nephrotoxicity.

Preface

More than 35 years after President Nixon declared the war on cancer, this disease is still one of the greatest scourges of humanity. In Switzerland, about 25% of all deaths are attributable to cancer, thus making malignant tumors the second most frequent death cause after cardiovascular diseases (PANORAMA, Swiss Federal Statistical Office, 2006). While the rate of cardiovascular fatalities has been decreasing since the 1960ies, the death toll due to cancer has remained stable (National Center for Health Statistics, 2005). Of the 7-year increase in life expectancy between 1960 and 2000, about 4.9 years resulted from a reduced rate of death from cardiovascular disease. It is altogether disappointing and disillusioning that only 0.2 years are due to a reduction in the rate of cancer deaths (Cutler et al., 2006).

In general, the treatment of childhood cancer is more successful than that of adult cancer. The current therapies, however, are toxic. A survey of adult survivors of childhood cancer showed that these patients are burdened with significant chronic health conditions. As compared with siblings, the relative risk of a survivor for a major joint replacement is 54.0, for congestive heart failure 15.1, for a second malignant neoplasm (in particular sarcomas and Hodgkin lymphomas) 14.8, for severe cognitive dysfunction 10.5, and for coronary artery disease 10.4. The risk of a cerebrovascular accident, renal failure, hearing loss, blindness and ovarian failure was also increased (Henderson et al., 2007 and Oeffinger et al., 2006).

These figures illustrate the current dilemma in the field of medical oncology: most malignant tumors are not curable, unless they are detected at an early, often asymptomatic stage. But if a neoplasm can be cured, the therapy is usually toxic and leads to chronic health conditions in about two thirds of the patients (Oeffinger et al., 2006). Thus, additional research efforts are indispensable if significant advances in oncology shall be achieved. Advances will only be possible with an unprejudiced approach to new techniques, and a stronger interaction between bench and bedside. Physicians and biologists alike face the challenge to broaden their views on cancer in order to solve the dilemma.

In this thesis, we tackle two problems of cancer. In the first part, we look at the mechanisms of tumor invasion, in particular investigating the molecular basis of single and collective cell invasion. In the second part, we concentrate on molecular imaging and targeted therapy of insulinoma. As experimental systems, we used human and mouse cell lines, transgenic and knock-out mice, and human tumor biopsies. Both parts can be read independently, but are held together by one central theme – the molecular mechanisms of cancer, and new approaches to targeted therapy.

The purpose of a general introduction might best be served by the following encyclopedia entry. It points out the difference between science, opinion and doubt, and sheds light on the role of skepticism.

SCIENCE, s. f. (Logiq. & Métaphys.) science, en terme de philosophie, signifie la connoissance claire & certaine de quelque chose, fondée ou sur des principes évidens par eux - mêmes, ou sur des démonstrations. Le mot science pris dans le sens qu'on vient de dire est opposé à doute; & l'opinion tient le milieu entre les deux.

Les sceptiques nient qu'il soit possible d'avoir la science sur rien, c'est - à - dire qu'il y ait rien sur quoi on puisse arriver à un degré de connoissance capable de produire une conviction entiere.

La science se partage en quatre branches, qui sont l'intelligence, la sagesse, la prudence & l'art. L'intelligence consiste dans la perception intuitive du rapport de convenance ou de disconvenance qui se trouve entre deux idées; telle est la science de Dieu, telle est la connoissance que nous avons des premiers principes. La sagesse s'éleve toujours aux vues générales, & ne considere dans les êtres que les rapports qu'ils ont les uns avec les autres, pour en tirer des conclusions universelles. Les êtres spirituels sont aussi de son ressort. La prudence s'applique à former les moeurs à l'honnêteté, conformément à des regles éternelles & immuables. On l'appelle dans les écoles, *habitus vera cum ratione activus*. L'art donne des regles sûres & immanquables pour bien raisonner. On le définit dans les écoles, *habitus vera cum ratione effectivus*.

The Encyclopedia of Diderot and d'Alembert, 1751-1777.

PART I:

Mechanisms of Tumor Invasion – Cancer Progression through EMT- and Non-EMT Mediated Pathways

Life is short, and art long; the crisis fleeting; experience
perilous, and decision difficult.
Hippocrates, Aphorisms, 400 BC

There are two ways of acquiring knowledge, one through
reason, the other by experiment. Argument reaches a
conclusion and compels us to admit it, but it neither
makes us certain nor so annihilates doubt that the mind
rests calm in the intuition of truth, unless it finds this
certitude by way of experience (...). It is necessary,
then, to prove everything by experience.
Roger Bacon, On Experimental Science, 1268

1. Introduction (part I)

1.1 Cancer and the mechanisms of tumor invasion

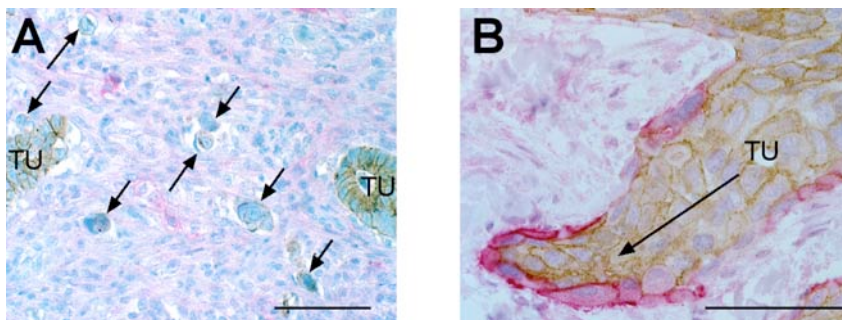
The human body is a conglomerate of more than 10^{13} cells, which are intricately linked and connected one to another. Each cell has a specific task assigned to it, and the fulfillment of this task is ultimately regulated by a delicate balance between active and inactive genes. To develop cancer, a healthy human cell or tissue needs to acquire a repertoire of new properties (Hanahan & Weinberg, 2000). These new functions can be organized into six major groups:

- limitless replicative potential
- sustained angiogenesis
- evading apoptosis
- self-sufficiency in growth signals
- insensitivity to anti-growth signals
- tissue invasion and metastasis

On a macroscopic level, the malignancy of a tumor is defined by the local progression, the relapse after extirpation, the involvement of the draining lymph nodes, and the formation of distant metastases (Virchow, 1863). On a cellular and molecular level, invasion, destruction and metastasis result from the interplay of the five other acquired capabilities of cancer cells, as outlined above.

Metastasis is the single most important prognostic factor for patient survival, and invasion is the first step in a multifaceted process leading to metastasis (Vernon & LaBonne, 2004). Morphological analysis of human cancer samples has revealed a plethora of different invasion patterns. For example, squamous cell esophageal tumors tend to invade by forming cone-like structures, lobular breast cancer is determined by invading cells forming Indian files, while anaplastic thyroid cancer often shows invasion of single dispersed cells in the surrounding tissue. Based on histological criteria, there are two fundamentally different patterns of invasion: single cell and collective cell invasion (Figure 1.1).

Figure 1.1: Single and collective cell invasion.



(A) This adenocarcinoma of the colon invades into the surrounding tissue by single cell invasion. Most of the cells of the tumour bulk (TU) express E-cadherin. Single cells invading the tissue (arrows) have downregulated E-cadherin. Podoplanin is not expressed in this cancer. (B) An esophageal carcinoma has formed an invasive cone that migrates into the surrounding tissue. Podoplanin (red) is expressed in the outer edge of the invading tumour. The tumour cells continue to express E-cadherin (brown) and migrate collectively. Size bar = $50\mu\text{m}$.

On tissue sections, single cell migration is characterized by the presence of isolated, dispersed tumor cells in an adjacent tissue (Figure 1.1 **A**). In an early stage of invasion, the architecture of the host tissue is maintained, although cell death may occur. During collective cell invasion, the cancerous tissue as a whole pushes forward, thereby displacing the healthy surrounding cells. (Figure 1.1 **B**). The host tissue is destroyed and its architecture altered. The morphogenesis of human cancer, i.e., the emergence of single or collective invasion, depends on the functionality of the adhesive apparatus of the cancer cells and may be regulated by a morphogenic code similar to that used during embryogenesis (reviewed by van den Brink & Offerhaus, 2007 and Hirohashi & Kanai, 2003).

Apart from morphologic criteria, staining of tumor tissue for molecular markers was used to define different forms of cancer cell invasion. The most prominent among those are cell surface molecules – in particular adhesion molecules – like E-cadherin, N-cadherin, integrins or ZO-1, and secreted factors like matrix-metalloproteases. Based on morphological and biochemical criteria, the categories of tumor invasion can further be refined (Friedl & Wolf, 2003).

Table 1.1: Invasion pattern of malignant human tumors

<i>Invasion pattern</i>	<i>Tumor type adopting the pattern</i>
single-cell amoeboid invasion	Lymphoma, leukemia, small-cell lung cancer (SCLC)
single-cell invasion after EMT	Fibrosarcoma, Glioblastoma, anaplastic tumors
invasion of cell chains after EMT	Lobular breast cancer
collective invasion of cell clusters and cohorts	Epithelial cancers, melanoma
collective invasion of multicellular strands or sheets	Epithelial cancers, vascular tumors

Cell migration is the result of a continuous cycle of repetitive steps: First, the cell becomes polarized and it elongates. Cell protrusions are formed, which initiate the recognition of and interaction with the extracellular matrix (ECM). These protrusions contain filamentous actin and a varying set of structural and/or signaling proteins. Then, the leading edge or the whole cell contracts, resulting in a forward gliding of the cell (Lauffenburger & Horwitz, 1996). This cycle underlies all forms of cancer cell invasion, but the molecular mechanism may vary from one invasion pattern to another.

Amoeboid invasion is defined by single cell migration and a low level of protease and β_1 integrin expression on the cell surface. Dictyostelium discoideum, a fungus abundant in soil or leaf mold, is a model organism for the study of amoeboid migration (Firtel & Meili, 2000). The translocation of Dictyostelium is characterized by

integrin-independent, low-affinity interaction with the substrate and a lack of surface protease expression. In metazoa, amoeboid migration is retained in leukocytes and certain cancer cells, including cells derived from hematological malignancies, but also from neuroendocrine tumors such as small-cell lung cancer. Cells with amoeboid migration are usually roundish, 10-30 μm in diameter, and they grow in suspension. The translocation velocity can be low (ca. 0.1 $\mu\text{m}/\text{min.}$) or high (ca. 20 $\mu\text{m}/\text{min.}$) (Friedl et al., 2001). Similar to Dictyostelium, these cells depend on a shape-driven migration, which allows them to circumnavigate, rather than degrade, the ECM (Friedl et al., 1998).

Single cell invasion is observed in sarcomas and anaplastic epithelial cancers. These malignancies often downregulate epithelial markers, such as E-cadherin, and upregulate mesenchymal markers, e.g., N-cadherin and/or vimentin. This switch in the expression pattern of adhesion and cytoskeleton molecules is part of a phenomenon called epithelial-mesenchymal transition (EMT). EMT had first been described in gastrulating and neurulating embryos. During embryogenesis, EMT is crucial to enhance cell motility and allow for organ formation. Cells that undergo mesenchymal invasion often have a fibroblast-like, spindle-shaped form. They usually express integrins and surface proteases, and they only grow on an adhesive culture dish (Sameni et al., 2000; Wolf et al., 2003 and d'Ortho et al., 1998). The translocation velocity is rather low (0.1-1 $\mu\text{m}/\text{min.}$; Friedl et al., 1998). Originally, EMT was thought to be necessary for any form of tumor cell invasion (Vernon & LaBonne, 2004). Recent results, including findings by our own laboratory, led to the conclusion that EMT is indeed important for single cell, but less so for collective cell invasion (reviewed by Gupta & Massague, 2006 and Friedl & Wolf, 2003).

Invasion of cell chains ("Indian files") is a typical feature of lobular breast cancer, but can also be observed in ovary cancer, melanoma and other neural crest cell tumors (Pitts et al., 1991; Sood et al., 2001 and Seftor et al., 2002). Lobular breast cancer cells often lose E-cadherin expression during tumor progression and thus show several characteristics of EMT-dependent invasion, including expression of integrins and surface proteases.

Finally, a hallmark of collective invasion is the continuing expression of adhesion molecules and other components of the adhesive apparatus by invading cells. *In vitro* studies of keratinocyte sheets and primary tumor explants or tumor cell lines showed that aggregates of cells can move as a functional unit (Vaughan & Trinkaus, 1966; Friedl et al., 1995 and Nabeshima et al., 1995). A subset of highly motile cells forms the invading front of the cell sheet. These cells are often referred to as path-generating cells (Hegerfeldt et al., 2002). They engage and cluster β 1-integrins in anterior protrusions towards the ECM, and show a high expression of matrix-metalloproteases (MMPs), which degrade the matrix in the cells' path (Hegerfeldt et al., 2002 and Nabeshima et al., 2000). Morphologically, there are two types of collective cell invasion: the first pattern consists of cell sheets that extend into the tissue, yet maintain contact with the primary site. It is observed in squamous cell cancers, basal-cell cancer, adenocarcinoma of the colon and ductal mammary

cancer (Nabeshima et al., 1999 and Bell & Waizbard, 1986). The second pattern is formed by cells that collectively detach from the primary tumor and generate cell nests (Nabeshima et al., 1999 and Bell & Waizbard, 1986). This type of invasion is frequently found in certain melanomas and rhabdomyosarcoma.

1.2. Tumor progression and signaling

Tumor progression is a complex process, which starts with the transformation of a benign into a malignant cell and potentially leads to tissue destruction, metastasis and finally death (Figure 1.2). The whole process can be divided into several, molecular and morphological distinct steps (Gupta & Massague, 2006).

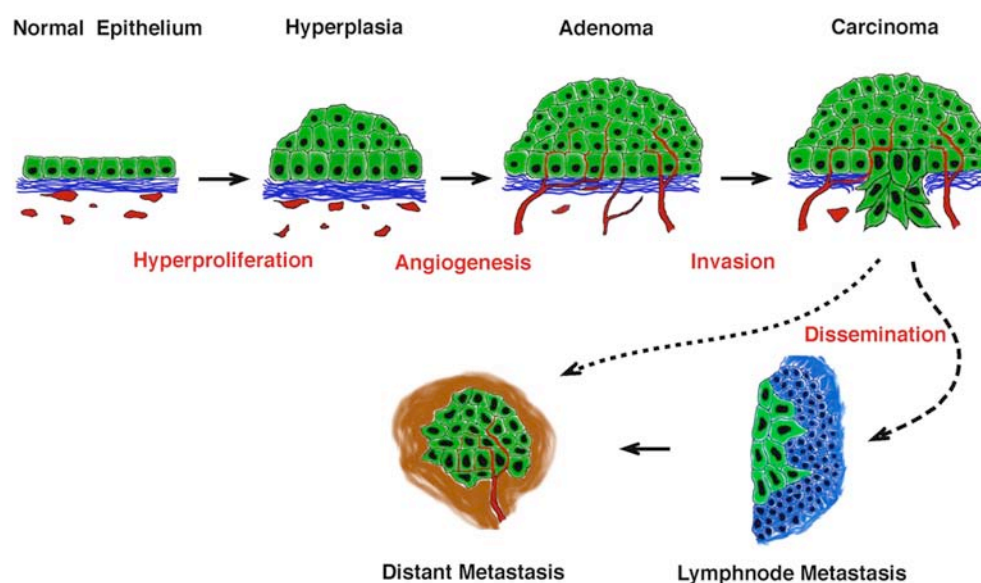
In a first stage, cellular heterogeneity originates through DNA mutations, chromosomal rearrangements, and epigenetic alterations. Damage to genomic DNA can be found even in apparently normal cells and continues to amplify during tumor progression (Bartkova et al., 2005). The same is true for epigenetic changes (reviewed by Ting et al., 2006). From the moment cellular heterogeneity arises, malignant cell clones are under an evolutionary pressure that selects for the fittest cancer cells. This pressure is determined by factors of the tumor microenvironment, including the availability of oxygen and nutrients, and the response of the immune system. Hypoxia is an exemplary selective factor that promotes the outgrowth of malignant cell clones. Hypoxic cells respond to a low oxygen tension by stabilizing hypoxia-inducible factor 1 α (HIF-1 α), a transcription factor that promotes angiogenesis, anaerobic metabolism, cell survival, and invasion (Harris, 2002). The induction of angiogenesis allows the tumor to grow in size and become independent of diffusion, while tumors that lack a sufficient blood supply may become dormant (Naumov et al., 2006). In addition, transformed cells become resistant to extracellular death signals, either by overexpression of anti-apoptotic factors, such as BCL2, or by loss of pro-apoptotic mediators, such as caspase 8 (reviewed by Mehlen & Puisieux, 2006 and Brodeur, 2003). Through autocrine stimulation they also become self-sufficient in growth factors, and they increase their replicative potential, for example through insensitivity to anti-growth signals, such as the retinoblastoma protein pathway (reviewed by Hayflick, 1997; Fedi P, 1997 and Weinberg, 1995).

In a second step, the malignant cells acquire the capability to invade into the surrounding tissue. Single and collective cell invasion and consequent tumor progression is induced by various cell signaling pathways. These pathways include induction of cellular migration and invasion by receptor tyrosine kinase-mediated signal transduction pathways, by changes in cell adhesion properties, and by the activation of small GTPases of the Rho family which in turn leads to the reorganization of the actin cytoskeleton (reviewed by Cavallaro & Christofori, 2004; Grunert et al., 2003; Sahai & Marshall, 2002 and Thiery, 2002). Migration and invasion of tumor cells are also promoted by the loss of interaction of adherens junctions with the cytoskeleton, and again subsequent changes in the activities of Rho family small GTPases, most prominently Rac1, Cdc42 and RhoA (Noren et al.,

2000 and Sahai & Marshall, 2002). Apart from adopting pro-migratory strategies, invading carcinoma cells must also disrupt the basement membrane. Invasion through the basement membrane depends on the expression of MMPs, but also on EGF signaling and the activity of the fos family of transcription factors (reviewed by Sherwood, 2006).

Thirdly, cancer cells become able to migrate through the ECM and intravasate into a blood or lymph vessel. The migration through the matrix is facilitated by stromal co-option, which manifests itself by fibrosis, leukocytic infiltration and (lymph) angiogenesis (reviewed by Condeelis & Pollard, 2006; de Visser et al., 2006 and Kalluri & Zeisberg, 2006). Targeted disruption of transforming growth factor β (TGF β) signaling in fibroblasts can by itself induce carcinomas of the forestomach and the prostate in mice, underlining the importance of the stromal co-option for tumor progression and development (Bhowmick et al., 2004). Intravital imaging studies of experimental mammary carcinomas showed that highly motile cancer cells are attracted to blood vessels owing to chemotactic gradients and extracellular matrix tracks originating from the vessels (Condeelis & Segall, 2003). The molecular mechanisms responsible for intravasation are poorly understood. However, the enhanced expression of Twist, an EMT-inducing transcription factor, promotes intravasation of a mouse mammary cell line into blood vessels (Yang et al., 2004).

Figure 1.2: stages of tumor progression



Tumor progression is regarded as a multistep process, leading from a healthy to a malignant tissue. Each step is characterized by the acquisition of new properties on the level of either single tumor cells or the whole tumor tissue.

During the fourth stage, the tumor cells have to survive in the blood stream and finally extravasate again. Circulating cancer cells may use platelets as shields in order to promote their survival. Platelets protect the tumor cells from the cytotoxic

effect of circulating $\text{TNF}\alpha$, enhance tumor embolization in the microvasculature and promote adhesion to the endothelium (Philippe et al., 1993 and Mehta, 1984). Indeed, the administration of aspirin to mice reduces the metastatic potential of cancer cells, presumably both by reducing the incidence of cancerous emboli and the $\alpha\text{V}\beta\text{3}$ integrin-mediated angiogenesis (Nash et al., 2002; Dormond et al., 2001 and Gasic et al., 1972). Homing of disseminated cancer cells to a secondary organ, however, may not only be achieved by embolization in a capillary field, but also by adhesive interactions between surface receptors and ligands on cancer and endothelial cells. For example, $\alpha\text{3}\beta\text{1}$ integrins and a novel receptor called metadherin were implicated in homing to the microvasculature of the lung (Wang et al., 2004 and Brown & Ruoslahti, 2004). For the actual extravasation process, both the motility of the cancer cells and the permeability of the endothelium are important. Knock-out of the cytoskeletal adaptor protein ezrin in osteosarcoma cells reduces the escape of cancer cells from the vasculature (Khanna et al., 2004). Vascular endothelial growth factor (VEGF) increases the permeability of the endothelium and thus facilitates extravasation (Weis & Cheresh, 2005). Knock-out of src family kinases in endothelial cells protects mice from lung metastasis, since src induces disruption of adhesive junctions upon stimulation of endothelial cells with VEGF (Criscuoli et al., 2005).

In a last step, the cancer cells colonize the secondary organ and grow out. More than a hundred years ago, Paget already proposed that cancer cells only colonized an organ with a suitable soil (Paget, 1889). Clinical observation suggests that the circulatory pattern alone is not enough to explain the incidence of metastasis in secondary organs (Fidler, 2003). Palliative peritoneo-venous shunting of ascites in ovarian cancer patients releases large amounts of metastatic cancer cells into the central venous system. Interestingly, up to two years after shunting, the majority of patients did not develop disseminated metastasis (Tarin et al., 1984). This demonstrates that successful tumors not only embolize but also generate a viable niche in the target organ. The preparation of a distant tissue before tumor cell arrival results in the establishment of a premetastatic niche. Specific upregulation of fibronectin and clustering of VEGFR1-positive haematopoietic bone marrow progenitors seem to play a role in the formation of this niche (Kaplan et al., 2005).

1.3 Signaling in EMT-mediated and EMT-independent tumor invasion

EMT-mediated tumor invasion

Loss of the adhesion molecule E-cadherin is a crucial event in EMT-mediated tumor invasion. E-cadherin, the prototype member of the classical cadherin family, is a 120kDa type 1 transmembrane glycoprotein. The 80kDa extracellular portion of E-cadherin consists of 5 Ca^{2+} -binding domains. It is responsible for homophilic interactions with other cadherin molecules and for heterophilic interaction with $\alpha\text{E}\beta\text{7}$ integrins (Higgins et al., 1998). The 40 kDa transmembrane and cytoplasmic part links E-cadherin via α , β and γ catenin to the actin cytoskeleton. Cadherins are the principal components of adherens junctions and desmosomes, which, together with

tight junctions, are the main adhesion junctions of vertebrate cells. The function of E-cadherin, however, is not limited to conferring adhesive abilities to cells. E-cadherin can modulate receptor tyrosin kinase (RTK) signaling, interfere with the Wnt pathway and influence RhoA, Rac1 and Cdc42 activity (reviewed by Cavallaro & Christofori, 2004). Thus, E-cadherin impacts on both the level of cell adhesion and the level of cell signaling in precancerous and malignant cells.

About 80—90% of human cancers originate from epithelial tissue. Precancerous lesions emerging from epithelia and early carcinoma stages usually express E-cadherin, since it is a major player involved in maintaining cell polarity and organizing the epithelium. E-cadherin is already expressed by the fertilized egg and knock-out of E-cadherin leads to early embryonic death (Larue et al., 1994). Loss of E-cadherin is often part of a more complex phenomenon called epithelial-mesenchymal transition (EMT). During EMT, differentiated epithelial cells lose the expression of epithelial markers, such as E-cadherin, and start to express mesenchymal markers, such as N-cadherin and vimentin. EMT is a phenomenon tightly linked to metazoan development, allowing for the formation of mesenchymal cells from primitive epithelium. Greenburg and Hay were the first to analyse EMT in epithelial tissue and they recognized the link between EMT and enhanced cell migration *in vitro* (Greenburg & Hay, 1982). Stoker and Perryman showed that EMT can be induced in epithelial Madin-Darby canine kidney (MDCK) cells by applying the supernatant of a fibroblast culture, which contained a scatter factor later identified as HGF (Stoker & Perryman, 1985). In general, EMT is induced by oncogenic events in tumor cells leading to activation of the wnt/ β -catenin, Notch and Hedgehog signaling pathways or by growth factors (TGF- β , HGF, EGF, IGF, FGF) secreted by tumor and stromal cells (reviewed by Huber et al., 2005; Grunert et al., 2003; Siegel & Massague, 2003 and Thiery, 2002). Ras signaling plays a central part in the induction of EMT (Thiery, 2003). Reactive oxygen species do not only induce EMT, but also genetic instability (Radisky et al., 2005). EMT of *in vitro* cultured cells resembles the metastatic process observed in patients, although this hypothesis is still under debate (Grunert et al., 2003). In a further step, cells that became mesenchymal can undergo a mesenchymal-amoeboid transition and thus become even more invasive. The inhibition of the E3 ligase Smurf1 induces a localized RhoA degradation and thereby promotes amoeboid cell migration (Sahai et al., 2007).

What is the link between loss of E-cadherin and EMT? The loss of E-cadherin at sites of EMT has been reported in mice and in gastrulation of *Drosophila*, chick and mouse embryos (Thiery, 2002). Downregulation of E-cadherin can occur through mutation of the E-cadherin gene, methylation and silencing of the E-cadherin gene, internalization by endocytosis and transcriptional repression (Thiery, 2002). Snail1, Twist and Slug1 are transcriptional repressors able of inducing EMT, and they also induce downregulation of E-cadherin. On the other hand, *in vitro* knock-down of E-cadherin leads to a EMT-like phenotype in MCF7 breast cancer cells (Wicki et al., 2006). Thus, EMT can induce loss of E-cadherin, while loss of E-cadherin can induce an EMT-like phenotype.

In many epithelial cancers cell adhesion is lost during tumor progression. Our laboratory has shown previously that introduction of dominant-negative E-cadherin into tumor cells enhances tumor cell invasion and metastasis formation *in vivo*. Re-introduction and forced expression of E-cadherin results in a reversion to a more benign phenotype. Therefore, the loss of E-cadherin mediated adhesion is a crucial step in tumor progression (Perl et al., 1998). Concomitant with the loss of E-cadherin, a strong upregulation of N-cadherin expression is observed. Such a cadherin switch has been previously described during the progression of various cancer types and is a crucial factor in EMT-mediated tumor progression (Cavallaro et al., 2002 and Hsu et al., 1996).

EMT-independent tumor invasion

A significant number of cancers, including certain subtypes of breast and ovarian cancers, are by pathological criteria characterized as invasive and malignant, yet they do not lose E-cadherin expression. Moreover, full EMT is rarely observed in biopsies from cancer patients. Based on these observations, it was postulated that non-EMT-mediated tumor progression and invasion must occur in those cancers. Morphologically, this form of invasion is usually accompanied by collective cell migration. TGF β family members (such as Nodal), fibroblast growth factors (FGF), Wnt signaling, cadherin cell adhesion molecules, and eomesodermin contribute to the collective migration of vertebrate embryonic tissue (reviewed by Locascio & Nieto, 2001). The molecular mechanisms of collective movement of neoplastic cell clusters is not well understood (Friedl et al., 2004). Recently, our laboratory has shown that podoplanin (PA2.26, T1 α -2, aggrus), a small, 38 kDa mucin-type transmembrane glycoprotein, is active in a signaling pathway leading to collective cell migration without EMT in the context of human carcinoma.

The expression of podoplanin is upregulated in a number of different cancers, including squamous cell carcinoma of the oral cavity, the lung, and the skin, in granulosa cell tumors and in mesothelioma (Kato et al., 2005; Kimura & Kimura, 2005; Martin-Villar et al., 2005 and Schacht et al., 2005). Podoplanin is expressed in human kidney podocytes and is homologous to T1 α -2, an antigen expressed on the apical surface of alveolar type I cells (Rishi et al., 1995). Other podoplanin homologues include OTS-8, RTI40, gp 38, canine gp 40, human gp 36 and murine PA 2.26 (Farr et al., 1992; Gonzalez & Dobbs, 1998; Martin-Villar et al., 2005; Nose et al., 1990; Zimmer et al., 1997 and Zimmer et al., 1999). Since podoplanin is expressed on lymphatic but not on blood vessel endothelium, it is widely used as a specific marker for lymphatic endothelial cells and lymphangiogenesis (Breiteneder-Geleff et al., 1999). Podoplanin-deficient mice die at birth due to respiratory failure exhibiting a phenotype of dilated, malfunctioning lymphatic vessels and lymphedema (Schacht et al., 2003). Yet, the physiological function of podoplanin is still unknown. Also, the functional contribution of podoplanin to tumor progression has remained elusive. First experiments addressing this issue have revealed that podoplanin co-localizes with ezrin, an ERM-protein (ezrin-radixin-moesin), at the cellular membrane

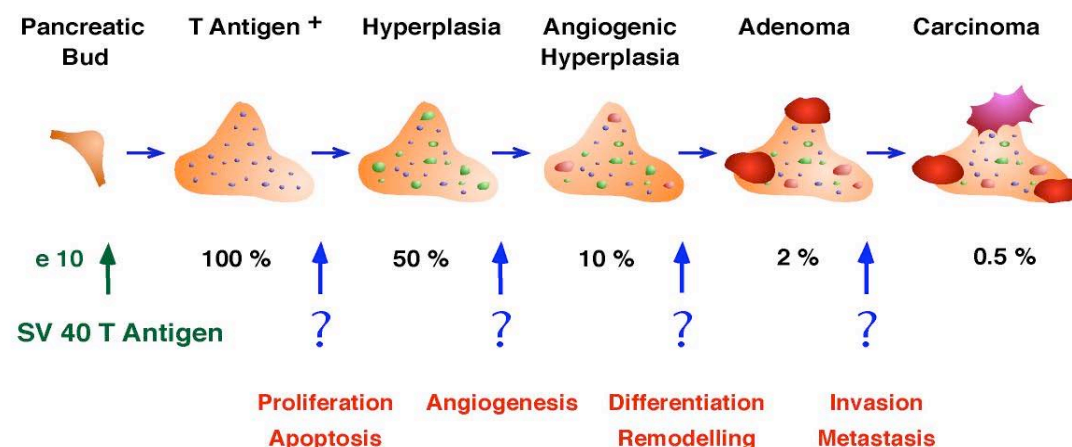
and that podoplanin promotes re-localization of ezrin to filopodia-like structures and reduces cell-cell adhesiveness (Martin-Villar et al., 2005). In this context, it is important to note that ezrin itself has been regarded as a tumor promoter, since its overexpression can enhance tumor progression in various cancer models (Hunter, 2004 and McClatchey, 2003).

1. 4. Models used for studying morphological patterns and molecular pathways present in tumor invasion

In vivo models

We used three different *in vivo* models to investigate the mechanisms of tumor invasion and the impact of different invasion patterns on tumor metastasis. The first mouse model of carcinogenesis we used is the Rip1Tag2 (= rat insulin promoter fragment 1, large T antigen 2) mouse (Hanahan, 1985). Over the last two decades, these mice have extensively been used to investigate the mechanisms of tumor progression. Rip1Tag2 mice express the simian virus (SV) large T antigen under the control of the rat insulin promoter and reproducibly develop tumors of the insulin-producing β -cells of the islets of Langerhans (Figure 1.3).

Figure 1.3: Multistep carcinogenesis is recapitulated in the Rip1Tag2 tumor mouse.



Incipient expression of the large T antigen in all β -cells of the Langerhans-islets at day E10 leads to an increased proliferation and apoptosis rate in the islets. About 50% of the islets become hyperplastic. A fifth of these hyperplastic islets undergo the angiogenic switch and thus start to attract a dense network of vessels. At 10-12 weeks of age, 2% of the islets have turned into an adenoma, while 0.5% have become a carcinoma.

To progress from a benign adenoma to malignant carcinoma, islet tumors of the Rip1Tag2 mouse need to lose E-cadherin expression and express N-cadherin instead. As mentioned above, this cadherin switch, a molecular event that is part of EMT, is a rate-limiting step in the transition from adenoma to a carcinoma (Li &

Herlyn, 2000 and Perl et al., 1998). Overexpression of E-cadherin in this system leads to inhibition of carcinoma formation and tumor progression is halted at the adenoma stage. In the Rip1Tag2 mice, the cadherin switch (and thus a partial EMT) occurs late in the development of islet cell tumors. Adenomas still express an epithelial set of cell surface markers (in particular E-cadherin and β -catenin), and only when they progress to a carcinoma they lose E-cadherin and gain the mesenchymal marker N-cadherin (Perl et al., 1998). This *late EMT* closely mimics tumor progression in human cancer.

To study different invasion patterns, we generated and analysed two additional transgenic mouse lines:

- the Rip1Podo;Rip1Tag2 mouse and
- the Rip1Cre;FloxEcad/ Δ Ecad;Rip1Tag2 mouse.

Rip1Podo;Rip1Tag2 mouse: We generated a double-transgenic mouse line that expresses the small mucin-like glycoprotein podoplanin (T1 α -2, aggrus) under the control of the rat insulin promoter and crossed this mouse with the Rip1Tag2 mouse to induce islets cell tumors. As we will discuss below, these mice do *not normally undergo a cadherin switch or EMT* and are a model for collective cell invasion.

Rip1Cre;FloxEcad/ Δ Ecad;Rip1Tag2 mouse: We obtained the Flox Ecad mouse from the laboratory of P. Derksen, Jos Jonkers and A. Berns (The Netherlands Cancer Institute, Amsterdam). Using a Cre-deleter mouse strain, we generated a monoallelic Δ Ecad mouse. We then crossed this mouse with Rip1Cre;FloxEcad and Rip1Tag2 mice to generate a Rip1Cre;FloxEcad/ Δ Ecad;Rip1Tag2 mouse. Thus, we obtained a mouse line that carries a deletion of E-cadherin specifically in the β -cells of the Langerhans islets and develops islets cell tumors derived from the same β -cells. These mice show a partial EMT (as defined by the loss of E-cadherin and the gain of N-cadherin expression) early in the development of islet tumors ("*early EMT*"). EMT is already present in morphologically (H&E staining) normal islets, before the induction of hyperplasia and the angiogenic switch. The Rip1Cre;FloxEcad/ Δ Ecad;Rip1Tag2 mouse is a model for EMT-induced tumor invasion. Table 1.2 gives an overview of the mouse models.

Table 1.2: Summary of mouse models used for studying tumor invasion

Rip1Cre;FloxEcad/ Δ Ecad;Rip1Tag2 ($=\beta$ -EcadKO;Rip1Tag2)	→	early EMT
Rip1Tag2	→	late EMT
Rip1Podo;Rip1Tag2	→	no EMT

In vitro models

We used several cellular systems, including MCF7 breast cancer cells, β -tumor cells and A549 alveolar carcinoma cells in order to investigate the molecular pathways

associated with different patterns of tumor invasion. In these cellular systems, we studied the influence of the overexpression or the knockdown of E-cadherin and podoplanin on tumor progression.

Human tumor biopsies

In collaboration with the group of D. Kerjaschki at the Institute of Clinical Pathology, Vienna, we analysed human tumor biopsies and stained them for E-cadherin and podoplanin. In our study we included 189 invasive tumor fronts from patients with squamous cell carcinomas of the lung, larynx, esophagus, cervix and skin, and adenocarcinomas of the mamma, colon and prostate.

1.5. Aim of the study (part I)

Although many different patterns of tumor invasion have been morphologically described through histopathological analyses performed on human tumors, the molecular basis of this phenomenon is still largely unknown. Yet, there is evidence that different types of tumor invasion are susceptible to different therapies. For example, collective cell invasion is more susceptible to MMP inhibitors than is single cell invasion (Friedl & Wolf, 2003). On the other hand, collective cell invasion leads to a higher packing density of cancer cells and thus to a decreased delivery of classical chemotherapeutics (Minchinton & Tannock, 2006). In order to develop new and innovative drugs against cancer, it is crucial to understand the molecular basis of tumor invasion.

In the first part of the thesis we will discuss molecular pathways leading to single or collective cell migration in cellular, animal and human tumor systems. In particular, we will provide experimental evidence that podoplanin is involved in a mechanism of collective cell invasion adopted by many human squamous cell carcinomas and we will further elucidate the role of loss of E-cadherin in tumor progression.

2. Materials and Methods (part I)

2.1 Transgenic and knock-out mice

Rip1Podo transgenic mice were generated according to standard procedures (Labosky et al., 1994). The entire coding region of mouse podoplanin was amplified by RT-PCR using the primer pair 5'-gcaattctagaatgtggaccgtgccag-3' and 5'-gcaataagcttttagggcgagaaccttc-3' and mouse kidney cDNA as template and cloned under the control of the rat insulin gene II promoter (Rip1; Hanahan, 1985). The genotypes of six founder mice were confirmed by Southern Blot and PCR analysis. Transgene expression was confirmed by RT-PCR, immunohistochemical and immunoblotting analysis. One podoplanin-expressing mouse line, with approximately 23 inserted transgene copies (as determined by Southern Blot), was used for further experimentation.

The E-cadherin conditional knock-out mice were a gift from Jos Jonkers (The Netherlands Cancer Institute, Amsterdam; Derksen et al., 2006). They carry loxP sites in introns 3 and 15. We crossed a Cre-deleter mouse (Ahlgren et al., 1998) with a heterozygous E-cadherin conditional knock-out mouse (floxEcad/wt) in order to generate a mouse with a heterozygous deletion of E-cadherin (Δ Ecad/wt). We back-crossed the Δ Ecad/wt mouse with floxEcad/wt mice and mice expressing Cre recombinase under the control of the rat insulin gene II promoter (RipCre; Ahlgren et al., 1998) in order to produce double-heterozygous (floxEcad/ Δ Ecad), RipCre expressing progeny. The expression of RipCre targets the conditional E-cadherin knock-out to the β -cells of pancreatic Langerhans islets. The tissue-specific deletion of E-cadherin was verified by western blot and immunofluorescence.

Generation and phenotypic characterization of Rip1Tag2 mice has been described previously (Hanahan, 1985). Rip1Podo and RipCre;floxEcad/ Δ Ecad (= β -EcadKO) female mice were crossed with Rip1Tag2 male mice to generate double-transgenic Rip1Podo;Rip1Tag2 and β -EcadKO;Rip1Tag2 mice. Mice were kept in a strict C57Bl/6 background. For genotyping, the following PCR primers were used:

Rip1Podo: 5'-CTGCAGCTTCAGCCCCTCTG-3' and 5'-CTGGCACGGTCCACATTCTAG-3';

floxEcad 3'loxP site: 5'-TCAATCTCAGAGCCCCACCTA-3' and 5'-CCTGCCATGATTGTCATGGAC-3';

Δ Ecad: 5'-ACATGTTTGTATCGATCTCAG-3' and 5'-CCTGCCATGATTGTCATGGAC-3';

RipCre: 5'-GGTGCTTTGGACTATAAAGC-3' and 5'-GTCAGTACGTGAGATATCTTTA-3'.

Rip1Tag2: 5'-GGACAAACCACAACCTAGAATGGCAG-3' and 5'-CAGAGCAGAATTGTGGAGTGG-3'.

All animal experiments were in accordance with the guidelines of the Swiss Federal Veterinary Office (SFVO) and the regulations of the Cantonal Veterinary Office of Basel-Stadt.

2.2 Histopathological analysis

Mice were sacrificed between one day and 12 weeks of age. Tumor number and diameter were measured, and tumor volumes were calculated assuming a spherical shape of the tumors. The preparation of paraffin and frozen tissue sections and immunohistochemical and immunofluorescent analysis was performed as described previously (Perl et al., 1998). The following primary antibodies were used at the dilutions indicated: hamster anti-mouse podoplanin 1:500 (DSHB, Iowa University), rabbit-anti-human podoplanin 1:100 (Breiteneder-Geleff et al., 1999), rat-anti-E-cadherin 1:100 (Zymed, San Diego, California), mouse-anti-N-cadherin 1:100 (Zymed, San Diego, California), rabbit-anti- β -catenin 1:150 (Sigma, St. Louis, Missouri), mouse-anti-p120-catenin 1:150 (Transduction Laboratories, San Jose, California), rat-anti-CD31 1:100 (BD Biosciences, San Jose, California), mouse-anti-moesin 1:100 (BD Biosciences, San Jose, California), mouse-anti-ezrin 1:100 (BD Biosciences, San Jose, California), rabbit-anti-phospho-ezrin/radixin/moesin 1:100 (Chemicon, Dietkon, Switzerland), rat-anti-ZO-1 1:100 (Chemicon, Temecula, California), mouse-anti-p115 1:200 (Transduction Laboratories, San Jose, California), mouse-anti-vimentin 1:100 (Sigma, St. Louis, Missouri), rabbit-anti-MMP2 1:200 (Oncogene, Dietikon, Switzerland and Chemicon, Temecula, California), goat-anti-MMP7 1:200 (Santa Cruz, Heidelberg, Germany), rabbit-anti-MMP9 1:200 (Chemicon, Temecula, California), goat-anti-insulin 1:1000 (Dako, Baar, Switzerland), rabbit-anti-glucagon 1:1000 (Linco, St. Charles, USA), Alexa fluor 488 phalloidin 1:50 (Molecular Probes, San Diego, California). In case of mouse-anti-mouse antibodies, background was reduced by additional blocking with the m.o.m. kit (Vector Laboratories, Burlingame, California). Alexa 488, 546, 568 and 633 (Molecular Probes, San Diego, California) as well as 1 μ g/ml 1,4,6-Diamidino-2-phenylindole (DAPI, Sigma, St. Louis, Missouri) were used to visualize the binding of primary antibodies and the nucleus, respectively.

For BrdU staining (proliferation assay), mice were injected with 100 μ g BrdU solution/g body weight intraperitoneally 2 hrs before sacrifice. BrdU (Zymed, San Diego, California) was diluted to 5 mg/ml in 10 mM TrisHCl pH 7.4; 0.8% NaCl; 0.25 mM EDTA. The pancreas was extracted and embedded in paraffin. Antigen retrieval on slides was done by incubation in 2N HCl for an hour and trypsinisation. Samples were incubated over night in a 1:100 solution of biotinylated mouse-anti-BrdU antibody (Zymed, San Diego, California). The staining was developed with the ABC-kit of Vectastain (Vector laboratories, Burlingame, California) and Sigma fast 3,3'-Diaminobenzidine tetrahydrochloride with metal enhancer (Sigma, St. Louis, Missouri). The mitotic index equals the percentage of BrdU-positive nuclei.

For TUNEL (apoptosis assay) antigen retrieval on slides was performed by digestion with proteinase K (Fluka, Buchs, Switzerland). Slides were incubated 1 hour in TUNEL reagent (Roche, Rotkreuz, Schweiz) at 37°C. The staining was developed

with the AEC-kit (Vector laboratories, Burlingame, California). The apoptotic index equals the number of tunel-positive nuclei.

Fluorescent stainings were evaluated on an AxioVert, a LSM 510 META confocal microscope (Zeiss, Oberkochen, Germany) or a Nikon epifluorescence microscope (Nikon, Egg, Switzerland). Immunohistochemical stainings were visualized with a AxioLab lightmicroscope (Zeiss, Oberkochen, Germany). Histological staging and grading was done in a blindfold manner and repeated twice.

2.3 MCF7 and A549 cell transfection and induction experiments

A cDNA fragment encoding human podoplanin was subcloned into pIRES (Clontech, Mountain View, California). Constitutive-active and dominant-negative Cdc42, RhoA and Rac1 cloned in pTriEx-4 (Kinexus, Vancouver, Canada) were a generous gift from O. Pertz (The Scripps Research Institute, La Jolla, California). Vectors and empty vector controls were transfected into MCF7 cells using the Amaxa electroporation system following the manufacturer's instructions (Amaxa, Köln, Germany). Cells were selected in 250 µg/ml G418. Transient transfections of MCF7 cells were performed with Fugene (Roche, Basel, Switzerland). Cells grown on a coverslip were fixed in 4% p-formaldehyde for 15 minutes, incubated with 0.2% Triton-X for 2 minutes, washed in PBS, blocked with 5% goat serum for 15 minutes and stained with the appropriate primary and secondary antibodies as described above.

To generate pSUPER-Ecad-shRNA and pSUPER-Control-shRNA constructs, the following oligonucleotides were annealed and inserted into the pSUPERretro-neo vector (OligoEngine, Seattle, Washington).

ShECAD oligos:

5'-GATCCCCATCTGAAAGCGGCTGATACTTCAAGAGAGTATCAGCCGCTTTCAG
ATTTTTGGAAA-3'

5'-AGCTTTTCCAAAAATCTGAAAGCGGCTGATACTCTCTTGAAGTATCAGCCG
CTTTCAGATGGG-3'

Sh_{mouse}NCAM control oligos:

5'-GATCCCCGTACAAGGCTGAGTGGAAGTTCAAGAGACTTCCACTCAGCCTTGT
ACTTTTTGGAAA-3'

5'-AGCTTTTCCAAAAAGTACAAGGCTGAGTGGAAGTCTCTTGAAGTACTTCCACTCA
GCCTTGTACGGG-3'

MCF7 cells were transfected with pSuperRetro-Ecad-shRNA and pSuperRetro-_{mouse}NCAM-shRNA (control) vectors using Fugene (Roche, Rotkreuz) and selected with 250 µg/ml G418 (neomycine). Positive clones were picked and analysed for E-

cadherin downregulation. One clone with E-cadherin knock-down was used for further experiments.

A549 alveolar cell carcinoma cells transfected with podoplanin (A549 podo) or an empty vector (A549 control) are a kind gift of B. Hantusch (Medical University, Vienna).

2.4 Immunoblotting of total cell lysates

For total cell lysates, cells were lysed at 4°C in RIPA-plus buffer (50 mM Tris-HCl pH8, 150 mM NaCl, 2 mM MgCl₂, 2 mM CaCl₂, 0.5% NaDoc, 10% glycerol, 1% NP40, 0.1% SDS, 1mM NaF, 2 mM NaVO₄, 0.1 mM PMSF, 1 mM DTT and protease inhibitor cocktail). 30µg of cleared protein lysates were separated by SDS-PAGE, electroblotted on PDVF membranes, and proteins were visualized with the appropriate primary and secondary antibodies and ECL (Amersham, Otelfingen, Switzerland) on superRX films (Fuji, Dielsdorf, Switzerland).

2.5 Isolation and preparation of pancreatic islets

About 200 islets = 200'000 cells are necessary to perform a Western Blot. One mouse pancreas harbors about 400 islets, but usually only about 100 islets per mouse can be isolated in one round of islet extraction.

Islet isolation: Mice of the appropriate genotype were sacrificed at 6-7 weeks of age. The peritoneal cavity was opened and the entry site of the D. hepaticus communis (common bile duct) in the duodenal wall was clamped using a fine seraphin clamp. The common bile duct was then isolated using fine pick-ups and cannulated with a 30 gauge needle. By retrograde perfusion the pancreas was then filled with 2-3 ml of collagenase solution (collagenase type IV; Worthington, Lakewood, New Jersey; 3 units/µl in HBSS/Ca²⁺/Mg²⁺) until it slowly inflated and rose off the retroperitoneal surface. Then the cannula and the clamp were removed and the pancreas was dissected. With scissors, the pancreas was cut into small pieces and put in an incubator at 37°C for 45 minutes. Then, the pancreas was re-suspended in 10 ml of RPMI + 10% FCS + 20 mM HEPES by pipetting up and down. The pancreatic fragments were diluted into 3 bacterial Petri dishes with 15 ml of medium in each dish. Islets were picked under dark field illumination of a dissection microscope and washed in fresh medium.

Islet preparation for Western Blotting: 200 isolated pancreatic islets were suspended in DMEM + 10% FCS in an Eppendorf tube and centrifuged for 5 minutes at 0.9G. The supernatant was tipped of and 1ml PBS was added. This washing step was repeated twice. Then, 50 µl of 2.5x SDS-sample buffer was added and the suspension was incubate for 5 minutes at 4°C in an ultrasound bath. Thereafter, the solution was incubated for 5 minutes in a cooking block. This extract was either

directly used for Western Blotting or stored at -20°C for later applications. Western blot of this extract was performed as described above.

2.6 Immunofluorescence of cultured cells

Exponentially growing cells were plated on coverslips. After 2-3 days of incubation cells were fixed in 3% p-formaldehyde/PBS/sucrose (pH7.4) for 10-15 minutes at 37°C and permeabilized with 0.2% TritonX-100/PBS for 2 minutes at room temperature, or fixed for 5 minutes in methanol/acetone at room temperature. All subsequent steps were carried out at room temperature. Coverslips were rinsed thrice with PBS and incubated for 1h with primary antibodies diluted in PBS / 1% BSA / 1% goat serum. The same 1^o antibodies as described in the histopathology section were used. After washing three times with PBS, the cells were incubated 30 minutes with the appropriate secondary antibodies (see above). DNA was counterstained with 1 $\mu\text{g/ml}$ 1,4,6-Diamidino-2-phenylindole (DAPI, Sigma, St. Louis, Missouri). Coverslips were then inverted and set on a drop of 5 μl Vectashield medium (Vector laboratories, Burlingame, California). Images were obtained with a LSM 510 META confocal scanning fluorescence microscope (Zeiss, Oberkochen, Germany).

2.7 Cell migration and invasion assays

Cell migration was determined by using a modified two-chamber migration assay (Falcon BD, Franklin Lakes, New Jersey) with a pore size of $8\mu\text{m}$. For the invasion assay, the membrane was coated with 20 μl of a 2.5mg/ml solution of matrigel (Falcon BD). For both assays, 10^5 MCF7 cells were seeded in 1% fetal calf serum/DMEM medium (Sigma, St. Louis, Missouri) in the upper chamber and the lower chamber was filled with 10% fetal calf serum/DMEM medium. After 24h incubation at 37°C , cells in the upper chamber were carefully removed with a cotton swap and the cells that had traversed the membrane were fixed in 4% p-formaldehyde/HBS- Ca^{2+} , stained with crystal violet (0.5% in 20% methanol), and counted. For functional assays, the Rock-inhibitor Y27632 (Sigma Aldrich, Basel) and the tissue-inhibitor of matrix metalloproteases 2 (TIMP2, a kind gift of A. Noel, Liege, Belgium) were added to the cell suspensions at a concentration of 10 μM and 200 nM, respectively.

2.8 Induction of podoplanin expression with stromal factors

MCF7 cells were treated with stromal factors at the following concentrations: IGF 100 ng/ml (Leinco, St. Louis, Missouri), TNF- α 50 ng/ml (R&D, Oxon, UK), HGF 10 ng/ml (R&D, Oxon, UK), EGF 100 ng/ml (Sigma, Basel, Switzerland), bFGF 50 ng/ml (Sigma, Basel, Switzerland), TGF- β 4 $\mu\text{g/ml}$ (R&D, Oxon, UK). Cells were lysed after

0, 2, 4, 8, 16 and 24 hours of incubation. Immunoblotting analysis was performed as described above.

2.9 MTT cell proliferation assay

The MTT cell proliferation assay (La Roche, Basel, Switzerland) was performed according to the manufacturer's instructions.

2.10 *In vitro* wounding assay

An artificial wound was generated using a 200 μ l pipette tip on confluent MCF7 cell monolayers in a 6-well culture plate in 10% serum containing DMEM-medium (Sigma, St. Louis, Missouri). Cells were then washed with fresh medium to remove floating cells. Photographs were taken at different time points.

2.11 Cell spreading assay

To determine cell spreading on fibronectin, 24-well plates were coated with 15 μ g/ml fibronectin (Sigma, St. Louis, Missouri). 10^4 cells were then plated in low serum medium (1% FCS in DMEM), and 30 minutes after seeding, the medium was changed to eliminate unattached cells. Cells were incubated at 37°C and monitored in regular intervals. Adherent cells were photographed under phase-contrast and counted as flattened or round cells. Cell spreading was confirmed in four independent experiments.

2.12 RhoA, Cdc42 and Rac activity assay

The RhoA, Cdc42 and Rac activity assays were performed as described (Sander et al., 1999). Briefly, 5×10^6 cells were lysed before incubation with GST-PAK (for Cdc42 and Rac) or GST-C21 fusion protein (for RhoA). After precipitation, complexes were washed with lysis buffer, resolved by SDS-PAGE, immunoblotted and analysed with antibodies against RhoA, Cdc42 and Rac (Transduction Laboratories, San Jose, California).

2.13 Xenograft assays with MCF7 and A549 cells

10^6 A549 podo or control cells were injected s.c. into female athymic (nude) mice (n=10 per group). Nude mice were purchased from Harlan Netherlands BV, Postbus, Netherlands. For the injection mice were anesthetized with isoflurane and every mouse was injected in both flanks. 52 days after injection mice were sacrificed and tumor number, tumor volume, macroscopic morphology, tumor histology and metastasis were analyzed.

For the transplantation of MCF7 cells, nude mice were implanted with 17 β -estradiol-releasing pellets (Innovative Research of America, Sarasota, Florida) one week before transplantation. The pellets have a mass of 0.72 mg, slowly release estrogen over a period of 90 days, and promote growth of MCF7 cells *in vivo*. Again, we injected 10⁶ MCF7 cells per flank into nude mice under isoflurane anesthesia and sacrificed the mice 52 days later.

2.14 Statistical analysis

Statistical analysis and graphs were performed employing the GraphPad Prism software (GraphPad Software Inc., San Diego, USA). Fisher's exact test was used for the binomial analysis of the adenoma and carcinoma frequency, E-cadherin presence or absence in carcinomas and flattened or round cells in the cell spreading assay. The chi-square test was employed to statistically analyze carcinoma gradings. Statistical analysis of the incidence of MCF7 cell filopodia as well as the quantification of MCF7 cell migration and invasion was done by unpaired, two-sided t-test. Normality testing was performed using the Kolmogorov-Smirnov test with Dallal-Wilkinson-Lilliefors p value.

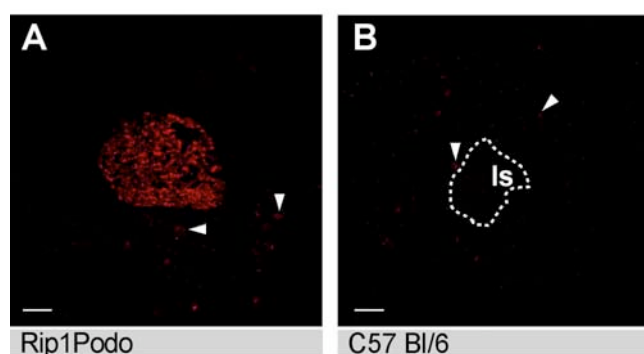
3. Results and Discussion (part I)

3.1. Tumor invasion in the absence of EMT: podoplanin-induced remodeling of the actin cytoskeleton

Generation of Rip1Podo transgenic mice.

We have generated transgenic mice expressing murine podoplanin specifically in the insulin-producing β cells of the pancreatic islets of Langerhans. A cDNA encoding murine podoplanin was cloned between a rat insulin II promoter fragment and a human growth hormone intron and polyadenylation signal, thus targeting podoplanin expression to pancreatic β cells (Hanahan, 1985). Six independent transgenic mouse lines were established that exhibited stable transmission of the transgene to their progeny. Rip1Podo transgenic mice were viable, normoglycemic and fertile. Analysis of transgene expression was examined at the RNA level by RT-PCR (data not shown) and by immunofluorescent staining of histological sections of pancreata of transgenic mice (Figure 3.1). Strong podoplanin expression was detected in all islets of several Rip1Podo mouse lines but not in non-transgenic littermate controls. In the exocrine pancreas, the only detectable podoplanin protein could be attributed to lymphatic vessels.

Figure 3.1: Expression of podoplanin (red) in β -cells of Rip1Podo mice.



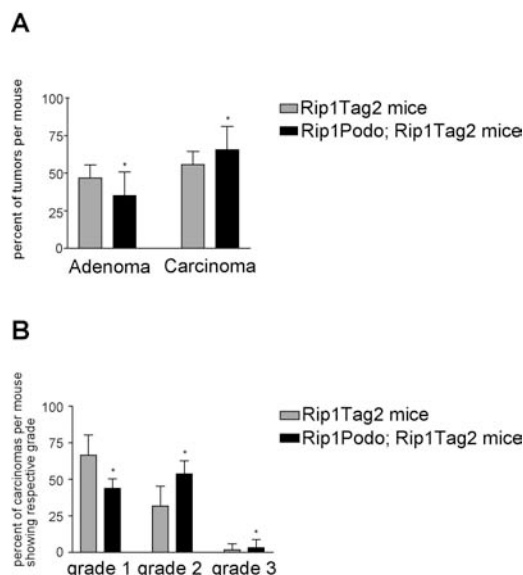
Immunofluorescent staining for podoplanin (red) on a section of a 10 weeks old Rip1Podo single-transgenic mouse (A) and a C57Bl/6 control mouse (B). Strong staining is detected in islets of Langerhans in Rip1Podo mice, whereas no podoplanin expression is detectable in islets of control mice. With the exception of lymphatic vessels (indicated by arrows), no podoplanin staining is visible in the exocrine pancreas. Size bar = 100 μ m.

Histopathological analyses of both adult and newborn pancreas did not reveal any significant differences in islet morphology between Rip1Podo mice and non-transgenic littermate controls, although transgenic podoplanin expression could be detected already in islets of newborn mice. Also, the presence and distribution of cells producing insulin, glucagon, pancreatic polypeptide and somatostatin was unaltered regardless of the age of the mice (data not shown). Moreover, the expression of podoplanin did neither affect blood vessel density and morphology within the islets of Langerhans nor the morphology and distribution of lymphatic vessels, which were exclusively found in the exocrine pancreas in control and in Rip1Podo mice (data not shown).

Podoplanin promotes invasion of β cell tumors

We next crossed Rip1Podo mice with Rip1Tag2 mice in order to generate double-transgenic Rip1Podo;Rip1Tag2 mice. Both single and double-transgenic mice were kept in a C57Bl/6 background. Single-transgenic Rip1Tag2 mice were used as experimental controls to identify podoplanin-specific effects on tumor progression in double-transgenic Rip1Podo;Rip1Tag2 mice. Obvious physiological or pathological differences or changes in life span were not detected between single-transgenic and double-transgenic mice. Mice were sacrificed between the age of 12 and 13 weeks, a time point when Rip1Tag2 mice succumb to hypoglycemia. Histological staging and grading was performed on paraffin sections of pancreata from double-transgenic Rip1Podo;Rip1Tag2 and from single-transgenic Rip1Tag2 mice on the basis of the 2001 WHO classification of rodent tumors (Mohr, 2001). Islets and β cell tumors were staged into normal islets, hyperplastic islets, adenoma (non-invasive tumor) or carcinoma (invasive tumor) with 3 grades: grade 1, invasive tumors with the invading front comprising less than 20% of the entire tumor periphery; grade 2, carcinoma with more than 20%; grade 3, carcinoma with high-grade invasion, nuclear atypia and anaplasia. Detailed analysis of pancreata from 18 double-transgenic and 13 single-transgenic mice revealed that podoplanin-expressing mice exhibited a higher incidence of carcinomas than single-transgenic controls (Figure 3.2 **A**). In particular, the number of grade 2 carcinomas was significantly higher in Rip1Podo;Rip1Tag2 mice (Figure 3.2 **B**). Lymph node and distant organ metastasis were not detected in both genotype mice.

Figure 3.2: tumor progression in podoplanin-overexpressing and control mice.

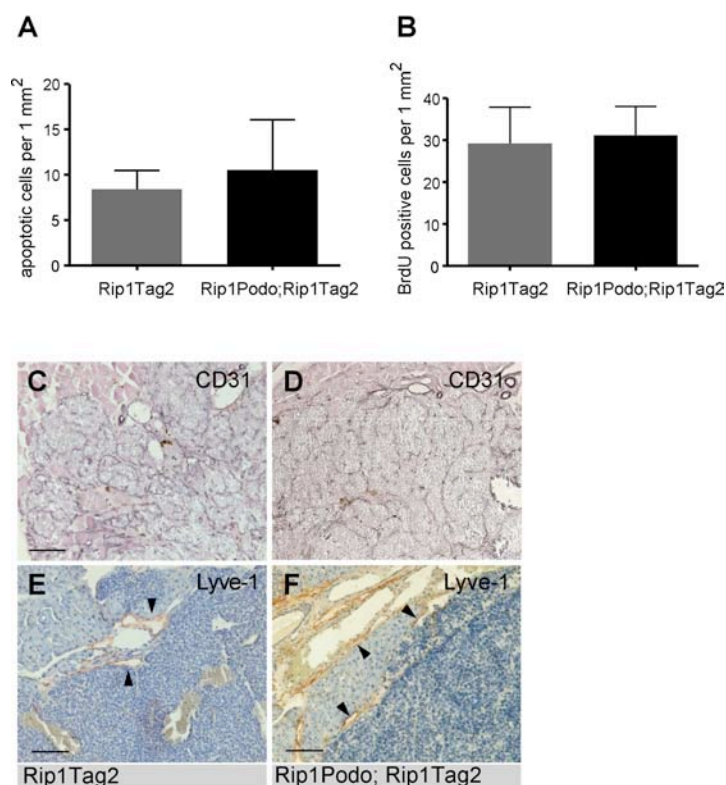


(A) Distribution of adenomas and carcinomas in Rip1Podo;Rip1Tag2 double-transgenic and Rip1Tag2 single-transgenic mice. The incidence of adenomas is reduced from 48% in Rip1Tag2 to 33% in Rip1Podo;Rip1Tag2 mice. Conversely, the incidence of carcinomas is increased in Rip1Podo;Rip1Tag2 mice (* $p = 0.04$, Fisher's exact test). (B) Grading of tumor stages in Rip1Podo;Rip1Tag2 and Rip1Tag2 mice. Carcinoma grading: see main text. Invasiveness of tumors in double-transgenic Rip1Podo;Rip1Tag2 mice was significantly enhanced (* $p = 0.005$, chi-square test). Data are shown as mean \pm SEM.

Expression of podoplanin during Rip1Tag2 tumorigenesis did neither affect tumor incidences nor tumor volumes. Moreover, the rates of tumor cell apoptosis and tumor cell proliferation, as assessed by TUNEL and BrdU incorporation assays,

respectively, were not significantly altered by podoplanin (Figure 3.3 **A** and **B**). Since podoplanin has been reported to play a role in the development of lymphatic vessels (Schacht et al., 2003), we also examined the morphology and density of blood and lymphatic vessels in Rip1Podo;Rip1Tag2 double-transgenic mice by immunohistochemical stainings with antibodies against CD31 and LYVE-1, respectively (Figure 3.3, **C-F**). No apparent difference in blood and lymphatic vessel morphology could be detected, and quantitation of vessel densities did not reveal any significant impact of podoplanin expression on blood vessel angiogenesis and lymphangiogenesis during tumor progression (data not shown). From these analyses, we conclude that podoplanin promotes tumor invasiveness *in vivo* by conferring migratory and invasive properties to tumor cells without affecting other tumor growth parameters.

Figure 3.3: Apoptosis, proliferation, blood vessel and lymphatic vessel density



Podoplanin overexpression does not significantly influence the rate of apoptosis (A) or proliferation (B) of insulinoma cells. Pancreatic sections from Rip1Tag2 (C, E) and Rip1Podo;Rip1Tag2 (D, F) mice were stained with antibodies against CD31 to visualize blood vessels (C, D) and with antibodies against LYVE-1 to detect lymphatic vessel (E, F). Counting of blood vessel and lymphatic vessel density per area did not show a significant difference between the two mouse lines. Data are shown as mean \pm SEM. Size bar = 100 μ m.

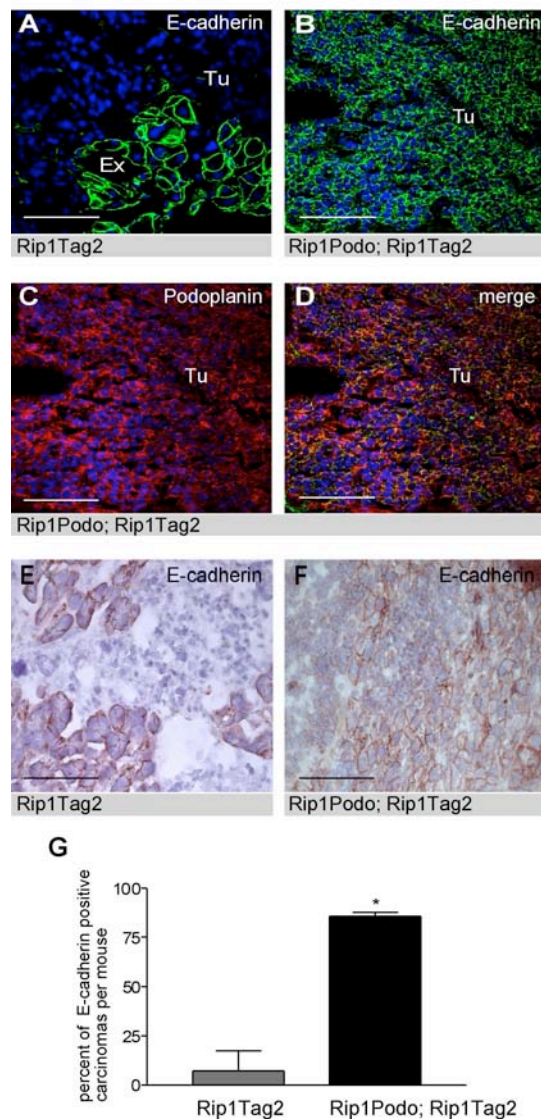
Podoplanin bypasses EMT during Rip1Tag2 tumor progression.

We have previously demonstrated that the loss of E-cadherin expression is a rate-limiting step in the transition from adenoma to carcinoma during Rip1Tag2 tumorigenesis (Perl et al., 1998). To assess whether podoplanin modulates the transition from adenoma to carcinoma by affecting the epithelial character of tumor

cells, E-cadherin expression in tumors from Rip1Tag2 mice and Rip1Podo;Rip1Tag2 mice was analyzed by immunofluorescence staining with antibodies against E-cadherin. As expected with Rip1Tag2 control mice, E-cadherin staining was absent in invasive tumors (Figure 3.4 **A**). In contrast, in podoplanin-expressing tumors, strong E-cadherin staining could be observed at the membranes of most tumor cells (Figure 3.4 **B**). Double-staining for the expression of E-cadherin and podoplanin revealed a strong co-localization of E-cadherin and podoplanin at cell-cell junctions, even of invasive tumor cells (Figure 3.4 **C** and **D**). To verify whether E-cadherin is present at the tumor rim and in the invading front, the expression of E-cadherin was also analyzed by immunohistochemical stainings on frozen sections. In tumors from Rip1Tag2 control mice, E-cadherin was undetectable in invasive tumor cells (Figure 3.4 **E**). In contrast, E-cadherin was still present in podoplanin-expressing tumor cells in the invading front of carcinomas (Figure 3.4 **F**). 86% of carcinomas in the podoplanin overexpressing mice were positive for E-cadherin, whereas 93% of carcinomas of control mice had lost E-cadherin expression (Figure 3.4 **G**, * $p=0.0009$, Fisher's exact test). This surprising observation suggests that in the presence of podoplanin the induction of tumor invasion is not dependent on the loss of E-cadherin function. Yet, the fact that approximately 14% of the podoplanin-expressing carcinomas are negative for E-cadherin expression indicates that podoplanin does not necessarily prevent the loss of E-cadherin expression in invasive tumor cells.

We next examined whether the expression of other epithelial markers, such as the cytoplasmic adherens junction proteins β -catenin and p120-catenin, was maintained together with E-cadherin at the cell membrane of podoplanin-expressing β tumor cells. No membrane staining for β -catenin and p120-catenin was detectable in carcinomas of Rip1Tag2 mice, except for vascular cells within the tumor area (Figure 3.5 **A** and **C**). In contrast, in the invasive fronts of podoplanin-expressing tumors, together with the continuing expression of E-cadherin, a strong membrane staining for both β -catenin and p120-catenin could be detected (Figure 3.5 **B** and **D**). Analysis of the expression of the tight junction protein ZO-1 revealed comparable results (Figure 3.6). Thus, markers of adherens and tight junctions are maintained at the cell membrane.

Figure 3.4: Podoplanin induces tumor invasion without loss of E-cadherin expression

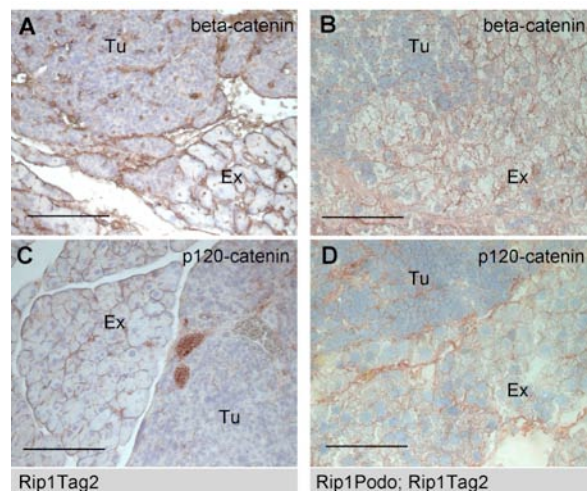


(A-D) Pancreatic sections from Rip1Tag2 (A) and Rip1Podo;Rip1Tag2 (B, C, D) were stained by immunofluorescence with antibodies against E-cadherin (green) and podoplanin (red) as indicated. Note that the invasive β cell carcinoma of a single-transgenic Rip1Tag2 mouse has lost E-cadherin expression (A), whereas podoplanin-expressing tumor cells, despite their apparent invasion into surrounding tissue, maintain the expression of E-cadherin (B, C). Podoplanin and E-cadherin colocalize at cell membranes in these cells (D). Blue staining = DAPI (nuclei).

(E, F) Immunohistochemical visualization of E-cadherin expression. E-cadherin expression (brown) is lost in an invasive carcinoma of a Rip1Tag2 mouse, while it is present in the exocrine pancreatic tissue (E). In an invasive carcinoma of a Rip1Podo;Rip1Tag2 mouse, E-cadherin expression (brown) is maintained even in the invading front of the tumor (F).

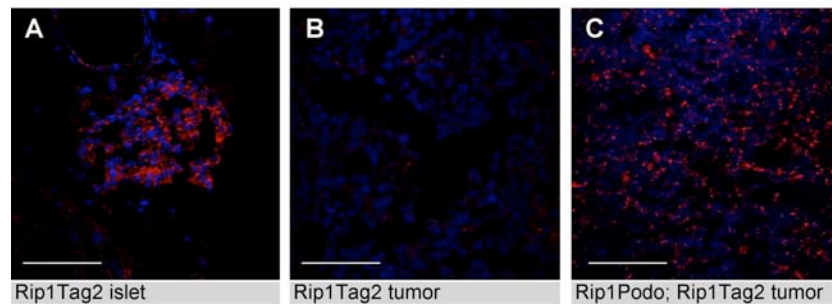
(G) Quantitation of E-cadherin expression in classified carcinomas of Rip1Tag2 and Rip1Podo;Rip1Tag2 mice. Data are shown as mean \pm SEM. Ex = exocrine tissue, Tu = tumor tissue. Size bar = 100 μ m.

Figure 3.5: Maintenance of epithelial markers in podoplanin-expressing tumor cells.



Immunohistochemical staining for β -catenin (A, B) and p120-catenin (C, D) in Rip1Tag2 (A, C) and Rip1Podo;Rip1Tag2 (B, D) mice. β -catenin and p120-catenin stainings are lost in tumors of Rip1Tag2 mice, except for vascular cells. In contrast, β -catenin and p120-catenin are maintained on membranes of tumor cells of a Rip1Podo;Rip1Tag2 mouse. Ex = exocrine tissue, Tu = tumor tissue. Size bar = 100 μ m.

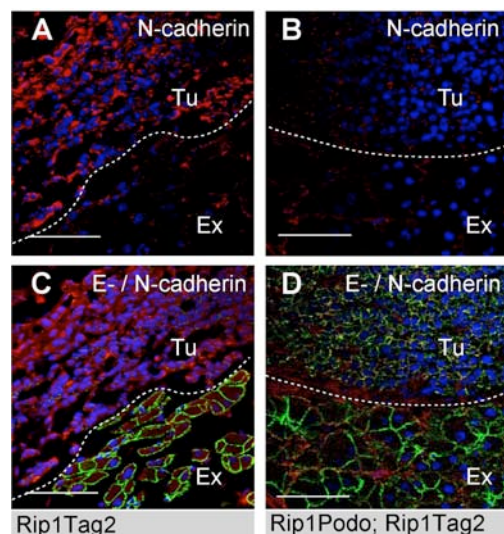
Figure 3.6: Expression of the tight-junctions protein ZO-1 is not lost upon podoplanin-mediated tumor invasion.



Immunofluorescence staining for ZO-1 (red) on pancreatic sections from Rip1Tag2 (A, B) and Rip1Podo;Rip1Tag2 (C) mice. A morphologically normal islet of a Rip1Tag2 mouse expresses ZO-1 at membranes of all islet cells (A), whereas β cell carcinomas of these mice have lost expression of ZO-1 (B). In contrast, expression of ZO-1 is maintained in an invasive tumor of a Rip1Podo;Rip1Tag2 mouse. Size bar = 100 μ m.

Next, we determined whether a cadherin switch, i.e. the switch from E-cadherin to N-cadherin expression, occurred in podoplanin-expressing tumors. In the carcinomas of Rip1Tag2 control mice, expression of E-cadherin was lost and the expression of N-cadherin was strongly upregulated (Figure 3.7 A and C). In contrast, in podoplanin-expressing tumors, only a very weak staining for N-cadherin was detectable, while E-cadherin expression remained present (Figure 3.7 B and D). Apparently, a switch in cadherin expression is not required for the development of invasive carcinomas in double-transgenic Rip1Podo;Rip1Tag2 mice. Instead, E-cadherin, together with other adherens and tight junction markers, remains at the membranes of invasive carcinoma cells. These results raise the intriguing possibility that podoplanin is able to induce tumor cell invasion without dissolving epithelial adherens and tight junctions.

Figure 3.7: Podoplanin-mediated tumor cell invasion does not involve a cadherin switch.



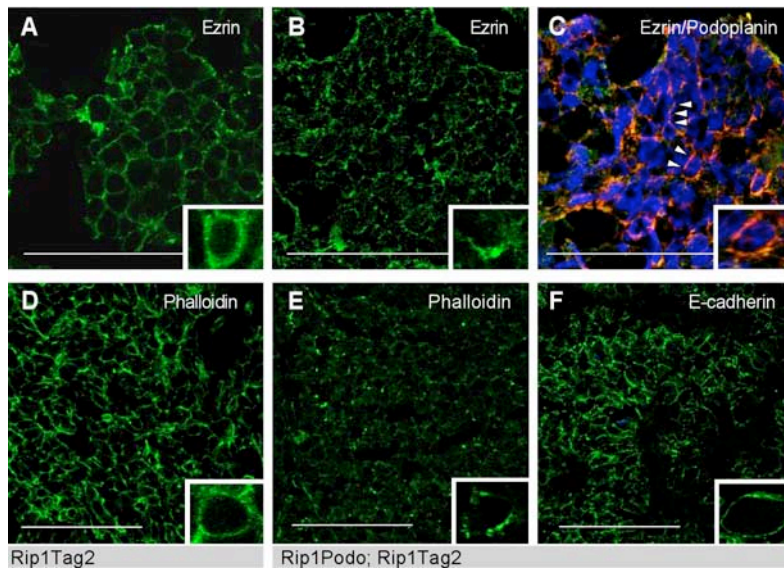
Immunofluorescence staining for N-cadherin (red) (A, B) and double-staining for N-cadherin (red) and E-cadherin (green) (C, D) on pancreatic sections from Rip1Tag2 (A, C) and Rip1Podo;Rip1Tag2 (B, D) mice. Note that in carcinomas of Rip1Tag2 single-transgenic mice, concomitant with the loss of E-cadherin expression, the expression of N-cadherin is upregulated. In contrast, in tumors of Rip1Podo;Rip1Tag2 double-transgenic mice, E-cadherin expression is maintained and N-cadherin is not upregulated. Blue staining = DAPI (nuclei), Ex = exocrine tissue, Tu = tumor tissue. Size bar = 100 μ m.

Podoplanin relocalizes ERM proteins and rearranges the actin cytoskeleton

Recently, it has been demonstrated that ezrin co-localizes with podoplanin at the cellular membrane in filopodia-like structures (Martin-Villar et al., 2005). Furthermore, ezrin is upregulated in invasive esophageal cancer cells (Shen et al., 2003) and may play a critical role in tumor metastasis (Hunter, 2004). We therefore investigated the distribution of ezrin both in tumors of podoplanin-transgenic mice and in control mice. In invasive tumors of Rip1Tag2 mice, ezrin was localized to the subcortical compartment of the cells, beneath the cellular membrane in the periphery of the cytoplasm (Figure 3.8 **A**). In tumors of podoplanin-expressing mice, ezrin was redistributed to the edges of invasive tumor cells (Figure 3.8 **B**). Double-stainings for ezrin and podoplanin confirmed the re-localization of ezrin and demonstrated a co-localization of podoplanin with ezrin in filopodia-like membrane foci (Figure 3.8 **C**). Staining for moesin, another ERM protein, showed a comparable pattern (data not shown). Thus, podoplanin overexpression exerts a profound effect on the cellular distribution of ERM proteins, and ERM proteins appear to co-localize with podoplanin in filopodia-like structures at the cell membrane of invasive tumor cells.

Both ZO-1 and ERM proteins are known to bind and modulate the actin cytoskeleton (McClatchey, 2003; Smalley et al., 2005). To investigate the consequences of podoplanin-overexpression on the actin cytoskeleton, we performed fluorescent phalloidin stainings on histological sections of tumors from Rip1Tag2 and Rip1Podo;Rip1Tag2 mice. In control mice, staining of actin filaments appeared in the subcortical compartment of the cells (Figure 3.8 **D**). In podoplanin-expressing tumor cells, actin filament staining was generally reduced, yet a significant subset remained in focal membrane areas which resemble filopodia (Figure 3.8 **E**). Proper membrane localization of E-cadherin indicated that the re-localization of actin filaments was not caused by damage to membrane structures in podoplanin-expressing tumor cells (Figure 3.8 **F**). Taken together, actin filament localization is strongly affected by the presence of podoplanin: subcortical actin filaments are markedly reduced in podoplanin-expressing tumor cells and are re-localized to filopodia-like foci at the plasma membrane.

Figure 3.8: Ezrin and actin filaments are re-localized by podoplanin.



Immunofluorescence staining for ezrin (green) and podoplanin (red) on pancreatic sections of Rip1Tag2 (A) and Rip1Podo;Rip1Tag2 (B, C) mice, as indicated. Note that ezrin is distributed cortically at the cell membrane throughout the tumor of a Rip1Tag2 mouse (A), whereas its presence is more irregular with significant localization to focal membrane regions in tumor cells of Rip1Podo;Rip1Tag2 mice (B). Double-staining of pancreatic sections from Rip1Podo;Rip1Tag2 mice reveals that ezrin (green) and podoplanin (red) co-localize (yellow) at filopodia-like structures at the plasma membrane of podoplanin-expressing β tumor cells, indicated by arrow heads (C). Inserts in panels A-D represent higher magnifications of single cells. Fluorescent phalloidin staining for actin (D, E) and E-cadherin (F) on pancreatic sections from Rip1Tag2 (D) and Rip1Podo;Rip1Tag2 (E, F) mice, as indicated. Note the regular subcortical distribution of actin in β tumor cells of Rip1Tag2 mice, yet an irregular pattern with foci of actin accumulation in tumor cells of Rip1Podo;Rip1Tag2 mice. Staining for E-cadherin on adjacent histological sections demonstrates intact cell membranes in the tumor cells of Rip1Podo;Rip1Tag2 mice. Blue staining = DAPI (nuclei). Size bar = 100 μ m.

Podoplanin induces filopodia formation, cell migration, invasion and spreading in vitro

To investigate whether the upregulated expression of podoplanin affected E-cadherin expression as well as cell morphology and function in cultured tumor cells *in vitro*, MCF7 breast carcinoma cells were stably transfected with a podoplanin expression construct or with empty vector as control. MCF7 cells are known to express high levels of E-cadherin and to exhibit epithelial morphology. Four control- and four podoplanin-transfected clonal cell lines were selected, and the expression of podoplanin was verified by immunoblotting and immunofluorescence analysis (Figure 3.9 A and Figure 3.10 B, D, F, respectively). As expected, MCF7-control cells formed epithelial layers with pronounced E-cadherin-mediated adherens junctions. No staining for podoplanin was detectable (Figure 3.10 A). Expression of podoplanin in MCF7-podoplanin cells caused a dramatic change in cellular shape and migratory behavior with the formation of many filopodia-like structures (Figure 3.10 B). Podoplanin was found to be evenly distributed in all plasma membranes. Similar to β tumor cells in Rip1Podo;Rip1Tag2 mice, podoplanin expression did not result in a loss of E-cadherin function, yet co-localization between E-cadherin and podoplanin was restricted to cell-cell junctions where no filopodia-like protrusions were observed (Figure 3.10 B). No upregulation of EMT-markers such as N-cadherin or vimentin

could be observed in podoplanin-transfected MCF7 cells (Figure 3.9 **B**). To demonstrate that MCF7 cells were actually able to undergo EMT, we ablated E-cadherin expression in these cells by transfection of a vector expressing a specific shRNA targeting E-cadherin (pSuperRetro Ecad). Indeed, upon marked reduction of E-cadherin expression, MCF7 cells upregulated the expression of N-cadherin and vimentin, an indication for EMT (Figure 3.9 **B**). This finding underlines the observation that podoplanin does not induce a cadherin switch or EMT.

Double-stainings for podoplanin and ezrin in podoplanin-expressing MCF7 cells confirmed the co-localization of podoplanin and ezrin at the cell membrane of microspikes and filopodia (Figure 3.10 **C** and **D**). Double-staining for podoplanin and phalloidin/actin revealed a dramatic reduction in actin stress fibers in podoplanin-transfected cells, with an evident re-localization of actin to filopodia (Figure 3.10 **E**, **F**, **G** and **H**). To investigate a direct physical interaction between podoplanin, E-cadherin, ezrin and actin, we performed immunoprecipitation experiments with specific antibodies against podoplanin. However, none of the aforementioned molecules co-precipitated with podoplanin (data not shown). Yet, these experiments revealed that the phosphorylated form of ezrin was much more abundant in podoplanin-transfected cells (Figure 3.10 **I**), suggesting that podoplanin indirectly affects ezrin function and with it the actin cytoskeleton.

Figure 3.9: Podoplanin does not induce EMT in MCF7 cells. The expression of podoplanin can be induced upon stimulation with stromal factors.

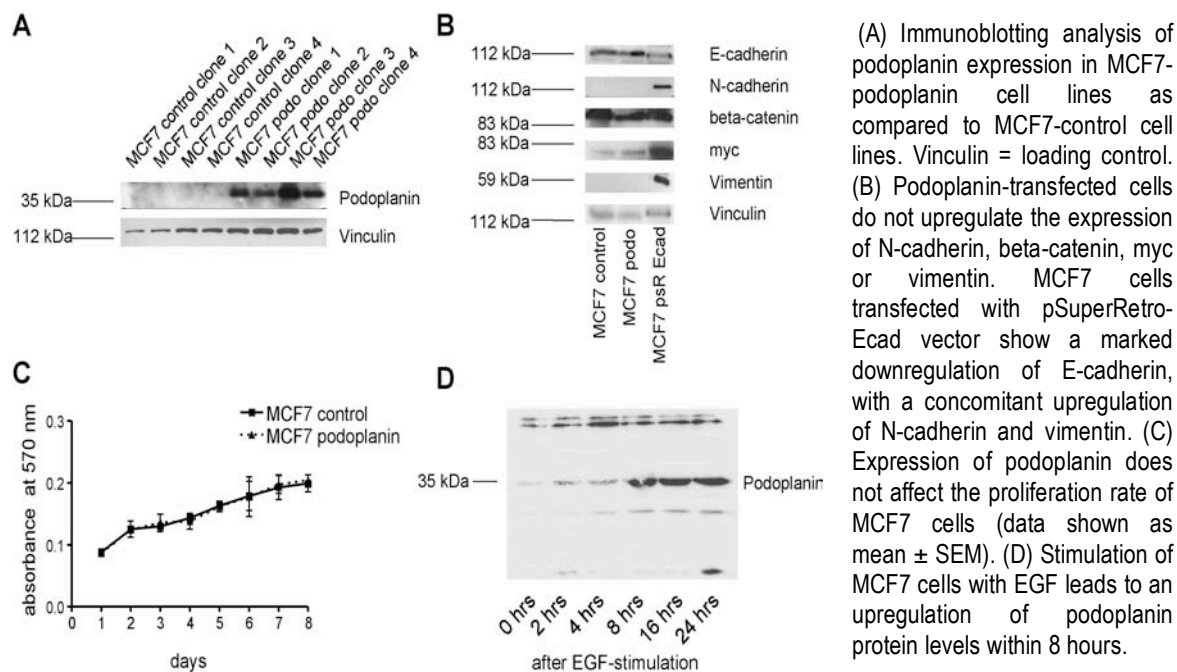
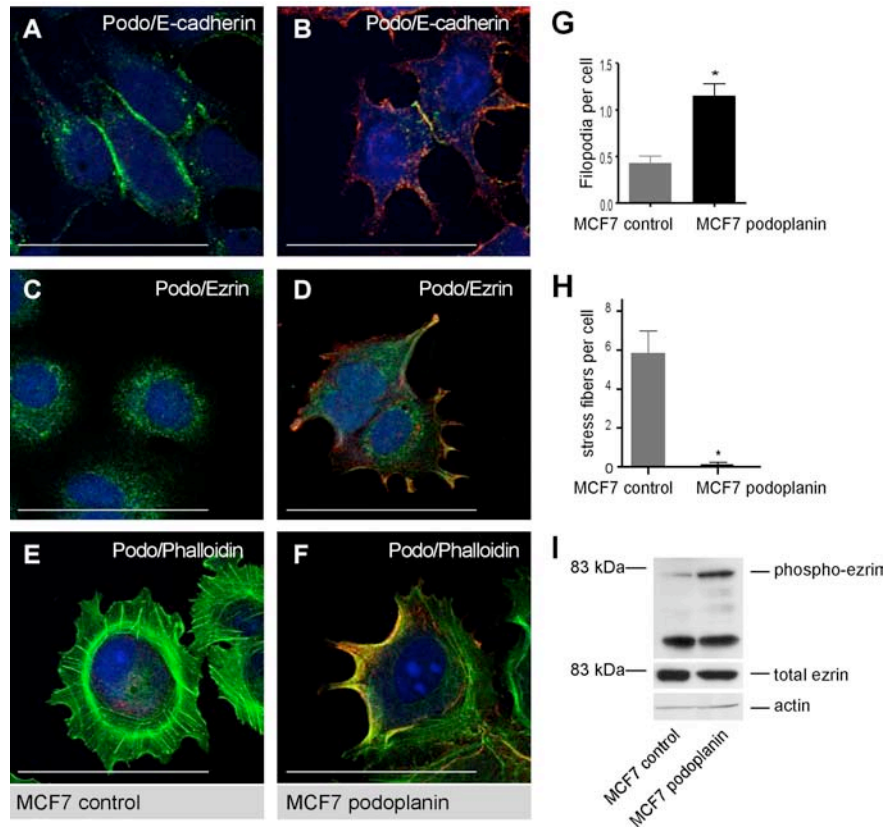


Figure 3.10: Podoplanin induces a migratory phenotype in MCF7 cells.



Double staining against podoplanin and E-cadherin in MCF7-control cells does not reveal any podoplanin (red) expression, yet demonstrates high levels of E-cadherin (green) in cell-cell junctions (**A**). Expression of podoplanin (red) in MCF7-podoplanin cells does not abrogate E-cadherin (green) expression at cell junctions (**B**).

Double-staining for podoplanin (red) and ezrin (green) reveals a regular, subcortical distribution of ezrin (green) in MCF7-control cells (**C**). In contrast, a strong co-localization of both molecules is evident in filopodia-like structures of podoplanin-expressing MCF7 cells (**D**, yellow).

Immunofluorescence stainings of podoplanin (red) and actin/phalloidin (green) reveals many stress fibers in MCF7 control cells (**E**), whereas stress fibers are dissolved and actin filaments are redistributed to filopodia-like structures in podoplanin-transfected cells (Yellow) (**F**).

The number of filopodia (defined as F-actin positive membrane protrusion of $> 5\mu\text{m}$ length) is significantly increased in podoplanin-transfected MCF7 cells as compared to control cells (**G**, $*p < 0.0001$, two-sided t-test). Conversely, the number of stress fibers is dramatically reduced in podoplanin-transfected cells (**H**, $*p < 0.0001$, two-sided t-test). Data are shown as mean \pm SEM.

(**I**) Immunoblotting analysis of ezrin phosphorylation. The level of phospho-ezrin (but not total ezrin) is increased in podoplanin-transfected cells as compared to control MCF7 cells. Size bar = $20\mu\text{m}$.

Cell spreading has been shown to be mediated by filopodia formation (Price et al., 1998). To assess whether the filopodia that formed upon the expression of podoplanin were functional, we compared control and podoplanin-transfected cells for their ability to spread on culture dishes pre-coated with fibronectin. Cell spreading was significantly accelerated in podoplanin-transfected cells (Figure 3.11 **A** and **B**), which could be repressed by neutralizing antibodies against β_1 integrin (data not shown).

Next, we performed *in vitro* scratch wounding assays on confluent monolayers of MCF7 cells (Figure 3.12). With podoplanin-transfected cells, a broad migrating front was visible in the gap after 8 hours, and after 24 hours the gap had closed, whereas with MCF7-control cells, only a few single migrating cells were detectable after 8 hours and the gap had not closed after 24 hours. Rates of cell proliferation were not different between podoplanin-transfected and control cells, excluding any proliferation effects on cell migration (Figure 3.9 C). To determine whether the podoplanin-mediated increase in cell migration was accompanied by cell polarization, the cells in the scratch wounding assays were stained with antibodies against the specific *cis*-Golgi marker p115 (Gadea et al., 2002). While 25% of the control cells exhibited a polarized orientation of the Golgi apparatus, 42% of podoplanin expressing cells migrated in a polarized manner ($p < 0.016$, chi-square test).

The effect of podoplanin expression on cell migration and invasion was quantified by two-chamber migration and invasion assays, where podoplanin-expressing and control MCF7 cells were seeded in the upper chamber of trans-well inserts, and migration of cells along a serum gradient through a membrane was observed. In the invasion assay, trans-well membranes were additionally coated with a layer of polymerized matrigel. These experiments revealed that migration of podoplanin-transfected cells was significantly higher as compared to control cells (Figure 3.11 C), and that the invasion rate was even more pronounced in podoplanin-expressing cells as compared to control cells (Figure 3.11 D).

Figure 3.11: Podoplanin induces spreading, migration and invasion of MCF7 cells.

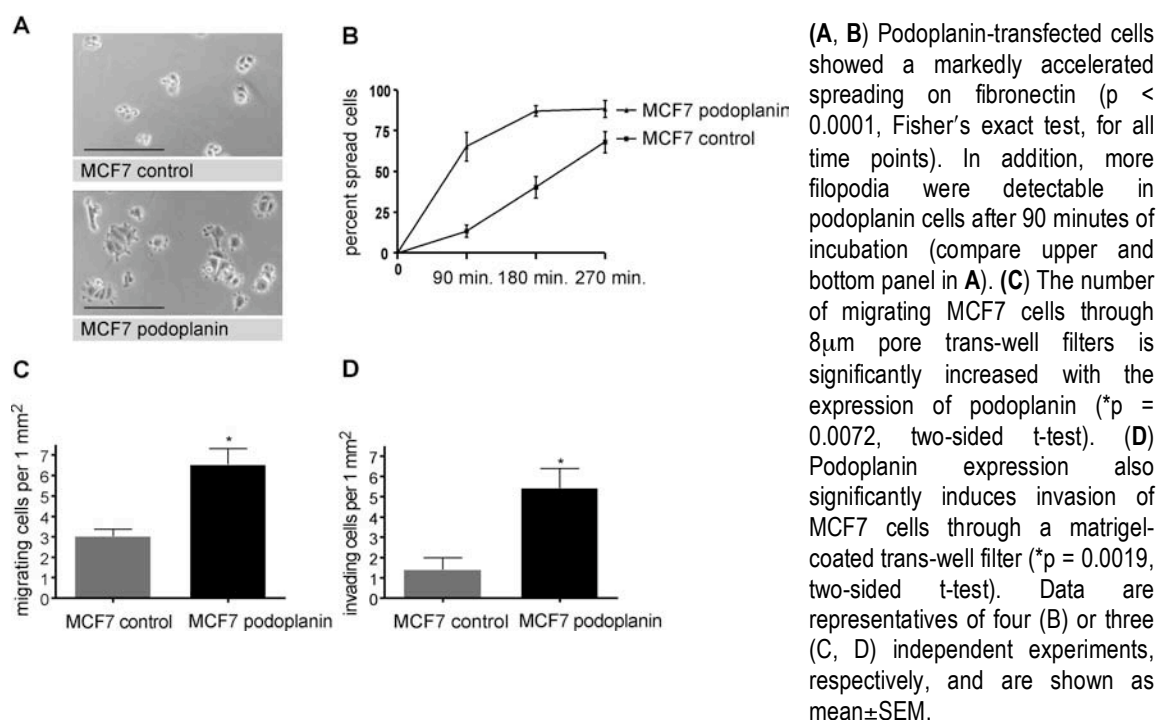
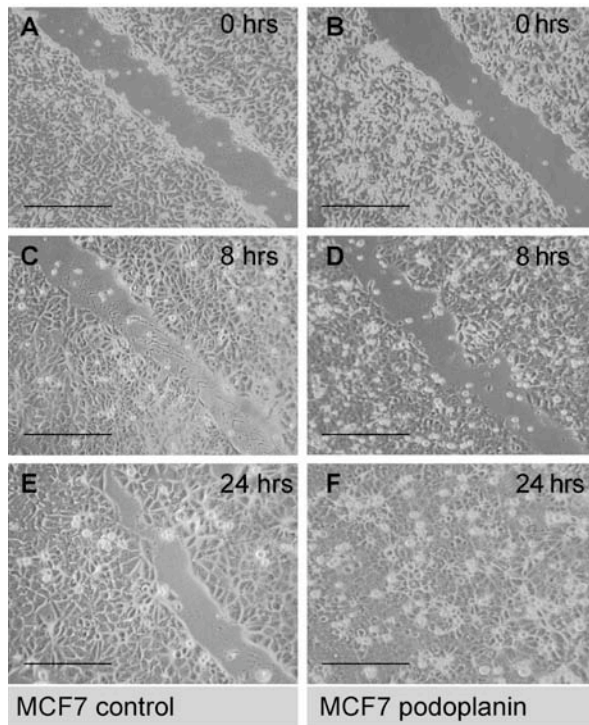


Figure 3.12: Scratch wound assay.



Scratch wound assay on confluent monolayers of podoplanin-expressing MCF7 cells and MCF7-control cells. Microphotographs were taken at various time points as indicated. Size bar = 100 μ m.

Since the invasive behavior of tumor cells and in particular of cells of the invading front is known to be influenced by growth factors derived from the tumor stroma, we set out to investigate whether podoplanin-expression can be induced by stromal factors. MCF7 cells were stimulated for different time periods with FGF2, EGF, TGF β , IGF1, TNF- α or HGF and podoplanin expression was determined by immunoblotting. Of all the factors tested, only EGF markedly upregulated podoplanin expression in MCF7 cells (Figure 3.9 D), while a somewhat weaker induction could be observed with FGF2 and TGF β (data not shown).

Taken together, the results from these *in vitro* experiments confirm that the pro-migratory and pro-invasive effect of podoplanin is independent of EMT or a cadherin-switch and is rather due to a dramatic re-organization of the actin cytoskeleton. In podoplanin-transfected cells, the loss of stress fibers is accompanied by the formation of microspikes and filapodia, indicating highly motile cell membranes. As a consequence, these cells exhibit enhanced spreading on extracellular matrix components and increased migratory and invasive capabilities. Thereby, the induction of podoplanin in the invading tumor front may be mediated by stromal growth factors, such as EGF, FGF2 and TGF β .

Podoplanin downregulates RhoA activity but acts independently of Cdc42

Our results indicate that podoplanin prevents stress fiber formation. Disruption of stress fibers can also be caused by an inactivation of the small GTPase RhoA pathway (Izawa et al., 1998). To test whether RhoA inactivation may be involved in the podoplanin-mediated reduction of stress fiber formation, we transfected control and podoplanin-expressing MCF7 cells with constitutive-active or dominant-negative

forms of RhoA (Figure 3.13 **A**). In addition, we also treated MCF7 cells with Y27632, an inhibitor of the Rho signaling effector, RhoA-associated kinase (Rock). Expression of constitutive-active RhoA efficiently reversed the loss of stress fibers in podoplanin-transfected cells ($p < 0.0001$, one-way ANOVA with Newman-Keuls post-test). Dominant-negative RhoA and the Rock inhibitor Y27632, on the other hand, repressed stress fiber formation in control cells to levels observed in podoplanin-expressing cells. To investigate whether podoplanin-mediated loss of stress fibers was due to an inactivation of RhoA, we performed RhoA activity assays. These experiments revealed a strong downregulation of activated RhoA in podoplanin-transfected cells as compared to control cells (Figure 3.13 **C**).

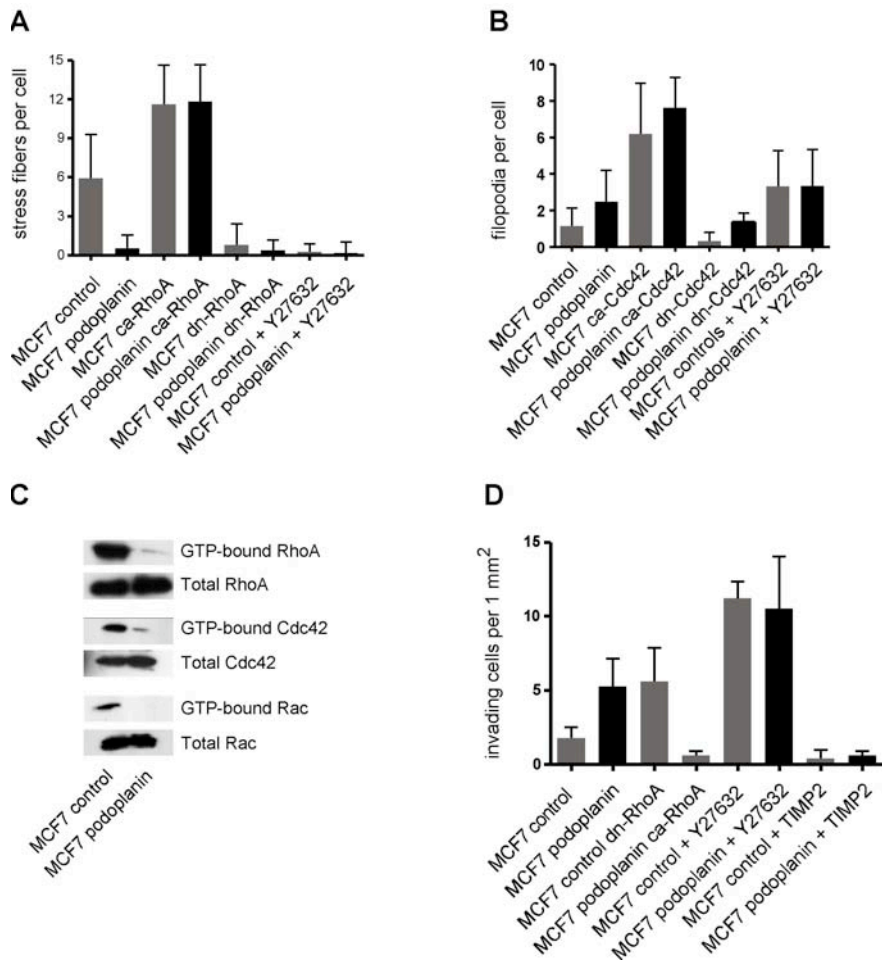
In contrast to stress fiber formation by RhoA, the Rho family GTPase Cdc42 and Rac1 are known to induce filopodia and lamellipodia, respectively (Fukata et al., 2003)(Sahai & Marshall, 2002). To investigate the mechanisms of filopodia formation in podoplanin-transfected MCF7 cells, we transfected these cells with either constitutive-active Cdc42 or dominant-negative Cdc42. In dominant-negative Cdc42-transfected cells, podoplanin still mediated the formation of filopodia, although a modest reduction in filopodia formation was observed in both podoplanin-expressing and MCF7-control cells (Figure 3.13 **B**). Conversely, constitutive-active Cdc42 dramatically increased filopodia formation in both cell types. Interestingly, the Rock inhibitor Y27632 also induced filopodia formation in MCF7 control cells (Figure 3.13 **B** and Figure 3.14). To verify these results, we performed Cdc42 activity assays, which revealed a significant reduction in Cdc42 activities between podoplanin-transfected and control cells (Figure 3.13 **C**). Activity assays for Rac1, the third member of the Rho family of small GTPases, also showed a downregulation of Rac1 activity upon podoplanin expression (Figure 3.13 **C**). Yet, transfection of MCF7 and MCF7 podoplanin cells with constitutive-active and dominant-negative Rac1 did not result in a significant change in cell morphology (data not shown). Together, these results suggest that podoplanin-mediated formation of filopodia does not involve the activation of Cdc42 or Rac1. Rather, inhibition of RhoA or Rock activities directly caused the formation of filopodia.

To investigate the functional impact of RhoA downregulation on cell invasion, MCF7 cells stably transfected with constitutive-active RhoA, dominant-negative RhoA or treated with Y27632 were analyzed in a matrigel invasion assay (Figure 3.13 **D**). Stable expression of constitutive-active RhoA inhibited invasion of control MCF7 cells. Conversely, MCF7 cells transfected with dominant-negative RhoA or treated with Y27632 exhibited markedly increased cell invasion (Figure 3.13 **D** and Figure 3.14). These results support the notion that podoplanin induces tumor cell invasion by inhibiting the RhoA pathway. Treatment of both control and podoplanin-transfected MCF7 cells with tissue inhibitor of MMPs (TIMP2), a general MMP inhibitor, almost completely abrogated cellular invasion (Figure 3.13 **D**).

These results indicate that podoplanin downregulates RhoA activity, thereby ablating stress fibers, inducing filopodia formation, and promoting tumor cell

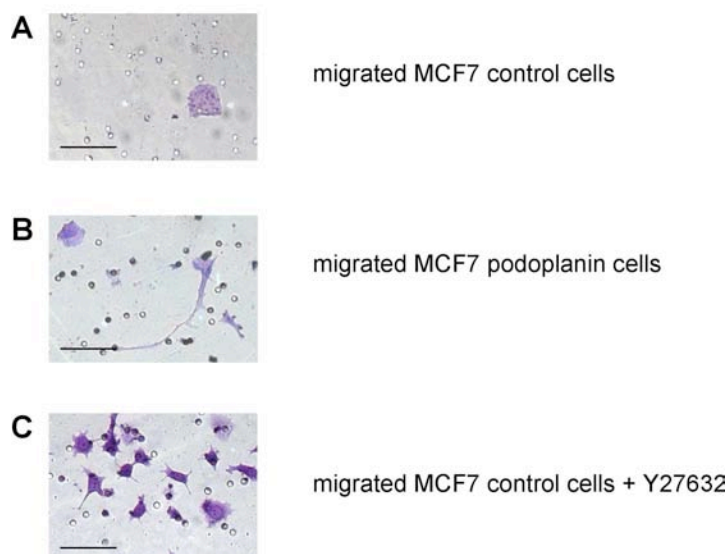
migration and invasion. Thereby, the enhanced invasion properties of podoplanin-expressing cells appear to depend on the activity of MMPs.

Figure 3.13: Podoplanin downregulates RhoA, Cdc42 and Rac activity.



(A) Expression of podoplanin represses stress fiber formation in MCF7 cells. Expression of dominant-negative RhoA (dn-RhoA) abrogates stress fiber formation in control-transfected cells, indicating that RhoA activity is required for stress fiber formation in MCF7 cells. Expression of constitutive-active RhoA (ca-RhoA) increases the number of stress fibers in both control and podoplanin-transfected cells. The Rock inhibitor Y27632 inhibits the formation of stress fibers in MCF7 cells. (B) Podoplanin induces filopodia formation. Transfection of constitutive-active Cdc42 (ca-Cdc42) in control- and podoplanin-transfected cells results in a strong increase in the number of filopodia. Transfection of dominant-negative Cdc42 (dn-Cdc42) in podoplanin-transfected cells does not significantly affect filopodia formation, whereas the Rock inhibitor Y27632 induces filopodia formation in MCF7-control cells. (C) Analysis of RhoA, Cdc42 and Rac1 GTPase activity by GST-C21 and GST-PAK pull-down assays, respectively. Note that podoplanin expression strongly reduces RhoA, Cdc42, and Rac1 activities. (D) Invasion of MCF7 cells is promoted if cells are transfected with podoplanin or dominant-negative RhoA or are treated with the Rock-inhibitor Y27632. Invasion of MCF7 cells is reduced if cells are transfected with constitutive-active RhoA. Upon treatment with TIMP2, invasion is markedly reduced in both podoplanin-expressing and control MCF7 cells. Data are shown as mean \pm standard deviation.

Figure 3.14: Morphology of MCF7 cells after migration through a matrigel-coated membrane.



(A) Migrated MCF7 control cells: cells are flat and do not display filapodia.

(B) Migrated MCF7 podoplanin cells: cells are elongated and form filapodia.

(C) Migrated MCF7 control cells treated with the Rock inhibitor Y27632: cells are elongated and form multiple filapodia.

Size bar = 20 μ m.

Podoplanin promotes tumor engraftment in a mouse xenograft model

To further elucidate the role of podoplanin in carcinogenesis, we transplanted podoplanin- or empty vector transfected MCF7 and A549 (alveolar carcinoma) cells subcutaneously in athymic (nude) mice. One week before xenotransplantation, nude mice destined for the transplantation of MCF7 podo and control cells were implanted with an estrogen-releasing pellet in order to promote MCF7 cell engraftment. We sacrificed the mice 52 days after the injection of the cells and analysed tumor engraftment, tumor volume, exulceration and metastasis (Figure 3.15 and table 3.1). All xenotransplanted A549 cells engrafted and formed subcutaneous tumors. In about 50% of the A549 control tumors, the overlying epidermis was infiltrated and destroyed by the tumor and exulceration ensued (Figure 3.15 **A**). Podoplanin shifted tumor growth to an expansive, subcutaneous spreading and protected the skin from exulceration ($p < 0.001$, chi-square test, cf. table 3.1). In contrast, MCF7 cell tumors never led to exulceration. However, MCF7 cells expressing podoplanin showed a significantly better engraftment (92% vs 69%, $p < 0.001$, chi-square test) than MCF7 control cells. The median volume of successfully engrafted tumors was identical for podoplanin-transfected and control A549 and MCF7 cells (Figure 3.15 **B**). These results confirm the concept that podoplanin can (i) actively promote carcinogenesis, as reflected by the improved engraftment of MCF7 podo cells and (ii) shift tumor invasion to an expansive growth pattern that reduces the likeliness of exulceration in this xenograft model.

Figure 3.15: Subcutaneously grafted A549 or MCF7 cells transfected with podoplanin or empty vector

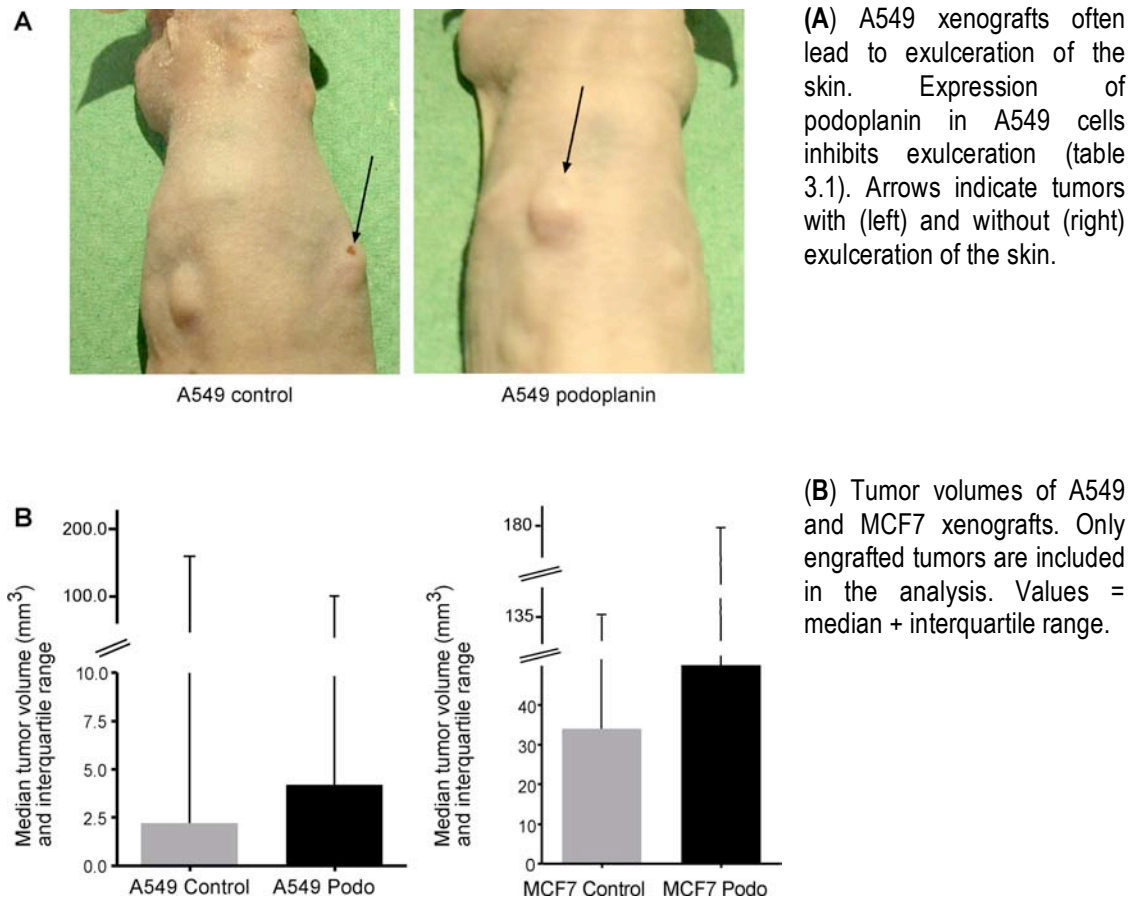


Table 3.1: Engraftment and exulceration of A549 and MCF7 xenografts in nude mice

	<i>A549 control</i>	<i>A549 podo</i>	<i>MCF7 control</i>	<i>MCF7 podo</i>
Engraftment (%)	100	100	69*	92*
Exulceration (%)	50*	0*	0	0

* = $p < 0.001$, chi-square test

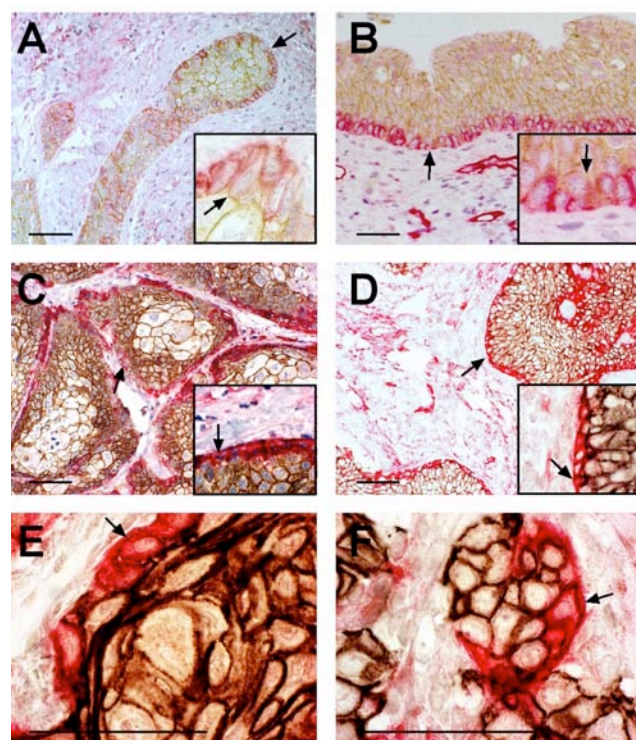
Co-expression of podoplanin and E-cadherin in the invasive front of human cancer

To investigate whether podoplanin possesses an invasion-inducing function in human cancers, histological sections of squamous cell carcinomas (from esophagus, skin, larynx, cervix and lung) and adenocarcinomas (from lobular breast cancer, prostate and colon) were stained with antibodies against podoplanin (red) and E-cadherin (brown) (Figure 3.16). A total of 189 tumor fronts were analysed. Approximately 80% of the investigated tissue samples of human squamous cell cancers of the lung, skin, esophagus, larynx and the cervix expressed podoplanin. Notably, in all these samples, podoplanin-expression was restricted to the outer cell layer of the invading tumor fronts (Figure 3.16 A-E). Similar to podoplanin-expressing β tumor cells and MCF7 cells, podoplanin and E-cadherin were co-expressed in the

invasive front of squamous cell carcinomas (Figure 3.16A-E). In contrast to squamous cell carcinomas, adenocarcinomas did not express podoplanin in their invading fronts, although E-cadherin expression was partially maintained in the tumor tissue samples analyzed. The notable exception was lobular breast cancer, which co-expressed podoplanin together with E-cadherin in areas of the invading front (Figure 3.16F). The results of the analysis of human cancer biopsies suggest an important role for podoplanin in the progression of squamous cell carcinomas and possibly of specific adenocarcinomas. Apparently, human squamous cell carcinomas reveal a phenotype of large invading tumor fronts without microinvasion, which corresponds to the phenotype of collective cell migration (Friedl & Wolf, 2003).

Together, the experimental results from human cancer biopsies, cultured MCF7 breast cancer cells and the Rip1Tag2 mouse model of carcinogenesis indicate that upregulated expression of podoplanin is causing tumor cell invasion by a pathway that is independent of EMT or the ablation of E-cadherin function. It most likely acts via specific changes in RhoA signaling, in the organization of ERM-proteins and the actin cytoskeleton and, as a result, mediates collective cell migration in cancers with cone-like invasion patterns.

Figure 3.16: Podoplanin and E-cadherin are co-expressed in the invasive front of human cancers.



Immunohistochemical staining for podoplanin (red) and E-cadherin (brown) reveals high expression of both molecules in the invading front of (A) invasive human esophageal carcinoma, (B) human skin squamous cell carcinoma, (C) human larynx carcinoma, (D) human cervix carcinoma, (E) human lung squamous cell carcinoma and (F) human lobular breast cancer. Whereas E-cadherin is expressed in all carcinoma cells, podoplanin is detectable exclusively in the outer cell layer of the invading front. Inserts: 10x higher magnification of the panel showing co-expression of E-cadherin (brown) and podoplanin (red) in cells of the invasive tumor front (arrows). Size bar = 50 μ m.

Discussion

We employed a transgenic mouse model of carcinogenesis, cultured human breast cancer cells and biopsies from cancer patients to investigate the functional contribution of podoplanin to tumor progression. Transgenic expression of podoplanin in Rip1Tag2 transgenic mice caused an acceleration of tumor progression with a higher incidence of tumor invasion and tumor malignancy, without the formation of lymph node or distant organ metastasis.

The presence of podoplanin during tumor progression in Rip1Tag2 mice had a rather unexpected impact on cell adhesion molecules in β tumor cells. Notably, expression of the epithelial adherens junction protein E-cadherin and its cytoplasmic linker molecules β -catenin and p120-catenin and the tight junction protein ZO-1 was maintained during the progression from a benign tumor (adenoma) to an invasive tumor (carcinoma) in double-transgenic Rip1Podo;Rip1Tag2 mice. In addition, we could not detect any upregulation of N-cadherin or any other mesenchymal marker in the invasive tumors of double-transgenic mice. This is surprising, since the loss of E-cadherin has been shown to be a rate-limiting step in the transition from adenoma to carcinoma in Rip1Tag2 single-transgenic mice (Perl et al., 1998). Apparently, podoplanin is able to induce tumor cell invasion without the need for a cadherin-switch or epithelial-mesenchymal transition (EMT).

Consistent with this intriguing observation, immunohistochemical analysis of squamous cell cancers of the lung, skin, esophagus, larynx and cervix of cancer patients revealed expression of podoplanin in the invading tumor front in the presence of E-cadherin. In addition, podoplanin was also expressed in human lobular breast cancer. Notably, podoplanin was found to be exclusively expressed in the outer cell layer of the invasive tumor front, whereas E-cadherin was found in both the podoplanin-expressing cancer cells as well as in the inner cells of the invasive tumor front. This particular localization of podoplanin expression raises the question whether factors secreted from stromal cells can induce podoplanin expression. Indeed, we found that EGF, FGF2 and TGF β can upregulate expression of podoplanin in MCF7 cells, raising the possibility that stroma-derived growth factors may induce the specific expression of podoplanin in the invading tumor front.

Together, the results demonstrate that overexpression of podoplanin (i) induces filopodia formation and cell polarization, (ii) enhances β_1 -integrin mediated cell spreading and adhesion on extracellular matrix, (iii) leads to increased cell invasion which is dependent on the action of MMPs and (iv) increases cell migration. These processes resemble the steps necessary for collective cell migration as recently described (Friedl et al., 2004; Friedl & Wolf, 2003). In the case of collective cell migration, epithelial markers, E-cadherin-mediated cell-cell adhesion, and β -integrin-mediated cell-matrix adhesion are maintained, while EMT does not occur. Many human cancers, including most squamous cell carcinomas and a few adenocarcinomas, exhibit such a histological phenotype of collective cell migration. Here, we have shown that E-cadherin is co-expressed with podoplanin in the invasive front of most human squamous cell carcinomas. Such organisation of an

invading sheet of cells is not only present in the mouse model and the human cancer biopsies, but is also observed in podoplanin-expressing MCF7 cells: while the cells seem to adhere by their rear ends via E-cadherin-mediated adhesion to their next neighbor, they display filopodia on their invading fronts. This observation is also consistent with the fact that podoplanin-expressing MCF7 cells migrate as a front and not as single cells in scratch wounding assays (Figure 3.12). Thereby, the cells exhibit polarized migration, as determined by the re-orientation of the Golgi apparatus (data not shown). Taken together, these results strongly suggest that podoplanin mediates a novel molecular pathway of collective cell migration. This mechanism stands in contrast to the invasion of single disseminating tumor cells, a process that in most cases involves a cadherin switch and EMT. While the latter process certainly promotes metastasis formation, the contribution of podoplanin-mediated collective cell migration to the metastatic process remains to be determined.

A first analysis on the signaling events that may underlie podoplanin-induced tumor invasion reveals that the activity of the small GTPase RhoA is reduced in podoplanin-expressing cells, which also lack stress fibers. Conversely, stress fibers of podoplanin-transfected cells could be reconstituted by the expression of a constitutive-active form of RhoA, suggesting that podoplanin is acting upstream of RhoA. Unexpectedly, the activity of Cdc42, which is known to play an important role in filopodia formation, is not upregulated by podoplanin. Moreover, the expression of a dominant-negative form of Cdc42 does not significantly repress podoplanin-induced filopodia formation, suggesting a pathway that induces filopodia independently of Cdc42-activity. Podoplanin-mediated downregulation of Rho activity is sufficient to induce filopodia formation and increased cell migration: inhibition of Rho activity by the expression of a dominant-negative form of RhoA or by an inhibitor of the RhoA effector kinase Rock promotes filopodia formation. Rac activity is also downregulated in podoplanin-transfected cells, but seems to be without functional relevance for the cellular parameters analyzed in MCF7 cells.

Podoplanin is highly glycosylated on its extracellular domain, and the intracellular terminus consists of only nine amino acids. Moreover, there is no apparent homology to any other protein domains and, hence, podoplanin may act by novel molecular pathways involving thus far unknown binding partners, including soluble ligands or cell surface molecules interacting with podoplanin's carbohydrate moiety or signaling effector molecules at the inside of the cell. However, immunoprecipitation experiments did not reveal any direct binding partner of podoplanin. The significant co-localization of ezrin and podoplanin in filopodia-like structures together with increased phosphorylation of ezrin in podoplanin-expressing cells suggest that ERM proteins may play a major role in podoplanin's modulation of the actin cytoskeleton. The Rho family of small GTPases exerts multiple effects on the phosphorylation of ERM-proteins: RhoA and Cdc42 are thought to promote, Rac to inhibit ERM protein phosphorylation (Ivetic & Ridley, 2004; Matsui et al., 1998). However, in our experiments the activities of all three Rho GTPases are found to be

downregulated, whereas ezrin is highly phosphorylated. Hence, whether the increased phosphorylation of ezrin and other ERM proteins is due to an overall repression of Rho GTPase activities or involves a hitherto unknown pathway, mediated by podoplanin, remains to be elucidated.

3.2. Tumor invasion in the presence of EMT: The role of E-cadherin in early carcinogenesis, microinvasion and metastasis

Generation of E-cadherin knock-out mice

The E-cadherin conditional knock-out mice were a gift from Jos Jonkers (The Netherlands Cancer Institute, Amsterdam; cf. Derksen et al., 2006). We crossed a Cre-deleter mouse strain with a heterozygous E-cadherin conditional knock-out mouse (floxEcad/wt) in order to generate a mouse with a heterozygous deletion of E-cadherin (Δ Ecad/wt). We then back-crossed the Δ Ecad/wt mouse with floxEcad/wt mice and mice expressing Cre recombinase under the control of the rat insulin promoter (RipCre) in order to produce double-heterozygous (floxEcad/ Δ Ecad), RipCre expressing progeny (β -EcadKO mice). β -EcadKO mice were finally crossed with Rip1Tag2 mice, thus generating the tumor- and knock-out-bearing β -EcadKO;Rip1Tag2 mouse line.

Analysis of E-cadherin knock-out mice

The knock-out of E-cadherin in β -cells was verified by western blot and immunofluorescence (Figure 3.17). The western blot was performed on pancreatic islets isolated from β -EcadKO mice and showed a slightly reduced expression of E-cadherin in an islet protein extract. Immunofluorescence analysis revealed that about 50% of the β -cells had lost E-cadherin expression completely. E-cadherin expression was maintained in α -cells and in vascular islet cells. Immunostaining for insulin and glucagon showed a normal organization with α -cells forming the periphery and β -cells the centre of the islets (Figure 3.17 **A**). This is surprising, since the introduction of a dominant-negative E-cadherin in β -cells leads to a sorting phenotype with a mixture of α - and β -cells throughout the islet (Perl et al., 1998). β -cells which had lost E-cadherin expression were never found in the rim of the islet, indicating that the complete loss of E-cadherin does not hinder a correct cell sorting in pancreatic islets. The sorting phenotype observed in β -islets overexpressing a dominant-negative E-cadherin might thus rather be due to a gain of function of the overexpressed E-cadherin c-terminal fragment (Ecad-CTF) than to a loss of function.

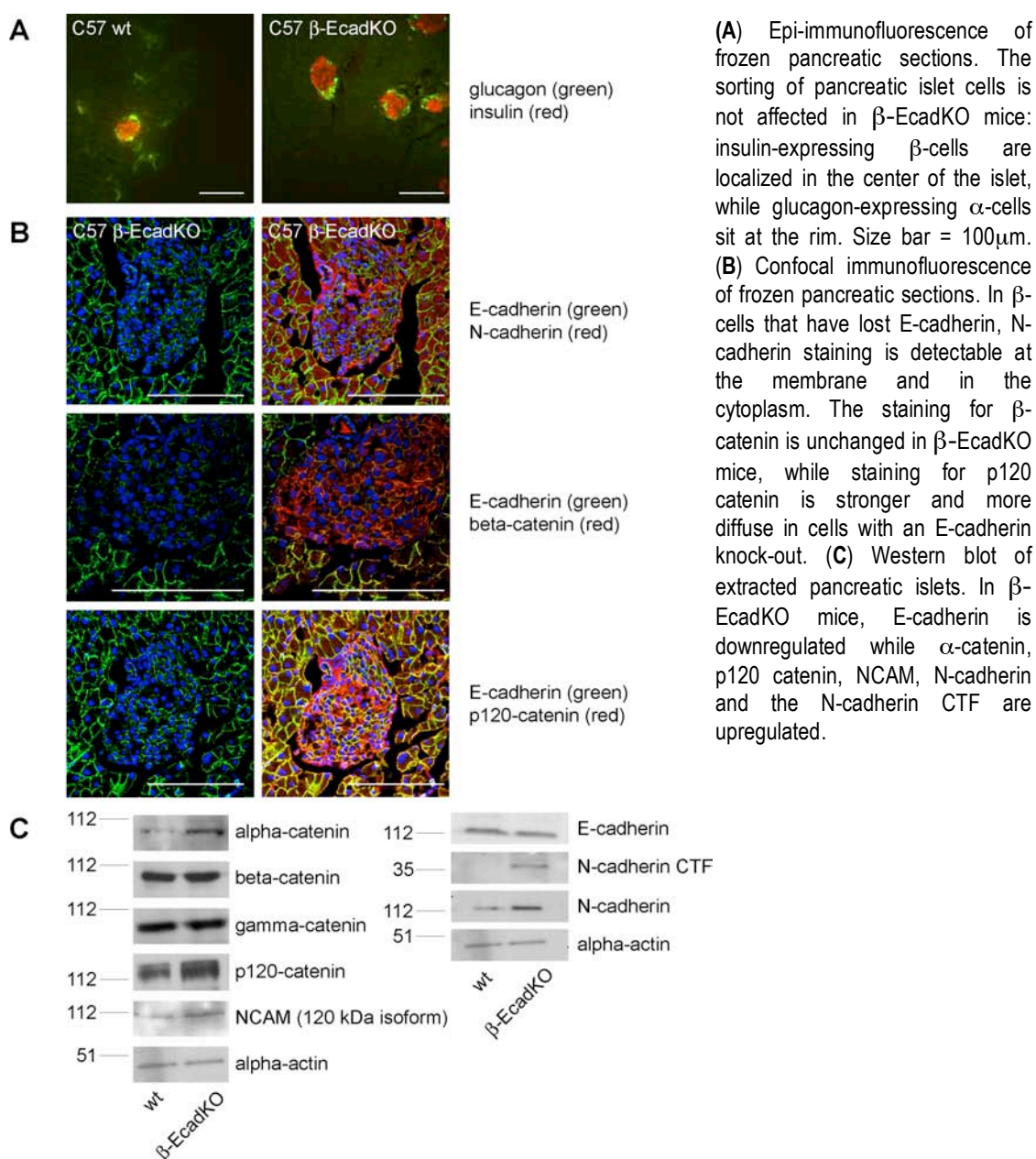
Knock-out of E-cadherin in β -cells did not lead to the formation of tumors within an observation period of 20 months. Knock-out mice were healthy and showed no growth impairment or organ abnormalities. Thus, the loss of E-cadherin in β -cells can fully be compensated for, probably by other adhesion molecules, including N-cadherin and NCAM.

Alterations of the adhesive apparatus depending on the loss of E-cadherin

We analysed the impact of E-cadherin knock-out on the adhesive apparatus of β -cells *in vivo*. To this end, we performed immunofluorescence of mouse pancreata and western blots of islet protein preparations for α -, β -, and γ -catenin, p120-catenin, NCAM, E-cadherin, and N-cadherin. Loss of E-cadherin led to a marked upregulation of N-cadherin, both at the cellular membrane and in the cytosol (Figure 3.17 **B**). This

could be confirmed by western blot of pancreatic islets of β -EcadKO mice (Figure 3.17 C). In particular, we noted a strong upregulation of the N-cadherin C-terminal fragment (Ncad CTF), which corresponds to the cytosolic staining observed for N-cadherin. The upregulation of N-cadherin was accompanied by a discrete increase of the 120 kDa isoform of NCAM (Figure 3.17 C).

Figure 3.17: Knock-out of E-cadherin has a profound impact on the adhesive apparatus of β -cells.



Concerning the catenins, there was a significant change in the expression of p120 catenin: p120 catenin levels were increased, and the immunofluorescence shows that in β -EcadKO cells p120 catenin is not only present at the cell membrane, as in cells that express E-cadherin, but also in the cytosol (Figure 3.17 B and C). In contrast, both the protein level and the distribution of β -catenin were unaltered in

Ecad KO β -cells. γ -catenin levels were also unchanged, while α -catenin protein levels were upregulated upon loss of E-cadherin (Figure 3.17 C). These findings show that the knock-out of E-cadherin in the absence of a tumor setting has a profound and specific impact on both the cytosolic apparatus that links E-cadherin to α -actin and the expression of other adhesion proteins.

Loss of E-cadherin increases the incidence of carcinomas and microinvasive islets

To investigate the impact of the E-cadherin knock-out on tumor progression, we crossed the β -EcadKO mouse with the Rip1Tag2 mouse. These mice express the large T antigen under the control of the rat insulin promoter and reproducibly develop carcinomas of the β -cells of the Langerhans islets (Hanahan, 1985). The β -EcadKO;Rip1Tag2 mice were sacrificed and analysed at 11 weeks. They had a significantly increased tumor volume (Figure 3.18 A, $p = 0.005$, Mann-Whitney test). This increase in volume was the result of a higher incidence of macroscopic tumors ($p = 0.024$, two-sided t-test; Figure 3.18 B). We analysed the tumor stages according to the international classification of rodent tumors (Mohr, 2001). Carcinoma grade 1 was defined as less than 20% invasive tumor front, grade 2 as more than 20% invasive tumor front, and grade 3 as high-grade invasion and nuclear atypia (Figure 3.18 C). β -EcadKO mice showed a shift towards more carcinomas and a higher carcinoma grade as compared to single-transgenic Rip1Tag2 mice ($p < 0.0001$, chi-square test). In a sub-analysis we quantified the presence of invasion in islets (Figure 3.18 D and 3.19 C). To qualify as an islet, the β -cell cluster had to be smaller than 100 μ m in diameter and exhibit a normal round or oval shape. Invasion was virtually absent in Rip1Tag2 islets, whereas about 50% of the islets in the β -EcadKO;Rip1Tag2 mice were invasive ($p < 0.0001$, chi-square test). We termed this phenotype microinvasion, in contrast to the invasion seen in large tumors. Microinvasion was usually not accompanied by visible tissue destruction.

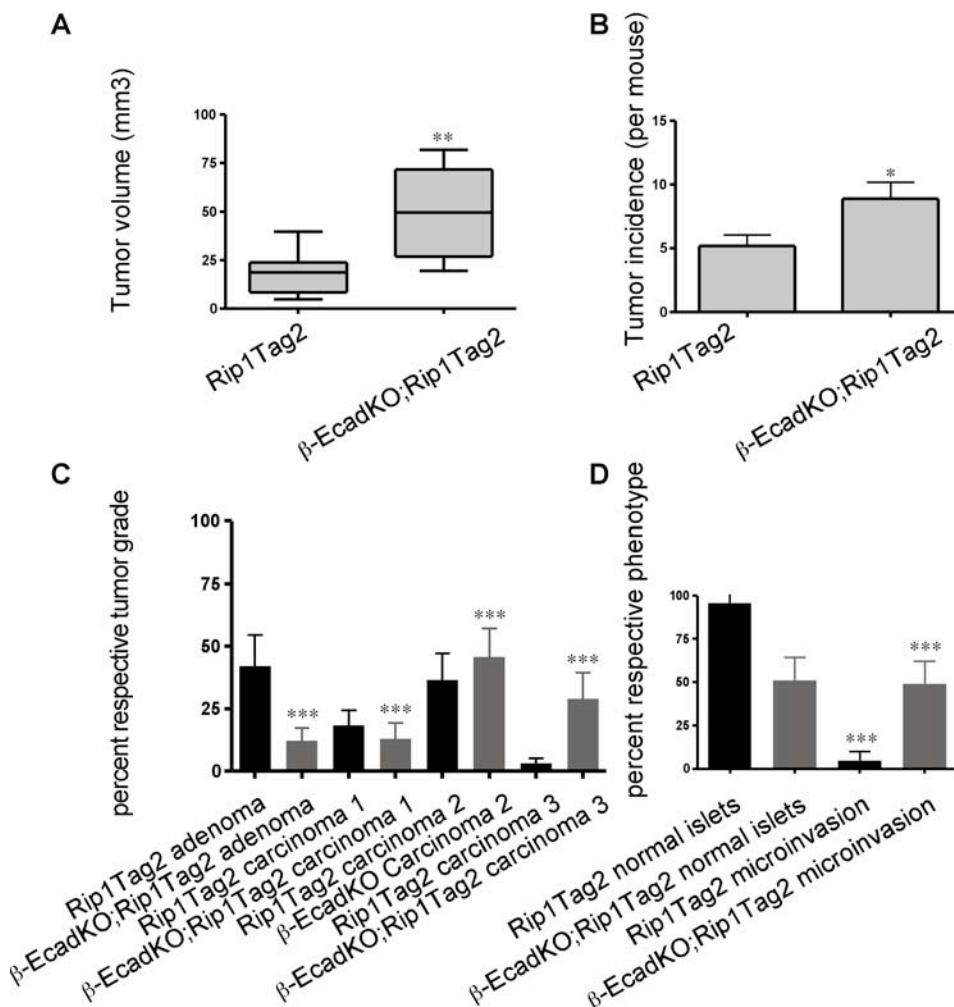
Microinvasion and micrometastasis

Staining for tumor cell apoptosis (TUNEL) and tumor cell proliferation (BrdU) failed to show a significant difference between Rip1Tag2 single transgenic and β -EcadKO;Rip1Tag2 mice (Figure 3.19 A and B). Surprisingly, microinvasive islets (Figure 3.19 C) had the same apoptosis rate as other normal sized islets and only a moderately increased proliferation rate ($p > 0.05$ for apoptosis, $p < 0.05$ for proliferation; Newman-Keuls post-test). Thus, the proliferation and apoptosis pattern of microinvasive islets differed significantly from that of larger invasive tumors. Loss of E-cadherin therefore enhances cell invasion without influencing apoptosis rates and only moderately increasing the proliferation rate *in vivo*.

These results demonstrate that the loss of E-cadherin per se is enough to induce tumor cell invasion. This phenomenon is particularly conspicuous in small, normal-sized islets (<100 μm in diameter), where microinvasion occurs. The invasion phenotype is characterized by single cell invasion and invasion of cells in Indian files. However, microinvasive tumors do not show obvious tissue destruction (as usually seen in carcinomas), and the proliferation and apoptosis pattern is still similar to that of hypertrophic islets and very distinct from that of larger carcinomas.

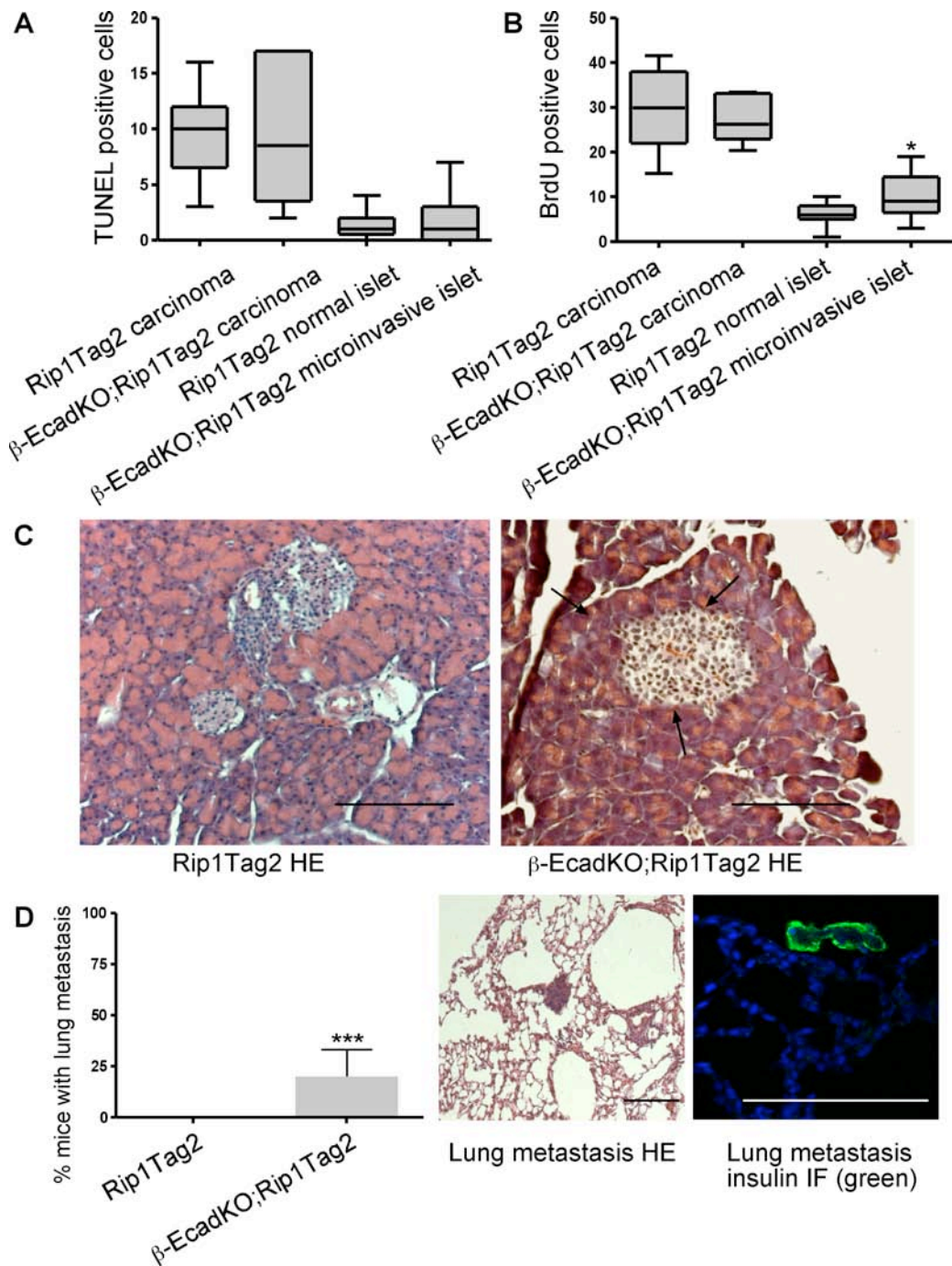
A thorough analysis of lungs and liver for metastasis revealed the presence of lung micrometastasis in 2 out of 10 β -EcadKO;Rip1Tag2 animals, whereas no lung metastases were observed in Rip1Tag2 control mice (Figure 3.19 D, $p < 0.0001$, chi-square test). In both groups, the liver was free of metastases. These findings underline the notion that the loss of E-cadherin contributes to metastasis formation.

Figure 3.18: Knock-out of E-cadherin promotes microinvasion



(A) The tumor volume is increased in β -EcadKO mice. Values = median \pm range. (B) There are more macroscopic tumors in β -EcadKO mice. Values = mean \pm SD. (C and D) In β -EcadKO mice, the ratio of adenoma:carcinoma is shifted in favor of carcinomas. This is owed to the increased incidence of microinvasive islets (see main text). Values = mean \pm SD.

Figure 3.19: Knock-out of E-cadherin induces metastasis

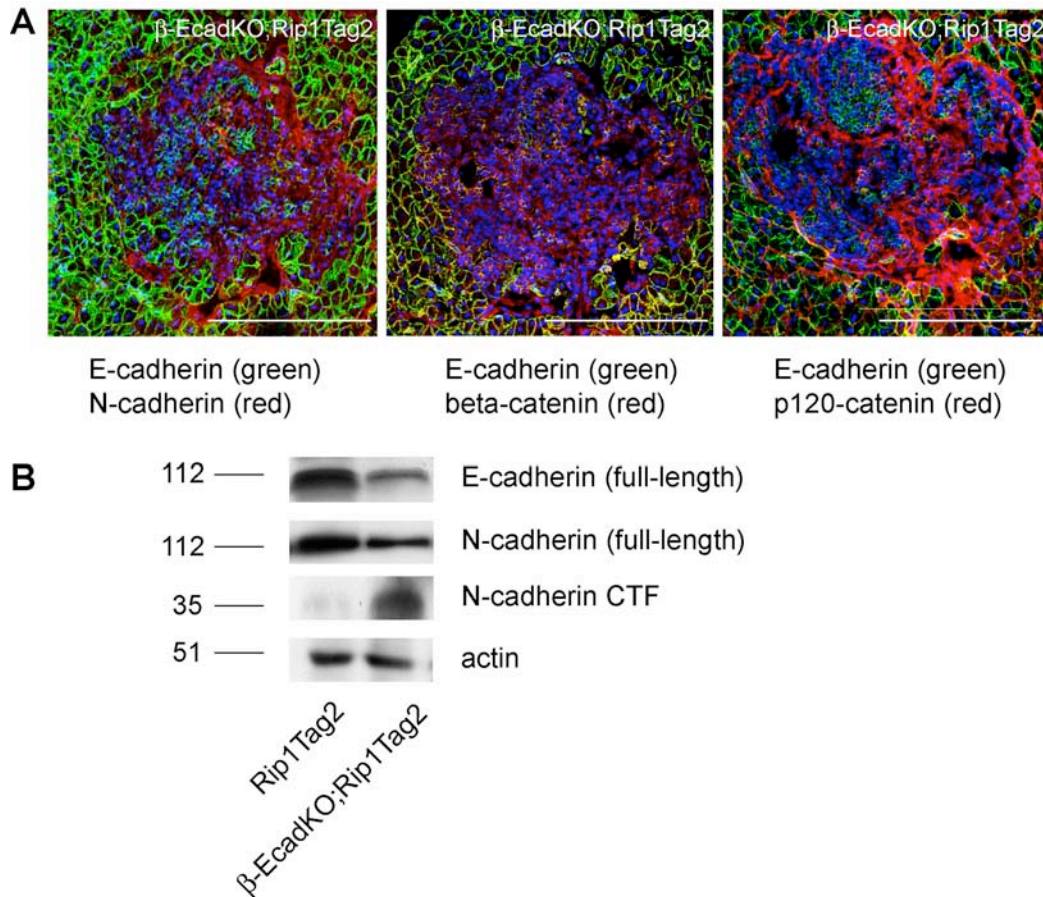


(A) Quantification of apoptosis by tunel staining. Large invasive carcinomas show more apoptosis than small invasive islets. There is no significant difference between microinvasive and non-invasive islets. Values = mean \pm SD. (B) Quantification of proliferation by BrdU staining. Microinvasive islets have a higher proliferation rate than non-invasive islets, but proliferate much less than larger carcinomas. Values = mean \pm SD. (C) H&E staining of non-invasive (left) and microinvasive (right) islets. (D) Left panel: Quantification of lung metastasis. Values = mean \pm SD. Right panel: H&E and immunofluorescence staining of a micrometastasis in the lung of an β -EcadKO;Rip1Tag2 mouse.

The adhesive apparatus in *EcadKO;Rip1Tag2* mouse tumors

We then analysed the adhesive apparatus of β -EcadKO;Rip1Tag2 mouse tumors by immunofluorescence of pancreas sections and Western blot of whole tumor protein extracts (Figure 3.20). The invasive front of the tumors was characterized by a strong expression of N-cadherin and p120-catenin, while the expression of β -catenin was unchanged (Figure 3.20 **A**). In the tumor center, E-cadherin expressing cells persisted, usually forming tumor nests.

Figure 3.20: The adhesive apparatus of β -EcadKO;Rip1Tag2 mouse tumors



(**A**) Immunofluorescence staining for E-cadherin (green), and N-cadherin, β -catenin or p120-catenin (red; as indicated). The outer tumor edge shows a strong staining for N-cadherin and p120-catenin, while cells positive for E-cadherin sit in the center of the tumor. Size bar = 100 μ m. (**B**) Western blot of whole protein extracts of Rip1Tag2 and β -EcadKO;Rip1Tag2 mice. Full-length E- and N-cadherin are downregulated in β -EcadKO;Rip1Tag2 mouse tumors, while the N-cadherin CTF is upregulated.

By Western blot analysis we could confirm the downregulation of E-cadherin in the β -EcadKO tumors (Figure 3.20 **B**). Interestingly, the total level of full-length N-cadherin was reduced in β -EcadKO tumors, while the expression of the N-cadherin CTF was markedly increased (Figure 3.20 **B**). Since we used a C-terminal antibody to detect N-cadherin, this probably reflects the cleavage of full-length N-cadherin. Taken together, the invasive margin is characterized by a strong expression of N-

cadherin at the cell membrane, N-cadherin CTF in the cytosol and p120-catenin both at the membrane and in the cytosol.

Discussion

We have generated a mouse line with a conditional knock-out of E-cadherin in the Langerhans islets of the pancreas. Knock-out of E-cadherin resulted in an upregulation of N-cadherin, N-cadherin CTF and p120-catenin, while β -catenin levels were unaltered. The knock-out of E-cadherin did not induce tumor formation within a surveillance interval of two years, and both the morphology of the Langerhans islets and the sorting of the islet cells was without pathological findings. By crossing the β -EcadKO mice with Rip1Tag2 transgenic mice we induced formation of β -cell tumors in E-cadherin deficient mice. The loss of E-cadherin early in carcinogenesis induced a distinct tumor stage, which was characterized by invasion of single tumor cells, but not the full phenotype of a large, destructive carcinoma. Following the nomenclature of human tumors, we called this intermediate state a microinvasive carcinoma. Interestingly, in the TNM system used to stage human tumors, the tumor size (T) is an important prognostic parameter. Our β -EcadKO tumor model provides a possible explanation for the success of this classification, since we could show that the loss of E-cadherin can induce single cell invasion without necessarily influencing other factors of tumor progression, such as cell proliferation and apoptosis. Indeed, the size of the tumor was a better predictor for a carcinoma-like proliferation and apoptosis pattern than the presence of tumor invasion. On the other hand, early loss of E-cadherin during carcinogenesis opens a window of opportunity for metastasis, as reflected by the increase in pulmonary metastasis found in β -EcadKO;Rip1Tag2 mice.

The mechanisms that underlie tumor progression in the absence of E-cadherin are only poorly understood. In our study, we identified two new candidates, p120-catenin and the N-cadherin CTF, which may play a role in loss-of-E-cad-dependent tumor progression. p120-catenin interacts with Kaiso, a zinc finger protein involved in transcriptional repression (Daniel & Reynolds, 1999). As we have seen, loss of E-cadherin increases the cytoplasmic pool of p120-catenin and thus might influence its function as a transcriptional regulator. The N-cadherin CTF was shown to interact with the transcription factor CBP and to promote its proteasomal degradation, thereby inhibiting CRE-dependent transactivation (Marambaud et al., 2003). Further studies in both *in vitro* and *in vivo* systems are needed to define the possible function of these two candidates.

4. Conclusions (part I): Mechanisms of Tumor Invasion

Invasion of cells into the surrounding tissue and destruction of normal tissue architecture are two hallmarks of malignant tumors. Morphologically, two patterns of tumor invasion can be distinguished: single cell and collective cell invasion. Investigations aimed at unraveling the molecular mechanisms underlying tumor cell invasion have identified various pathways that determine the invasive potential and the invasion pattern of tumor cells (Friedl & Wolf, 2003).

The invasion of cells is often correlated with dramatic changes in the expression and function of adhesive (e.g. cadherins, immunoglobulin-domain-containing cell adhesion molecules) and regulatory proteins (e.g. Snail family members, transforming growth factor β). These changes are reminiscent of early developmental processes, in particular during neurulation and gastrulation, when cells acquire a migratory, mesenchymal phenotype. During this so-called epithelial-mesenchymal transition (EMT) cells lose epithelial markers, such as E-cadherin, and gain the expression of mesenchymal markers, such as N-cadherin and vimentin. The exact role of EMT in tumor progression is still under debate. EMT is seen in most animal models of cancer progression, but studies in human tumor biopsies did only produce scarce evidence for the occurrence of EMT in human tumors (Lee et al., 2006 and Thiery, 2002). In many human cancers, invasion is characterized by large tumor cell sheets pushing into the surrounding tissue. These cell sheets maintain the expression of epithelial adhesion structures but can nonetheless invade and thereby destroy the host organ.

In fact, the distinction between these different forms of invasion has a long-standing tradition. In colorectal cancer, pathologists distinguish between a pushing and an infiltrating invasive margin, and they showed that the morphology of the invasive margin is an independent predictor of prognosis (Cianchi et al., 1997). On a biological level, pushing invasion corresponds to collective cell migration, while infiltrating invasion relates to single cell invasion. Moreover, the morphology of the invasive tumor margin is important for therapeutic considerations, since a pushing border relates to an intact adhesive apparatus and thus a higher cell density in the tumor. The cell density and the presence of intact adhesive complexes critically regulate the penetration of drugs in solid tumors (Minchinton & Tannock, 2006).

However, the invasive tumor front should not only be classified morphologically, but also on a molecular level. There is growing evidence that the expression pattern of cells in the invading front of solid tumors is different from that of cells in the tumor interior. For example, nuclear localization of β -catenin and up-regulation of β_1 -integrin and the L1 cell adhesion molecule were specifically observed in cells of the invasive margin (Gavert et al., 2005; Hegerfeldt et al., 2002 and Brabletz et al., 2001).

To investigate different mechanisms of tumor invasion, we have generated and/or studied three mouse models of pancreatic β -cell carcinogenesis: the β -EcadKO;Rip1Tag2 mouse, the Rip1Tag2 mouse and the Rip1Podo;Rip1Tag2 mouse.

The β -cell tumors of the β -EcadKO;Rip1Tag2 mouse undergo an early, though incomplete, EMT. We showed that the early loss of E-cadherin and the subsequent changes in the adhesive apparatus (upregulation of full-length N-cadherin, NCAM and p120 catenin; shift to a cytoplasmic expression of p120 catenin and the N-cadherin CTF) lead to a distinct tumor stage: the microinvasive carcinoma. This tumor is characterized by its small size (<100 μ m), the invasion of single cells in the surrounding exocrine pancreas, an intermediate tumor proliferation rate that is between the values found in non-invasive islets and in large invasive tumors, and an apoptosis rate which is still identical to that of morphologically normal islets and much smaller than in large carcinomas. However, the knock-out of E-cadherin also results in the formation of lung metastasis, a phenotype not normally found in Rip1Tag2 mice. The formation of lung metastasis underlines the concept that single cell invasion and early EMT contribute to a metastatic phenotype of tumors. Our findings are in line with a recent report from Derksen and co-workers. In a mouse model of mammary carcinoma they found that the knock-out of E-cadherin shifts the invasion pattern of the tumor from an expansive to an infiltrating phenotype and increases the incidence of metastasis (Derksen et al., 2006).

The tumors of the Rip1Tag2 mice grow to be adenomas without losing the expression of E-cadherin. An EMT (loss of E-cadherin, upregulation of N-cadherin) occurs late in tumor progression and is necessary for the formation of carcinomas. No distant metastases could be observed in these mice.

In RipPodo;Rip1Tag2 mice carcinomas can develop without the loss of E-cadherin and thus collective cell invasion is predominant. EMT was not necessary for tumor progression in these mice. Lymph node or distant metastasis was not observed.

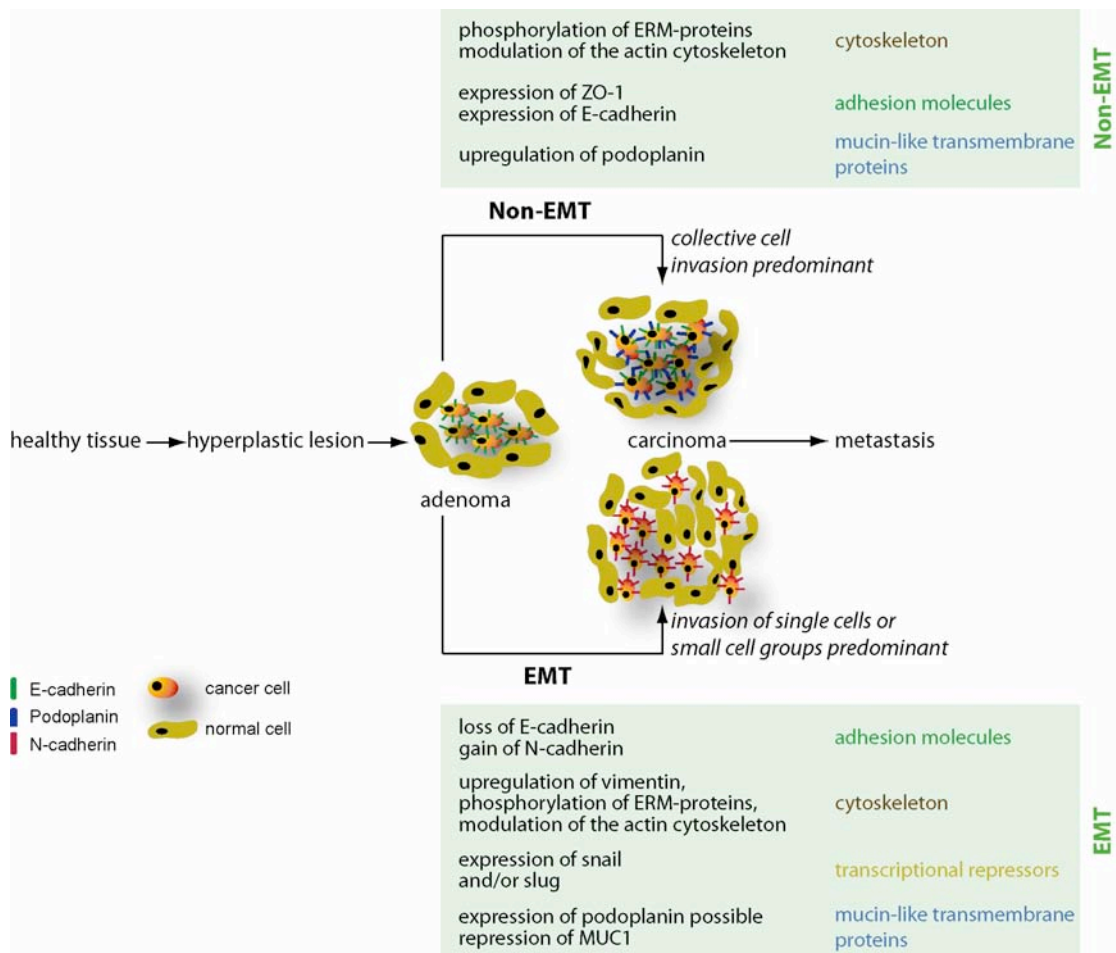
Table 4.1: Progression of β -cell carcinomas in β -EcadKO;Rip1Tag2, Rip1Tag2 and Rip1Podo;Rip1Tag2 mice.

Mouse line	Carcinoma formation	Invasion pattern	(partial) EMT	Distant metastasis
β -EcadKO;Rip1Tag2	+++	single cell or mixed	+ (early)	+
Rip1Tag2	+	mixed	+ (late)	-
Rip1Podo;Rip1Tag2	++	collective	- (absent)	-

Taken together, we could show that tumor invasion can occur by both EMT-mediated and EMT-independent mechanisms. *In vitro* experiments with cell lines derived from the three tumor models (β -EcadKO/Rip1Tag2 β -cells, Rip1Tag2 β -cells and Rip1Podo/Rip1Tag2 β -cells) as well as human tumor cell lines (MCF7 podo,

MCF7 pSREcad, A549 podo) were used to study the mechanisms underlying tumor invasion. Interestingly, there is a considerable overlap in the molecular profile found in both invasion types. For example, EMT- and non-EMT mediated mechanisms of tumor invasion modulate the expression of mucin-like transmembrane proteins and the morphology of the actin cytoskeleton. The alterations of the cytoskeleton are critically influenced by ERM-proteins, which were also shown to play a role in both the context of EMT and non-EMT. EMT, as defined by the downregulation of E-cadherin and the up-regulation of Snail 1, can downregulate ezrin in an immortalized hepatic cell line, but increases ezrin phosphorylation levels in MDCK cells (Lan et al., 2006; Martin-Villar et al., 2006 and Wicki et al., 2006). Podoplanin itself can promote tumor invasion in both the setting of single and collective cell migration (Wicki & Christofori, 2007). Figure 4.1 outlines our current understanding of these distinct invasion phenotypes.

Figure 4.1: Mechanisms of tumor invasion.



Tumor invasion can occur by either EMT- or non-EMT-mediated mechanisms. Each invasion pathway is characterized by a particular expression profile. However, many effectors of tumor invasion have an overlapping function in both forms of tumor invasion.

These examples illustrate the concept that the effect of pro-migratory and pro-metastatic mediators heavily depends on the cell of origin (Gupta & Massague, 2006). However, they also show that in a given cellular context and therefore in a particular human cancer these mediators reproducibly induce a particular pattern of invasion. Friedl and co-workers have shown in a melanoma explant model of human cancer that cells can switch from one invasion pattern to another, depending on the tumor environment and in particular also on the selective pressure exerted by anti-tumoral drugs (Hegerfeldt et al., 2002). Nevertheless, in the Rip1Tag2 mouse model of β -carcinogenesis carcinomas do not spontaneously arise in the presence of E-cadherin and upon forced expression of E-cadherin the tumors cannot activate an alternative pathway of tumor progression but arrest at the stage of an adenoma (Perl et al., 1998). Only the transgenic introduction of podoplanin, as discussed in chapter 3.1, releases the blockage of tumor progression and allows tumors to proceed to a carcinoma stage in the presence of E-cadherin (Wicki et al., 2006). From this experimental evidence we may draw the following conclusion: (i) Invasive tumors (carcinomas, but probably also sarcomas, although the available evidence for sarcomas is less sound than for carcinomas) can invade into the surrounding tissue by either adopting EMT-dependent or EMT-independent molecular mechanisms. (ii) If they use an EMT-based strategy, a single-cell invasion pattern is more likely to occur. (iii) The opposite is true for non-EMT mediated invasion, where the persistence of adhesive junctions favors the migration of large interconnected cell sheets. (iv) Under the pressure of the microenvironment, tumor invasion can switch from one mechanism to another, thus eluding attempts to treat tumors with a single therapeutic agent. (v) There are intrinsic barriers that inhibit the switch from one tumor pattern to another *in vivo*. These barriers can be overcome by transgenic manipulation of tumors.

However, despite recent advances in understanding the molecular basis of tumor invasion and other forms of tumor progression, many a question remains open. The nature of factors that determine for example the result of podoplanin expression or ezrin phosphorylation on the invasion pattern, and which are defined by the cell of origin, is unknown. Furthermore, the molecular pathways responsible for the inhibition or the promotion of the switch between EMT- and non-EMT invasion remain unclear and thus warrant further study.

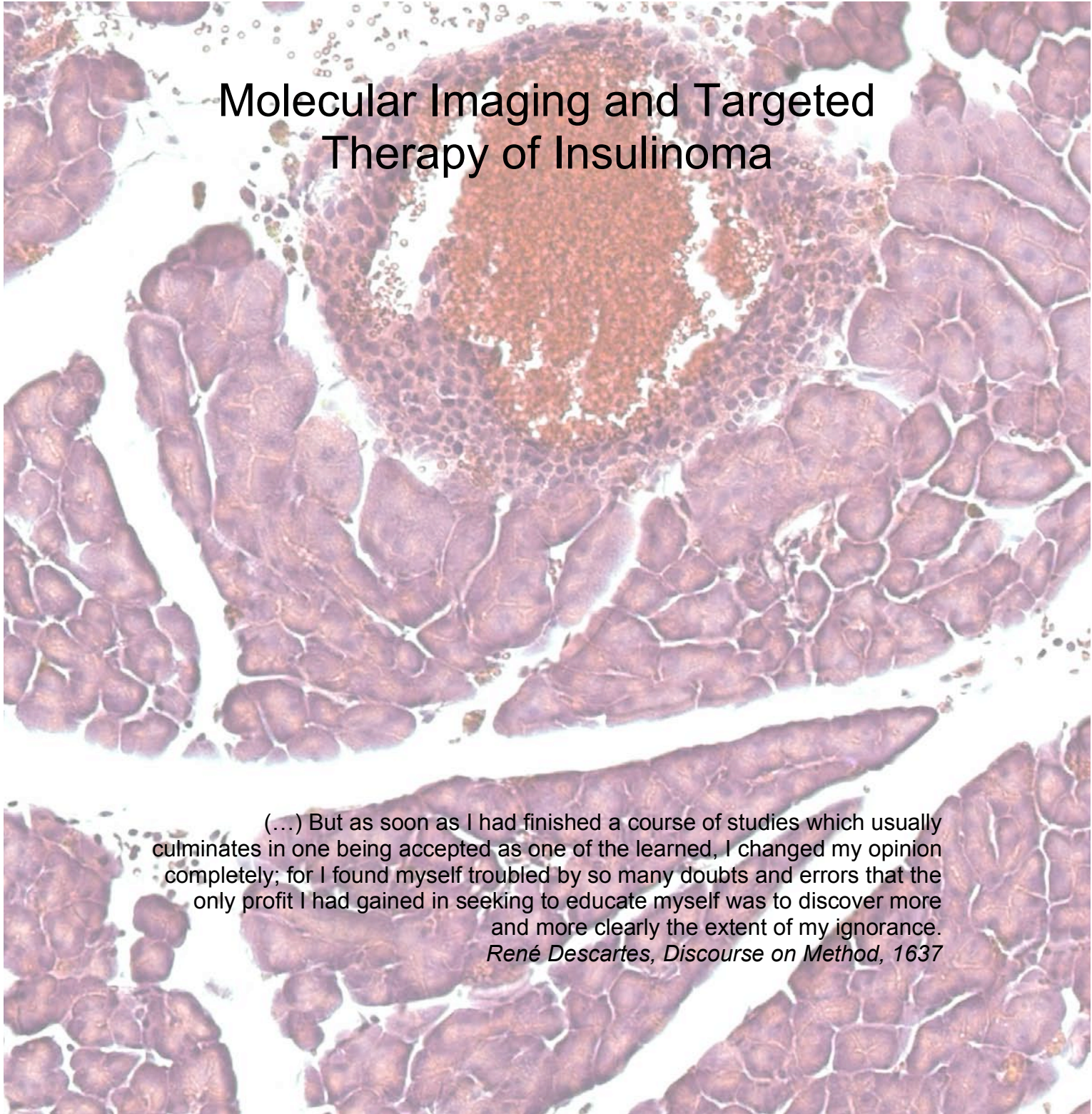
Outlook

The identification of different expression patterns in a population of tumor cells raises a number of important issues. In several cancers, the capacity to initiate and maintain tumor growth may be restricted to a sub-population of malignant cells called cancer stem cells (Reya et al., 2001). Although the term stem cell in the context of cancer is somewhat misleading, since normal stem cells are able to divide and produce cells that differentiate in a correct and timely fashion, while cancer stem cells decidedly lack that ability, it is clear that indeed there are slowly replicating tumor cells with a higher tumorigenic potential than other tumor cells. Looking back

at the expression of podoplanin, as described in chapter 3.1, figure 3.16, one might wonder whether the upregulation of podoplanin is due to a clonal expansion of cells of the basal layer, and if this is the case, whether the putative cancer stem cells of a squamous carcinoma might be found in the podoplanin-expressing cell layer. The cancer stem cell populations identified so far are notoriously difficult to kill, and their presence appears to be one of the reasons for the lacking efficiency of anti-cancer drugs (Al-Hajj et al., 2004). In most cancers, however, the stem cell compartment has not been identified yet, and further research is necessary in order to develop therapeutic strategies against this specific class of cancer cells. A recent study by Calabrese and co-workers showed that neuronal cancer stem cells in a brain tumor model can selectively be targeted by agents directed against ErbB2 and/or VEGF signaling (Calabrese et al., 2007). This is a prove of principle experiment for a future targeted therapy against cancer stem cells.

PART II:

Molecular Imaging and Targeted Therapy of Insulinoma



(...) But as soon as I had finished a course of studies which usually culminates in one being accepted as one of the learned, I changed my opinion completely; for I found myself troubled by so many doubts and errors that the only profit I had gained in seeking to educate myself was to discover more and more clearly the extent of my ignorance.
René Descartes, Discourse on Method, 1637

5. Introduction (part II)

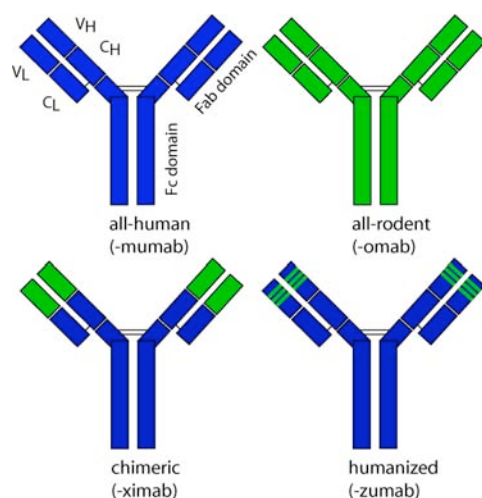
5.1 Targets in anti-cancer therapy

Cancer therapy is a major challenge for modern medicine. From 1960 through 2000, the life expectancy for newborns increased by about 7 years (Cutler et al., 2006). It is estimated that roughly one half of this increase is owed to medical progress. Of this half, 70% are attributable to a reduction in cardiovascular mortality, and 20% to a reduction in newborn and infant death. Only 3% result from a reduced rate of cancer death (Cutler et al., 2006). Thus, most obviously there is ample space for improvement of cancer therapy.

Most anti-cancer drugs currently in clinical use do not target a specific cell type or a specific signalling pathway, but rather act unselectively on proliferating cells. Although some of these drugs were used successfully even in advanced cancer stages (e.g., CHOP = cyclophosphamid+hydroxydaunorubicin+oncovin+prednisolon in lymphoma or cis-platin in seminoma), these drugs decidedly lack specificity, and in many cancers they are not able to eradicate the tumor. In the last years, many research facilities and pharmaceutical companies focused on the development of new compounds directed against cancer cell specific surface targets or specific signalling pathways active in cancer. In the clinic, the most successful of these new drugs are mabthera®, herceptin® and gleevec®.

Mabthera® and herceptin® are monoclonal antibodies (Figure 5.1), the first directed against the CD20 antigen expressed on B-lymphocytes, the second against ErbB2 expressed on mammary cancer cells. Mabthera® significantly improved the response of B-cell lymphomas to chemotherapy (Coiffier et al., 2002). Adjuvant treatment of ErbB2 positive, resectable breast cancer with herceptin increased the disease-free survival after 5 years from 67% to 87% (Romond et al., 2005). These examples show that the concept of targeted therapy harbours the promise of a major break-through in oncology.

Figure 5.1: Monoclonal antibodies



Monoclonal antibodies are used in targeted anti-cancer therapy. To reduce the incidence of immune reactions against antibodies of other species, immunoglobulines (Igs) were engineered in order to make them more similar to human antibodies. The generic name of antibodies used as drugs reveals the origin of the Ig: -mumab are human, -omab rodent, -ximab chimeric and -zumab humanized antibodies.

During the last years, other cell surface markers that are expressed preferentially by cancer cells were detected (Reubi, 2003). As mentioned above, monoclonal antibodies were the first compounds employed to target hormone or cytokine receptor-expressing cancer cells. There are two modes of action of the antibodies: first, they may directly block the function of their target. Second, they can induce complement-dependent cytotoxicity or antibody-dependent cellular cytotoxicity (Imai & Takaoka, 2006). To enhance the efficient clearance of peptide hormone receptor-expressing cancer cells, antibodies were also linked to radionuclides (Figure 5.2), thus combining the benefits of antibody-induced immunoresponses with the cytotoxic effects of radiation. Table 5.1 gives an overview of the FDA-approved antibodies against cancer as at 2006.

Table 5.1: targeted agents (antibodies) against cancer, FDA-approved as at 2006 (after Imai & Takaoka, 2006, modified)

<i>Agent (antibody)</i>	<i>Target</i>	<i>Approved for</i>
Cetuximab (Erbix)	EGFR	Colorectal cancer, head and neck squamous cell carcinoma
Trastuzumab (Herceptin)	ErbB2	Breast cancer
Bevacizumab (Avastin)	VEGF	Colorectal cancer
Rituximab (Rituxan)	CD20	B-cell lymphomas
Ibritumomab tiuxetan (Zevalin)	CD20	B-cell lymphomas
Tositumomab- ¹³¹ I (Bexxar)	CD20	B-cell lymphomas
Gemtuzumab ozogamicin (Mylotarg)	CD33	Acute myelogenous leukaemia
Alemtuzumab (Campath)	CD52	B-cell chronic lymphoid leukemia

To overcome the limitations imposed by the large molecular weight of antibodies, small chemical inhibitors were designed, which inhibit specific enzymatic or signalling activities in cancer cells (reviewed by Sebolt-Leopold & English, 2006). The most famous of these is Gleevec®. It is used against chronic myeloid leukaemia, where it inhibits the enzymatic activity of the bcr-abl fusion protein resulting from the translocation t(9;22). It is the first successful tyrosine kinase inhibitor introduced into the oncological routine and hopefully a herald of more to come (Krause & Van Etten, 2005). Table 5.2 summarizes the currently available small molecule enzyme inhibitors.

Table 5.2: targeted agents (small molecule inhibitors) against cancer, FDA-approved as at 2006 (after Imai & Takaoka, 2006, modified)

<i>Agent (small molecule inhibitor)</i>	<i>Target</i>	<i>Approved for</i>
Imatinib mesylate (Gleevec)	Tyrosine kinases (Bcr-Abl, c-kit, PDGFR)	Chronic myelogenous leukaemia, gastrointestinal stromal tumors
Gefitinib (Iressa)	Tyrosine kinase (EGFR)	Non-small cell lung cancer
Erlotinib (Tarceva)	Tyrosine kinase (EGFR)	Non-small cell lung cancer, pancreatic cancer
Sunitinib (Sutent)	Tyrosine kinases (VEGFR, PDGFR, c-kit, Flt3)	Gastrointestinal stromal tumors, renal cancer
Sorafenib (Nexavar)	Kinases (B-raf, VEGFR2, EGFR, PDGFR)	Renal cancer
Bortezomib (Velcade)	28S protease	Multiple myeloma

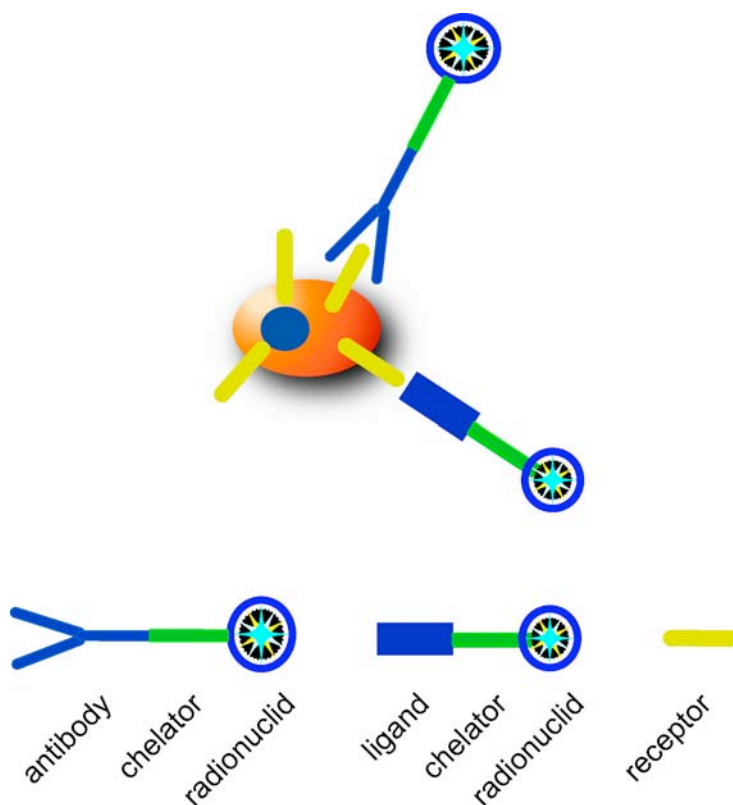
As an alternative to the inhibitors of enzymatic activity, small peptides ligands have been generated to specifically target suitable hormone or cytokine receptors on cancer cells. These ligands do not necessarily inhibit the activity of the target receptor, but they are coupled to cytotoxic compounds, thus inducing rapid cell death. The prototype of a radiolabelled small molecule ligand is the somatostatin receptor ligand octreotide, which is used for both diagnosis and therapy of a number of neuroendocrine tumors, including insulinoma (Reubi, 2003).

5.2 Radiolabelling of antibodies or small peptide ligands for imaging and therapy

The choice of the radionuclide depends on the application type and localization of the target molecule. Because of their long range, γ -emitters are preferred for diagnostic applications, while Auger-, β - or α -emitters have a higher linear energy transfer and are therefore used for therapeutic approaches. In our study, we used the radioisotope ^{111}In (Indium-111) for diagnostic and therapeutic purposes. ^{111}In is a γ - as well as an Auger- and conversion electron emitter. Auger- and conversion electrons have a tissue penetration of only 0.02-10 μm and 200-500 μm , respectively. Because of the short range of these electrons, the biological effects of Auger emitters are highly dependent on the subcellular distribution of the radionuclide (Kassis AI, 1988). Auger electrons have a high linear energy transfer (LET), which is comparable to that of α -emitters (Kereiakes & Rao, 1992). It has been shown that internalization and translocation of Auger-emitters to the cell nucleus results in cell death (Rao et al., 1989). In addition, accumulation of ^{111}In in the cytoplasm or in the cell nucleus increases the cellular absorbed dose fraction (Goddu et al., 1994). A number of chemotherapeutic compounds (e.g. bleomycin)

and antibodies (e.g. anti-EGF receptor, anti-CD74, and anti-HER2) have been labelled with ^{111}In and tested in both cellular and animal xenograft models with moderate therapeutic effects (Jaaskela-Saari et al., 2005; Reilly et al., 2000; Ochakovskaya et al., 2001 and Michel et al., 2005). A higher anti-tumor efficacy of Auger electron-emitters compared to β -emitting radio-metals or ^{131}I have also been detected when conjugated to internalizing antibodies (Behr et al., 2000). A clinical study investigating the effect of [^{111}In -DTPA]-octreotide in patients with neuroendocrine tumors has revealed a low incidence of clinical side-effects, yet only a moderate therapeutic response to the radiopeptide (Valkema et al., 2002). In all these studies, an efficient therapeutic effect of ^{111}In has been mainly hampered by a rather low uptake of the radiopeptide into the tumor cells. Hence, a significant improvement of tumor cell uptake would markedly enhance the therapeutic effect of ^{111}In -labeled compounds.

Figure 5.2: Targeted therapy in nuclear medicine



Antibodies or small peptides can be used to target specific molecular markers on cancer cells. After coupling the antibodies or peptides with a radionuclide, the compounds are used for either molecular imaging or targeted therapy.

5.3 The glucagon-like peptide-1 receptor (GLP-1R) as a drug target in human insulinoma

Glucagon-like peptide-1 receptor (GLP-1R) is highly expressed on both benign and malignant human insulinomas (Reubi & Waser, 2003). Insulinomas arise from pancreatic β cells and are the most frequent hormone-active tumors of the pancreas with an incidence of 0.4/100'000/year. 90% of insulinomas are benign and present as small, encapsulated, solitary tumors. Multiple tumors occur in 13% of the cases, and approximately 10% of insulinomas progress to malignant cancer and the formation of tumor metastases. Morbidity and mortality of benign insulinomas are also due to the induction of profound hypoglycemia by the tumor. For benign insulinoma, 10 years survival is about 88% after complete surgical removal of the tumor. In case of malignant, metastasizing insulinoma, prognosis is poor with a median survival of 2 years and a 10 years survival rate of 29% (Service et al., 1991). About 30% of the patients have a prolonged tumor-free survival due to the biology of the tumors rather than any treatment modality.

Diagnosis of insulinoma is possible by either a functional assay or by imaging techniques. Pathognomonic is the presence of hypoglycemia in the face of inappropriately elevated levels of insulin and C-peptide as well as low levels of β -hydroxybutyrate (Chammas et al., 2003). The diagnosis usually is established through a prolonged fasting up to 72 hours. In contrast to the functional diagnosis, imaging of insulinoma is rather cumbersome. The sensitivity of CT scans (44%) and MRI (57% with the contrast agent gadolinium) is not satisfying. Arteriography with selective sampling of hepatic vein insulin is more sensitive (up to 82%), but much more invasive. Endosonography is a valuable alternative to arteriography, but again the sensitivity is not over 90% (Gouya et al., 2003). Thus, new options for the imaging of insulinoma are warranted.

Therapeutic options in case of unresectable tumors are limited to palliative therapies, including transarterial tumor embolization, chemotherapy, radical surgery and radio-ablation (Hirshberg et al., 2005). Alternative therapy options include Octreotide (Sandostatin) and the radiolabelled somatostatin modification [^{90}Y]DOTA-TOC (DOTA = 1,4,7,10-tetraazacyclododecane-1,4,7,10-tetraacetic acid), which are used for somatostatin-receptor-2 (SSTR-2) targeting in insulinomas. In SSTR-2-positive endocrine pancreatic tumors, including SSTR-2-positive insulinomas, the response rate of [^{90}Y]DOTA-TOC is 38% (partial and complete remission; Waldherr et al., 2002). Unfortunately, in about 40% of insulinomas, expression of SSTR-2 is too low to allow for efficient targeting (Krenning et al., 1993). In contrast, the density of GLP-1R in insulinoma cells is considerably higher than that of other peptide hormone receptors, with an incidence of GLP-1R in 25 out of 27 insulinomas, as compared to SSTR-2 with 18 out of 26 (Reubi & Waser, 2003). Treatment of mice bearing a subcutaneously implanted rat insulinoma tumor (RINm5F) with ^{123}I -labeled GLP-1 [7-36] amide and [^{123}I]-Exendin-3 has demonstrated that the peptide is specifically internalized and that the implanted tumor cells can be detected by

scintigraphy (Gotthardt et al., 2002). However, the low peptide stability of [¹²³I]-GLP-1 and the less effective radio-iodination of Exendin-3 have limited their clinical use. Therefore, [Lys⁴⁰(Ahx-DTPA-¹¹¹In)NH₂]-Exendin-4, a novel radiopeptide with an enhanced peptide stability and more effective radiolabelling has been designed.

5.4 Aim of the study (part II)

We have employed the Rip1Tag2 transgenic mouse model of multistage insulinoma development to investigate the diagnostic and therapeutic efficacy of [Lys⁴⁰(Ahx-DTPA-¹¹¹In)NH₂]-Exendin-4. Rip1Tag2 transgenic mice express the simian virus 40 large T antigen under the control of the rat insulin promoter in β cells of islets of Langerhans (Hanahan, 1985). These mice reproducibly develop tumors in a well-defined multistage tumorigenesis pathway, whereby carcinomas begin to form at 9-10 weeks of age and represent 2-4% of all islets by 14 weeks of age (please cf. figure 1.3, chapter 1.4).

Here, we demonstrate that GLP-1R is a suitable target for the efficient molecular imaging and internal radiotherapy of insulinoma and that the Auger-electron emitting [Lys⁴⁰(Ahx-DTPA-¹¹¹In)NH₂]-Exendin-4 is a potent radiotherapeutic.

6. Materials & Methods (part II)

6.1 Reagents and instrumentation

All chemicals were obtained from commercial sources and used without further purification. $^{111}\text{InCl}_3$ was purchased from Mallinckrodt (Petten, The Netherlands). Analytical HPLC was performed on a Metrohm HPLC system LC-CaDI 22-14 and a Berthold LB 509 flow-through γ -detector with a Macherey-Nagel Nucleosil 120-3 C-18 column. Quantitative γ -counting was performed on a COBRA 5003 γ -system well counter (Packard Instrument Company, Switzerland). Analytic reversed-phase high-performance liquid chromatography (RP-HPLC) was performed on a Bischof HPLC system (Metrohm AG) with HPLC pumps 2250 and a I-1010 ultraviolet detector (Metrohm AG) using CC250/4 Nucleosil 120-3 C18 columns from Macherey-Nagel. The gradient systems consisted of mixtures of water with 0.1% trifluoroacetic acid (TFA) (solvent A) and acetonitrile (solvent B): Gradient I: 0 min 95% A (5% B), 5 min 95% A (5% B), 10 min 0% A (100% B), 15 min 0% A (100% B), 20 min 95% A (5% B); flow, 0.75 mL/min; λ 214 nm; and gradient II: 0 min 95% A (5% B), 30 min 55% A (45% B), 32 min 0% A (100% B), 34 min 0% A (100% B), 37 min 95% A (5% B); flow, 0.75 mL/min; λ 214 nm. Quantitative γ -counting was performed on a COBRA 5003 γ -system well counter from Packard Instruments. Rip1Tag2 mice were scanned in an MR scanner (Magnetom Expert; Siemens) and with an e.cam SPECT scanner (Siemens) that was modified with a multipinhole aperture. SPECT images were reconstructed using HiSPECT reconstruction program (SciVis). Afterward, MRI and SPECT images were manually fused on a HERMES workstation (HERMES Medical Solutions). In addition, hybrid SPECT/CT scans (Symbia T2; Siemens) were performed. The co-registered CT scan was performed with intravenous contrast medium (Telebrix 30 meglumine; Megluminoxitalamat, 300 mg/mL [Guerbet]). Images were displayed and analyzed on the Syngo (Siemens) computer system. Fasting blood glucose levels were measured with the Akku-Check system (Roche, Basel).

6.2 Peptide synthesis and radiolabelling

[Lys⁴⁰(Ahx-DTPA- ^{111}In)NH₂]-Exendin-4 was custom-synthesized by Peptide Speciality Laboratories (Heidelberg, Germany). An aliquot of 4 μg [Lys⁴⁰(Ahx-DTPA)NH₂]-Exendin-4 was dissolved in sodium acetate buffer (0.4 M/pH 5.0), incubated with 555 MBq high specific $^{111}\text{InCl}_3$ at room temperature for 30 min and then subjected to a quality control by analytical HPLC (eluent: A = 0.1% TFA in water and B = acetonitrile, flow: 0.75 ml/min; 0 min 95% A, 5 min 95% A, 10 min 0% A, 15 min 0% A, 20 min 95%).

6.3 Mice

Phenotypic and genotypic analyses of Rip1Tag2 transgenic mice in a C57Bl/6 background have been described previously (Hanahan, 1985). Rip1Tag2 and wild type C57Bl/6J mice were used for organ toxicity studies. Animals were maintained and treated in compliance with the guidelines of the Swiss Veterinary Office and the Kantonale Veterinärämter Basel-Stadt (approval 2085 and 789). Rip1Tag2 mice were injected into the tail vein with single doses of 1.1 MBq (2 pmol), 5.6 MBq (8 pmol) and 28 MBq (40 pmol) [$\text{Lys}^{40}(\text{Ahx-DTPA-}^{111}\text{In})\text{NH}_2$]-Exendin-4 or with 40 pmol non-radioactive [$\text{Lys}^{40}(\text{Ahx-DTPA-In}^{\text{nat}})\text{NH}_2$]-Exendin-4 as control. At indicated times, mice were sacrificed, tumor diameters were measured with a grid (for small tumors) or with a caliper (for large tumors), and tumor volumes were calculated assuming a spherical shape of the tumors. Mouse age at time of sacrifice was for all cohorts 11.4 ± 0.3 weeks.

6.4 In Vitro GLP-1 Receptor Autoradiography

GLP-1 receptor autoradiography was used to detect and quantify the GLP-1 receptors in mouse tumor, pancreas, lung, and kidney samples. 20-mm-thick sections were incubated for 2 h at ambient temperature in the presence of 32 pmol/L ^{125}I -labeled GLP-1 (74 TBq/mmol [2,000 Ci/mmol]) (Reubi & Waser, 2003). The incubation solution was 170 mmol/L Tris-HCl buffer (pH 8.2) containing 1% bovine serum albumin, bacitracin (40 mg/mL), and MgCl_2 (10 mmol/L) to inhibit endogenous proteases. Nonspecific binding was determined by adding 100 nmol/L solution of unlabeled GLP-1. Incubated sections were washed twice for 5 min in cold incubation buffer containing 0.25% bovine serum albumin, then washed in buffer alone, and dried quickly. Finally, the sections were apposed to Biomax MR films (Kodak) and exposed for 1 wk in x-ray cassettes. In selected cases, displacement experiments were performed on successive tissue sections using increasing concentrations of GLP-1, exendin-4, and the [$\text{Lys}^{40}(\text{Ahx-DTPA})\text{NH}_2$]-Exendin-4 analog to measure their respective binding affinity to GLP-1 receptors. In all experiments, the autoradiograms were quantified using a computer-assisted image processing system (Reubi et al., 2000 and Reubi et al., 2001). Tissue standards for iodinated compounds were used for this purpose.

6.5 Cell Culture, Radioligand Internalization, Externalization, and Peptide Stability Studies

GLP-1 receptor-expressing β -tumor cells were established from β -cell tumors of Rip1Tag2 mice. Tumors were homogenized and cells were initially kept in high-glucose DMEM containing 10% fetal calf serum and 10% heat-inactivated horse serum. Tumor cells were slowly expanded over 3 weeks and then maintained by serial passage in monolayers in DMEM in a humidified 5% CO_2 / air atmosphere at

37° C. Cell numbers were counted under a microscope with a Neubauer's counting chamber. For all cell experiments, the cells were seeded at a density of 0.8–1 million cells per well in 6-well plates and incubated overnight with internalization buffer (DMEM, 1% fetal bovine serum, amino acids, and antibiotics, pH 7.4) to obtain good cell adherence. The internalization rate was linearly corrected to 1 million cells per well in all experiments. The medium was removed from the 6-well plates and the cells were washed once with 2 ml internalization buffer. To each well, 1.2 ml internalization buffer were added and incubated at 37° C for about 1 h. To the medium, 0.25 pmol [Lys⁴⁰(Ahx-DTPA-¹¹¹In)NH₂]-Exendin-4 was added (final concentration, 0.17 nmol/l). Then the cells were incubated at 37° C for the indicated periods of time. Peptide concentration–dependent internalization was studied using 3 different concentrations of [Lys⁴⁰(Ahx-DTPA-¹¹¹In)NH₂]-Exendin-4 (0.17, 1.7, and 6.67 nmol/l). To determine nonspecific membrane binding and internalization, cells were incubated with the radioligand in the presence of 0.33 mmol/l unlabeled [Lys⁴⁰(Ahx-DTPA)NH₂]-Exendin-4. Cellular uptake was stopped by removing the medium and by washing the cells twice with 1 ml ice-cold phosphate-buffered saline (PBS). An acid wash with a glycine buffer (pH 2.8) on ice was performed twice for 5 min to distinguish between membrane-bound (acid-releasable) and internalized (acid resistant) radioligand. Finally, cells were treated with 1 mol/l NaOH. The culture medium, the receptor-bound fraction, and the internalized fraction were measured radiometrically in a γ -counter. For cellular retention studies, β -tumor cells (0.8–1 million) were incubated with 0.25 pmol per well (0.17 nmol/l) [Lys⁴⁰(Ahx-DTPA-¹¹¹In)NH₂]-Exendin-4 for 120 min; then the medium was removed and the wells were washed twice with 1 ml ice-cold PBS. In each experiment, an acid wash with a glycine buffer (pH 2.8) on ice was performed twice for 5 min to remove the receptor-bound ligand. Cells were then incubated at 37 C with fresh internalization buffer. At different time points, the external medium was removed for quantification of radioactivity in a γ -counter and replaced with fresh medium. Finally, cells were solubilized in 1 mol/l NaOH, and the internalized radioactivity was quantified in a γ -counter. The recycled fraction was expressed as the percentage of the totally internalized radiopeptide per 1 million cells, and the integrity of the externalized peptide after 1- and 2-h externalization was determined using RP-HPLC (gradient II). Peptide stability was determined after incubation of 7 pmol [Lys⁴⁰(Ahx-DTPA-¹¹¹In)NH₂]-Exendin-4 in 3 ml fresh human blood serum for at least 24 h. After certain time points, samples of 100 ml blood serum were taken and added to 200 ml methanol. After centrifugation, the radioactivity in the serum protein pellet and the supernatant was quantified in a γ -counter. Potential metabolites were analyzed by subjecting the supernatant to analytic HPLC (gradient II).

6.6 Biodistribution in Rip1Tag2 mice

Male and female Rip1Tag2 mice, 18-27g and 10-14 weeks old, were injected with 40 pmol (192 ng total peptide mass/ 28 MBq) [Lys⁴⁰(Ahx-DTPA-¹¹¹In)NH₂]-Exendin-4, in 100 μ l NaCl solution 0.9% into the tail vein. At 1h, 12h, 36h, 84h, 168h and 264h after injection, mice (n=5 per cohort) were sacrificed. Organs, blood and tumors were collected and the activity concentration C_{tissue} (percentage injected activity per gram [%IA/g]) was determined. In order to determine radiopeptide uptake in organs and tumors, mice were injected with 2 pmol, 10 pmol, 50 pmol and 250 pmol (0.1 – 14 MBq) [Lys⁴⁰(Ahx-DTPA-¹¹¹In)NH₂]-Exendin-4 as described above and sacrificed 4h after injection. The measured γ emission of ¹¹¹In is proportional to the emission of Auger electrons.

6.7 GLP-1 Receptor Imaging with Multipinhole SPECT/MRI

Rip1Tag2 mice were injected with 37 MBq [Lys⁴⁰(Ahx-DTPA-¹¹¹In)NH₂]-Exendin-4 (50 pmol) into the tail vein. Four hours after injection, multipinhole SPECT images of Rip1Tag2 mice were performed under isoflurane anesthesia in prone position. Images were taken from 60 angles with a minimum of 30 kilocounts per angle, and image reconstruction was done by HiSPECT. Shortly thereafter, Rip1Tag2 mice were scanned in an MR scanner in the same prone position. To enhance the signal-to-noise ratio, a specially designed and modified small animal saddle coil was used. Coronal high-resolution slices were obtained using a 3-dimensional (3D) double echo in steady-state sequence. Transversal slices were reconstructed from the 3D dataset to obtain slices for image fusion. Reconstructed transverse MRI and SPECT images were manually fused using the anatomic information obtained from both imaging modalities. After imaging, in both animals necropsy was performed and the size of tumors was measured.

6.8 GLP-1 Receptor Imaging with SPECT/CT

Rip1Tag2 mice were injected with 27.8 MBq [Lys⁴⁰(Ahx-DTPA-¹¹¹In)NH₂]-Exendin-4 (40 pmol) as described. One hour after injection of the radiopeptide, 100 mL of contrast medium were injected into the tail vein. Then the mice were sacrificed and bilateral nephrectomy was performed. During nephrectomy a drop of contrast medium (about 1 ml) was directly injected into the tumor for tumor visualization on the CT scan. Mice were then placed under a dual-head γ -camera with an integrated CT scanner, and SPECT images were obtained in a continuous mode. The angular range was 180 per γ camera head and the acquisition time was 25 s per frame. The image matrix was 256 · 256, and images were reconstructed as 5-mm-thick sections by using an iterative algorithm. The CT data from the SPECT/CT examination were reconstructed in the transverse plane as 1-mm-thick sections. The following parameters were used for imaging: 130 kV, 80 mA s, 1.5 s per rotation, and a table

speed of 1 mm/s. All images were viewed with software that provided multiplanar reformatted images of SPECT, CT, and fused data with linked cursors. After imaging, selected organs and the tumor were collected and the radioactivity was determined using a γ -counter. Finally, the size of the tumor was measured with a caliper.

6.9 Dosimetry

Determination of the absorbed dose in the tumor and normal tissue from ^{111}In was performed according to the MIRD formalism (Loevinger, 1988). The biodistribution data (40 pmol/ 28 MBq [Lys⁴⁰(Ahx-DTPA- ^{111}In)NH₂]-Exendin-4) were used to generate the time-activity curve between 1h and 264h. The mean cumulated activity (\tilde{A}) in selected organs was obtained by analytical integration over a bi-exponential fit to the time-activity curve:

$$\tilde{A} = \int_0^{\infty} A_{\text{tissue}}(t) dt = \frac{\alpha_1}{\lambda_1} + \frac{\alpha_2}{\lambda_2}$$

Fitting was done using the GNU ([http:// www.gnu.org/software/gsl](http://www.gnu.org/software/gsl)) implementation of the Levenberg-Marquard algorithm (Moré, 1978 and Moré et al., 1981). The mean absorbed dose D_{tissue} to a tissue with mass m_{tissue} was estimated for various tissues as:

$D_{\text{tissue}} = \tilde{A}nE\Phi/m_{\text{tissue}}$. nE is the mean energy emitted per nuclear transformation and Φ is the absorbed fraction. In these calculations we considered the energy (nE) of Auger- and conversion electrons only. The emission of Auger electrons is proportional to the emitted γ component, but the energy deposition of gamma-rays is negligible in small animals such as mice (Behr & Goldenberg, 1996). The absorbed fraction Φ for all measured organs was set to be 1 because of the very short path-length of Auger- (2-12 μm) and conversion electrons in tissues. TND_{tissue} , the tumor-to-normal tissue and blood absorbed dose ratio, was calculated as: $TND_{\text{tissue}} = D_{\text{tumor}}/D_{\text{tissue}}$

6.10 Histological analysis

Tissue was fixed in 4% p-formaldehyde overnight at 4°C and embedded in paraffin. For frozen sections, tissue was fixed in 4% p-formaldehyde, immersed overnight in 20% sucrose in HBS-Ca²⁺ (Hepes-buffered saline with 1mM CaCl₂), and embedded and snap-frozen in OCT-compound (Tissue-Tek, München, Germany). Immunohistochemistry on paraffin and frozen sections was performed by quenching the slides in 3% H₂O₂ in PBS for 10 minutes, blocking in 5% goat serum for 1 hour, incubation with primary antibody over night at 4°C, incubation with secondary antibody for 30 minutes, and development with the ABC-kit of Vectastain (Vector Laboratories, Burlingame, California) and Sigma Fast 3,3'-Diaminobenzidine tetrahydrochloride with metal enhancer (Sigma, Basel, Switzerland) or AEC-kit

(Vector Laboratories). Toluidine blue staining: Kidneys were fixed in 4% formalin and embedded in paraffin. Sections were deparaffinized, stained for 10 minutes in 0.1g/100ml toluidine blue, rinsed in distilled water and finally dehydrated in ethanol. BrdU (proliferation) and TUNEL (apoptosis) staining were performed as described in the methodology section of part I.

6.11 Immunofluorescent stainings

The protocol was as described above and in the methodology section of part I. In addition, the following primary antibodies were used: rat-anti-CD31 1:100, rat-anti-mouse CD45 1:100, rat-anti-mouse CD8a 1:100, rat-anti-mouse CD4 1:100 (all BD Biosciences, San Jose, California), rat-anti-mouse F4/80 1:100 (Serotec, Oxford, UK), rat-anti-mouse Gr-1 1:100 (Leinco Technologies, St. Louis, Missouri), rat-anti-cyclin D2 1:50 (Santa Cruz Biotechnology, Heidelberg, Germany). The following secondary antibodies were used: Alexa fluor 488 anti-rat and Alexa fluor 546 anti-rat (all Molecular Probes, San Diego, California).

6.12 Electron microscopy

Kidneys were extracted, put on ice, fixed in 2.5% glutaraldehyde and further analysed by standard protocols for tissue processing and transmission electron microscopy.

6.13 Light microscopy

Immunohistochemical stainings were analyzed on an AxioVert microscope (Zeiss, Oberkochen, Germany). Immunofluorescence stainings were analyzed on a LSM510 META confocal microscope using LSM510 software (Zeiss). Histological grading of tumors as hyperplastic islets, adenomas or carcinomas was performed following the WHO international classification of rodent tumors, part II, The Mouse. Histological staging and grading was done in a blindfold manner and repeated twice.

6.14 Statistical analysis

Statistical analysis was performed using the GraphPad Prism software (GraphPad Software Inc., San Diego, USA). Tumor volume and mass were calculated using non-parametrical statistical analysis (Kruskal-Wallis test) with Dunn's post-test. Proliferation, vessel density, number of immune cells, as well as blood glucose levels and animal weight were analyzed by parametric testing (one-way Anova and Newman-Keuls post-test).

7. Results and Discussion (part II)

7.1 [$\text{Lys}^{40}(\text{Ahx-DTPA-}^{111}\text{In})\text{NH}_2$]-Exendin-4, a promising ligand for glucagon-like peptide-1 (GLP-1) receptor targeting

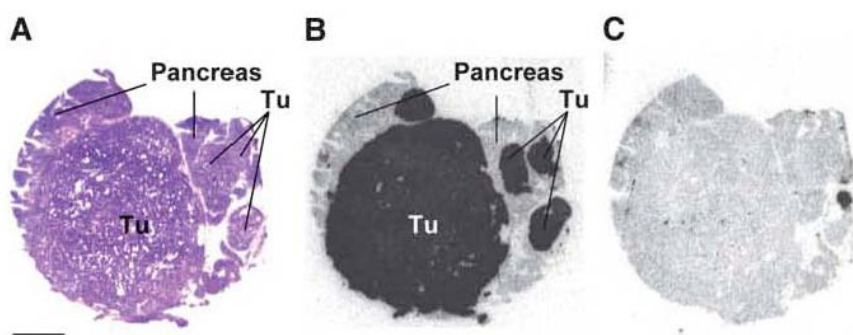
Synthesis and Radiolabeling

DTPA was coupled via the Lys side chain of the C-terminally extended exendin-4 using Ahx as the spacer between DTPA and the peptide. The composition and structural identity of [$\text{Lys}^{40}(\text{Ahx-DTPA})\text{NH}_2$]-exendin-4 was verified by analytic HPLC and MALDI-MS (calculated mass: 4'799.4 g; observed mass: 4'801.3 g ($[\text{M}+2\text{H}]^{2+}$, 100%; 2'402.1 g $[\text{M}+4\text{H}]^{2+}$, 20%). The labeling yield of [$\text{Lys}^{40}(\text{Ahx-DTPA-}^{111}\text{In})\text{NH}_2$]-Exendin-4 was >99% at a specific activity of 90 GBq/mmol and a radiochemical purity of >90%. The HPLC elution time on different gradient systems was 11.33 min (gradient I) and 29.5 min (gradient II).

Expression of GLP-1 Receptors in Mouse Insulinoma Tumors

Receptor autoradiography revealed a very high density of GLP-1 receptors homogeneously distributed in the tumor sample. Conversely, the adjacent exocrine pancreas expressed only a very low level of receptors (Fig. 7.1). The mean density of the GLP-1 receptor was quantified and found to be $17'269 \pm 1'906$ dpm/mg tissue ($n=5$; mean \pm SEM).

Figure 7.1: Receptor autoradiography for GLP-1R



GLP-1 receptors in tumors of Rip1Tag2 mice: receptor autoradiographic illustration of GLP-1 receptors in tumors (Tu) and pancreas of a representative example. (A) H&E staining. (B) Autoradiogram shows total binding of ^{125}I -labeled GLP-1 in tumors and pancreas. (C) Autoradiogram shows nonspecific binding in presence of 100 nmol/L GLP. Bar = 0.1 mm.

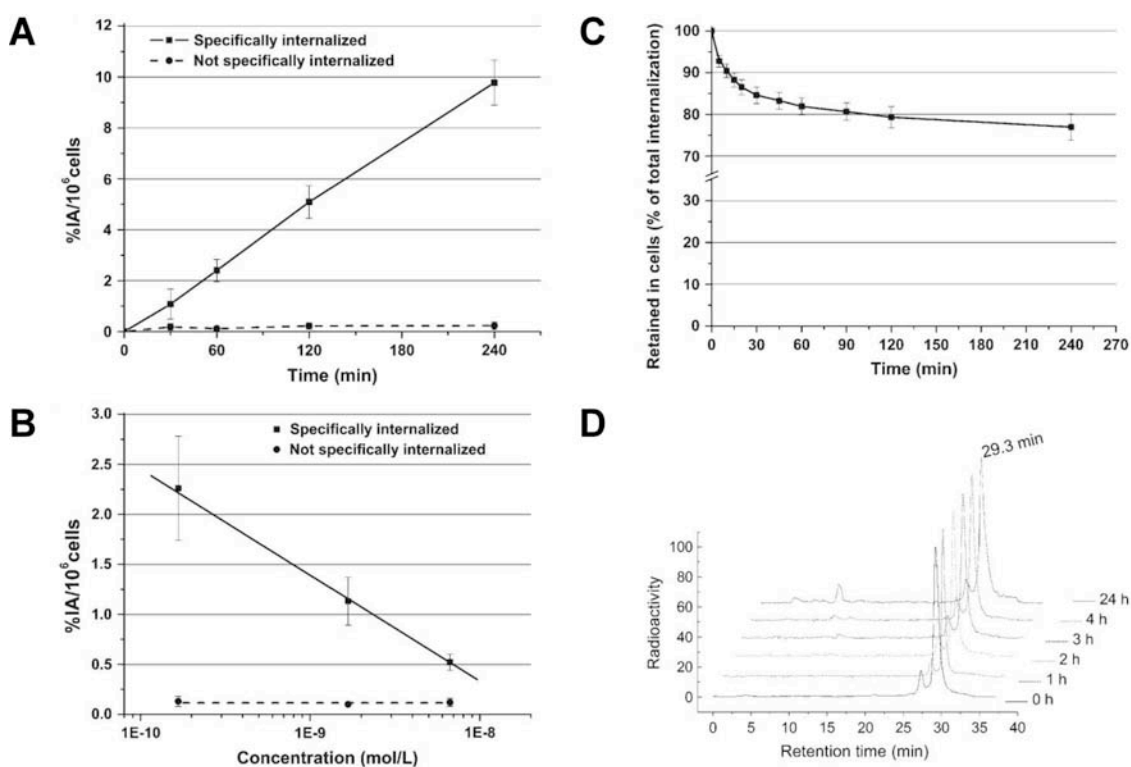
GLP-1 Receptor Binding Affinity for [$\text{Lys}^{40}(\text{Ahx-DTPA})\text{NH}_2$]-Exendin-4

High-affinity GLP-1 receptor binding was measured for [$\text{Lys}^{40}(\text{Ahx-DTPA})\text{NH}_2$]-exendin-4 in competition experiments. An IC_{50} value of 2.1 ± 1.1 nmol/L (mean \pm SEM, $n = 4$) was found for [$\text{Lys}^{40}(\text{Ahx-DTPA})\text{NH}_2$]-Exendin-4, compared with 0.65 ± 0.1 nmol/L (mean \pm SEM, $n = 11$) for exendin-4 and 2.4 ± 0.1 nmol/L for GLP-1 (mean \pm SEM, $n = 3$) using ^{125}I -labeled GLP-1 as radioligand.

In Vitro Internalization Studies in β -Tumor Cells

[Lys⁴⁰(Ahx-DTPA-¹¹¹In)NH₂]-Exendin-4 showed a linear uptake within 4 h of incubation in established β -tumor cells (Fig. 7.2 A). Between 85% and 97% of totally internalized radioligand was specifically internalized. At 1 h, the specific uptake into β -tumor cells was 2.4%±0.4% of the totally administered activity, increasing to 9.8%±0.9% at 4 h. The time–activity curve did not show a plateau during the first 24 h of internalization (data not shown). The percentage of internalized peptide measured at 1 h as a function of injected radiopeptide concentrations is shown in Figure 7.2 B.

Figure 7.2: internalization and peptide stability



(A, B) Specific (■) and nonspecific (●) internalization rates of [Lys⁴⁰(Ahx-DTPA-¹¹¹In)NH₂]-Exendin-4 into β -tumor cells. Values and SD are result of 2–4 independent experiments (triplicates in each experiment) and are expressed as percentage of activity internalized into 1×10⁶ cells. (A) In vitro kinetic of [Lys⁴⁰(Ahx-DTPA-¹¹¹In)NH₂]-Exendin-4 at 0.17 nmol/L peptide concentration. (B) Radiopeptide concentration–dependent specific internalization at 60 min. (C) Externalization rate ± SD of [Lys⁴⁰(Ahx-DTPA-¹¹¹In)NH₂]-Exendin-4 after internalization for 120 min. Retained fraction is expressed as percentage of totally internalized radiopeptide per 1 million cells. (D) Stability of [Lys⁴⁰(Ahx-DTPA-¹¹¹In)NH₂]-Exendin-4 in human serum. After centrifugation, supernatant was analyzed on analytic HPLC at different time points.

Cellular Retention

The kinetics of externalization was studied with β -tumor cells exposed to the radiopeptide for 2 h. Within 4 h, only 23% ± 3% of the radioligand were released from the β -tumor cells and the externalization curve showed a flattening (Fig. 7.2 C). The externalized radioactivity represented intact peptide as identified by HPLC.

Stability in Human Serum

For the determination of peptide stability, [Lys⁴⁰(Ahx-DTPA-¹¹¹In)NH₂]-Exendin-4 was incubated in human blood serum at 37 °C. After 4.5 h incubation, the protein fraction obtained as a pellet contained ≤6% of radioactivity and increased to 14.8% at 24 h. The supernatant was analyzed by analytic HPLC and showed 82.1% of intact peptide after 4.5 h and 73.7% after 24 h (Fig. 7.2 D).

Animal Biodistribution Studies

The levels of [Lys⁴⁰(Ahx-DTPA-¹¹¹In)NH₂]-Exendin-4 uptake, determined 4, 24, and 48 h after injection, in kidneys, liver, spleen, femur, and blood as well as in GLP-1 receptor–positive organs (lung, pancreas, stomach, and tumor) are shown in Table 1.

Table 7.1: Biodistribution and tissue radioactivity ratio in tumor-bearing Rip1Tag2 mice at 4, 24 and 48 hours after injection of 2 pmol [Lys⁴⁰(Ahx-DTPA-¹¹¹In)NH₂]-Exendin-4

Organ	Time (h)	[Lys ⁴⁰ (Ahx-DTPA- ¹¹¹ In)NH ₂]exendin-4	
		Nonblocked (%IA/g)	Blocked* (%IA/g)
Lung	4	65.08 ± 18.62	0.86 ± 0.04 [†]
	24	51.58 ± 4.25	
	48	31.21 ± 2.73	
Pancreas	4	21.13 ± 7.35	1.44 ± 0.43 [†]
	24	20.05 ± 4.29	
	48	13.59 ± 0.47	
Stomach	4	4.68 ± 0.73	0.72 ± 0.23 [†]
	24	2.86 ± 0.25	
	48	2.75 ± 0.53	
Tumor	4	287.37 ± 62.37	7.28 ± 3.50 [†]
	24	181.82 ± 81.77	
	48	132.01 ± 41.04	
Kidneys	4	208.77 ± 34.68	214.91 ± 4.71
	24	148.16 ± 35.98	
	48	104.10 ± 15.04	
Liver	4	0.97 ± 0.27	0.35 ± 0.09
	24	0.68 ± 0.10	
	48	0.53 ± 0.07	
Spleen	4	1.55 ± 0.73	1.77 ± 0.31
	24	1.18 ± 0.16	
	48	0.91 ± 0.14	
Bone	4	0.40 ± 0.13	0.07 ± 0.04
	24	0.30 ± 0.08	
	48	0.42 ± 0.19	
Blood	4	0.29 ± 0.22	0.16 ± 0.03
	24	0.10 ± 0.01	
	48	0.06 ± 0.01	
Ratio		[Lys ⁴⁰ (Ahx-DTPA- ¹¹¹ In)NH ₂]exendin-4	
		4 h after injection	48 h after injection
Tumor/blood		991	2,200
Tumor/kidneys		1.38	1.27
Tumor/lung		4.42	4.23
Tumor/pancreas		13.6	9.71

*Blocked with 2 nmol [Lys⁴⁰(Ahx-DTPA-^{nat}In)NH₂]exendin-4.

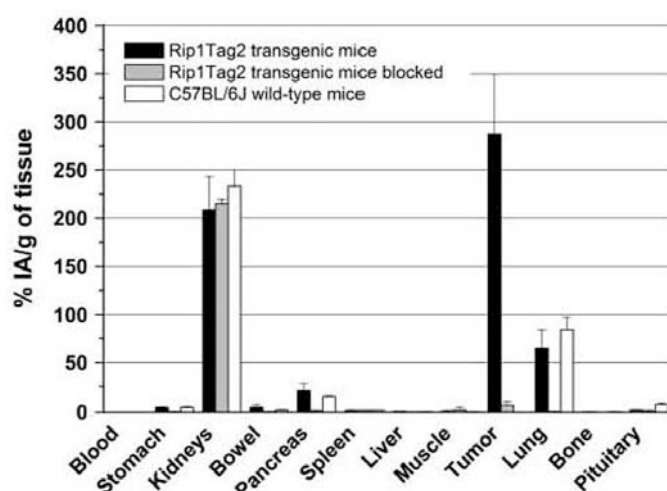
[†]GLP-1 receptor–positive organs.

Values are given as %IA/g tissue ± SD.

Blood clearance was fast with 0.3% IA/g remaining in blood 4 h after injection, resulting in very high tumor-to-normal organ ratios, especially tumor-to-blood ratios. By contrast, the organ and tumor excretion rate of the radiopeptide was slow. The

accumulated activity in organs with the highest uptake, including kidneys, lung, pancreas, liver, and tumor, was $81\% \pm 9.1\%$ of the totally injected activity at 4 h. Four hours after injection of 2 pmol $[\text{Lys}^{40}(\text{Ahx-DTPA-}^{111}\text{In})\text{NH}_2]\text{-Exendin-4}$ the uptake in the tumors (tumor weight, 5.6 ± 3.6 mg) was very high with 287 ± 62 %IA/g tissue. Only the uptake in the kidneys (209 ± 35 %IA/g) was nearly as high as in the tumors. Blocking with 1,000 times excess of cold ligand reduced the tumor uptake by $>95\%$, whereas the kidney uptake was not affected. The tumor-to-kidney ratio was 1.38 at 4h and 1.27 at 48 h. An important value for diagnostic use of $[\text{Lys}^{40}(\text{Ahx-DTPA-}^{111}\text{In})\text{NH}_2]\text{-Exendin-4}$ is the tumor-to-pancreas ratio, which was 13.6 at 4 h and 9.71 at 48 h. One hour after injection, only weak and unspecific uptake was found in the lymphatic reticular tissue, such as spleen ($2.6 \pm 1\%$ IA/g) and bone marrow ($1.5 \pm 0.3\%$ IA/g). A comparison of radiopeptide uptake in tumor, blood, and organs of Rip1Tag2 mice and wild-type C57BL/6J mice is shown in Figure 7.3. In all normal organs, the uptake in the transgenic mice was the same as that in the wild-type mice.

Figure 7.3: Biodistribution of $[\text{Lys}^{40}(\text{Ahx-DTPA-}^{111}\text{In})\text{NH}_2]\text{-Exendin-4}$ in Rip1Tag2 and wt mice



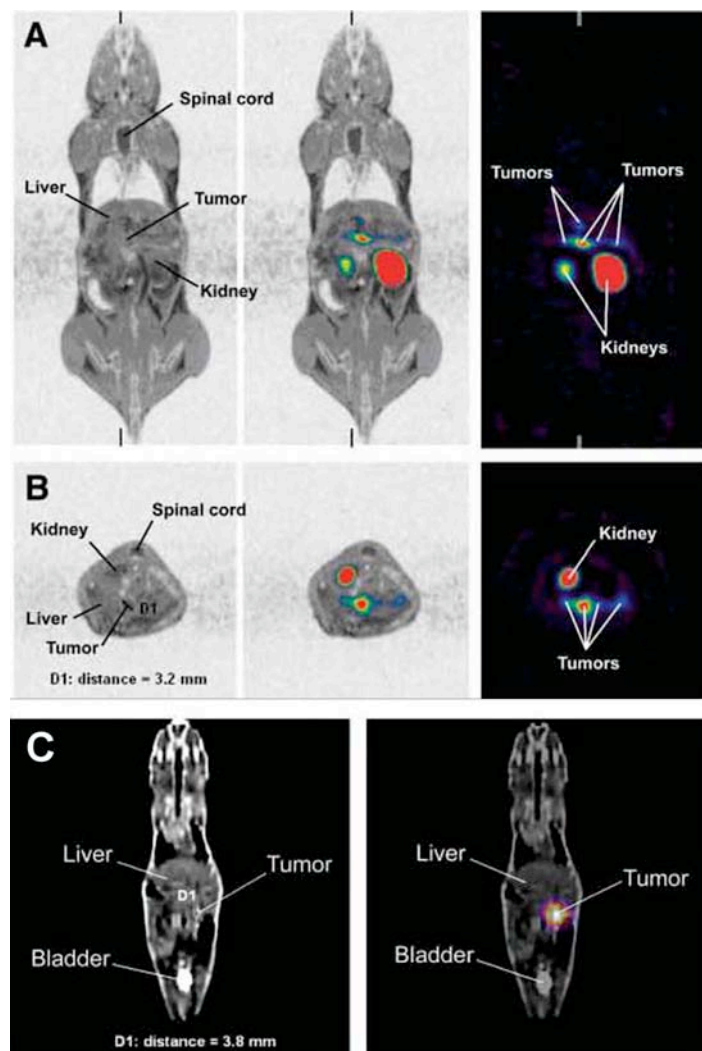
Biodistribution of $[\text{Lys}^{40}(\text{Ahx-DTPA-}^{111}\text{In})\text{NH}_2]\text{-Exendin-4}$ in C57BL/6J wild-type mice and tumor-bearing Rip1Tag2 mice 4 h after injection of radiopeptide. Values and SD are result of 2 independent experiments with a total of 6 Rip1Tag2 mice (black and gray bars) and 3 wild-type mice (white bars). Gray bars show uptake in tumors and organs of Rip1Tag2 mice after co-injection with excess cold peptide.

In Vivo GLP-1 Receptor Imaging

Iteratively reconstructed multipinhole SPECT/MR images were performed to visualize tumors in Rip1Tag2 transgenic mice 4 h after injection of 37 MBq $[\text{Lys}^{40}(\text{Ahx-DTPA-}^{111}\text{In})\text{NH}_2]\text{-Exendin-4}$ (Fig. 7.4 **A** and **B**). In pinhole SPECT, 5 small pancreatic tumors (1–3.2 mm) and both kidneys were visible. Other GLP-1 receptor-positive organs, such as lung and pancreas (Mayo et al., 2003) were not detectable. In contrast to high-resolution MRI, pinhole $[\text{Lys}^{40}(\text{Ahx-DTPA-}^{111}\text{In})\text{NH}_2]\text{-Exendin-4}$ SPECT visualized small insulinoma tumors with a maximal diameter of 1 mm. In comparison with pinhole SPECT, the resolution of ordinary SPECT is limited. Nevertheless, iteratively reconstructed SPECT/CT images of Rip1-Tag2 mice 1 h

after injection of 27.8 MBq [Lys⁴⁰(Ahx-DTPA-¹¹¹In)NH₂]-Exendin-4 demonstrated very high uptake exclusively in the tumor after bilateral nephrectomy (Fig. 7.4 C).

Figure 7.4: Molecular imaging of GLP-1R expression by multipinhole SPECT/MRI and conventional SPECT/CT.



(A) Coronal MR image (left), multipinhole SPECT/MR fusion image (center), and multipinhole SPECT image (right). (B) In corresponding transversal sections, maximal tumor diameter in MR image is 3.2 mm. In the MR image, only the largest tumor is visible—in contrast to the pinhole SPECT image, where 4 additional small tumors are apparent. (C) Right panel: Coronal SPECT/CT image of a tumor-bearing Rip1Tag2 mouse 1 h after injection of [Lys⁴⁰(Ahx-DTPA-¹¹¹In)NH₂]-Exendin-4. Left panel: Corresponding contrast medium-enhanced CT scan with tumor size of 3.8 mm. Tumor size measured with a caliper was 4.5 × 3 × 3 mm.

Discussion

This study describes the preclinical evaluation of a DTPA linker-conjugated exendin 4 derivative for the labeling with the γ - and Auger-emitter ¹¹¹In and the targeting of GLP-1 receptor-positive tumors in the Rip1Tag2 transgenic mouse model of pancreatic β -cell carcinogenesis. The main rationale to develop a radiopeptide for the targeting of the GLP-1 receptor is based on the need to develop tools for imaging and localization of insulinomas by SPECT, PET, or use of a surgical probe for

intraoperative localization. Although sst2 receptor targeting with radiopeptides is a very successful method for the diagnosis and therapy of neuroendocrine tumors, radiolabelled peptides have not been effective enough for a curative approach (Krenning et al., 2004). In addition, about 50% of insulinomas are not detectable using [^{111}In -DTPA 0]octreotide because the sst2 receptor density on the cell membrane is too low for visualization with [^{111}In -DTPA 0]octreotide (Krenning et al., 1993; Modlin & Tang, 1997). Therefore, detection of receptors expressed in higher density, leading to higher tumor uptake, is desirable. The GLP-1 receptor, which is expressed at high levels in human insulinomas, is such a promising receptor. In this regard, the Rip1Tag2 transgenic mouse model that develops insulinoma-like tumors appears to be a suitable tumor model to study and optimize different GLP-1/exendin-based radiopeptides. Indeed, an high [$\text{Lys}^{40}(\text{Ahx-DTPA-}^{111}\text{In})\text{NH}_2$]-Exendin-4 uptake of 287 ± 62 %IA/g tissue was found 4 h after injection in the tumor of Rip1Tag2 mice, which could be blocked by >95% when co-injected with a 1,000 times excess of cold peptide. ^{111}In -coupled peptides are predominantly used for tumor imaging in the clinic, but recently ^{111}In was also proposed for therapeutic application using the radiotoxic effect of Auger electrons (Behr et al., 2000; Chen et al., 2006). Therefore, [^{111}In -DTPA 0]-octreotide was used for targeted radionuclide therapy of neuroendocrine tumors with encouraging results (Valkema et al., 2002). Unfortunately, the dose-limiting factor was bone marrow toxicity. In the Rip1Tag2 mouse model, the bone marrow uptake 1 h after injection was $1.5 \pm 0.3\%$ IA/g tissue, resulting in a favorable tumor-to-bone marrow ratio of 181. However, not only a high tumor uptake but also a high kidney uptake was found in this animal model (tumor-to-kidney ratio 4 h after injection, 1.38). The high kidney uptake was not GLP-1 receptor mediated, as the uptake by kidneys could not be blocked by an excess of [$\text{Lys}^{40}(\text{Ahx-DTPA-}^{\text{nat}}\text{In})\text{NH}_2$]-Exendin-4, suggesting that the accumulation of [$\text{Lys}^{40}(\text{Ahx-DTPA-}^{111}\text{In})\text{NH}_2$]-Exendin-4 in the kidney tissue is most likely due to tubular cell reabsorption as found with most radiopeptides. However, patients with neuroendocrine tumors treated with a cumulative dose of 100 GBq [^{111}In -DTPA 0]octreotide showed no kidney toxicity at all (Valkema et al., 2002). Therefore, kidney toxicity is not expected from diagnostic doses of [$\text{Lys}^{40}(\text{Ahx-DTPA-}^{111}\text{In})\text{NH}_2$]-Exendin-4. Previous *in vivo* studies used the ^{125}I -labeled GLP-1 (7–36) amide and ^{125}I -labeled exendin-3 for GLP-1 receptor targeting in a rat insulinoma model (RINm5F cells). The radiopeptides were shown to target specifically the xenografted tumor shortly after injection, yet the tumor-to-background ratio was low during the time period studied (Gotthardt et al., 2002). In Rip1Tag2 mice, the tumor-to-background ratio was favorable (4 h after injection: tumor-to-pancreas ratio, 13.6; tumor-to-intestine ratio, 58; tumor-to-stomach ratio, 61; tumor-to-muscle ratio, 299; tumor-to-liver ratio, 296). The tumor-to-lung ratio (4.4 at 4 h) is relatively low in Rip1Tag2 mice. It is not known whether human lung expresses high densities of GLP-1 receptors. However, it is established that human pancreatic β -cells express high levels of GLP-1 receptors (Kreymann et al., 1987; Thorens et al., 1993). Yet, because of their small size, pancreatic islets may not be visible within the pancreas

on a SPECT scan. Indeed, only multiple pancreatic tumors and both kidneys were visible on the pinhole SPECT, which was performed in Rip1Tag2 mice. The normal pancreatic tissue was not visible because the tumor-to-pancreas ratio was >10 in our animal model. In addition, pinhole SPECT visualized small tumors with a size of 1 mm because of high tumor uptake. However, on the MR scan of the same animal such small tumors were not visible, although a small animal saddle coil was used to enhance the signal-to-noise ratio.

Pinhole SPECT is not often used on patients because sensitivity and short scan time are more important than a higher image resolution. Therefore, we performed additional SPECT scans with the same hybrid camera as that used for patients. As expected, a differentiation between tumor and kidney was not possible in these small animals. Nevertheless, the tumor with a size of only $4.5 \times 3 \times 3$ mm was visible with a good contrast after bilateral nephrectomy. At a very high threshold level, only the lungs were distinguishable from the tumor with a weak signal. To confirm these findings the activity of relevant organs was measured with a γ -counter. One hour after injection, the absolute uptake in the kidneys was 35% IA each, followed by the tumor (5.7% IA) and the lung (1.0% IA). These findings indicate that a small tumor (<5 mm) can be visualized by a normal SPECT camera if the absolute tumor uptake is high. Insulinomas are very difficult to visualize by any method because of their small size of <2 cm in 90% of the cases (Gouya et al., 2003). Nevertheless, preoperative localization and staging are essential because of the possibility of multiple insulinomas, malignancy, and metastatic disease. In addition, many surgeons emphasize the importance of preoperative localization of insulinomas because these lesions cannot be identified during surgical exploration in 10%–20% of the cases (Angelini et al., 1987). Hence, not only pre-operative but also intra-operative tumor localization using a normal or endoscopic γ -probe might be an additional clinical application of radiolabeled Exendin-4.

7.2 A new therapeutic approach to insulinoma: [Lys⁴⁰(Ahx-DTPA-¹¹¹In)NH₂]-Exendin-4 is a highly efficient radiotherapeutic for glucagon-like-peptide-1 (GLP-1) receptor targeted therapy

Biodistribution and dosimetry

As we discussed in chapter 7.1, GLP-1R is expressed with a density of 17269±1906 dpm/mg in insulinoma cells of Rip1Tag2 transgenic mice. We have also seen that the synthetic ligand [Lys⁴⁰(Ahx-DTPA-¹¹¹In)NH₂]-Exendin-4 is linearly internalized into β -cells, resulting in an uptake of 9.8%±0.9% 4 hours after incubation. Thus, the GLP-1R might be a suitable target to attack the insulinoma cells directly and specifically. Here, we set out to employ [Lys⁴⁰(Ahx-DTPA-¹¹¹In)NH₂]-Exendin-4 for therapeutic intervention studies of insulinoma development in Rip1Tag2 transgenic mice. By using highly specific ¹¹¹InCl₃, [Lys⁴⁰(Ahx-DTPA-¹¹¹In)NH₂]-Exendin-4 was labelled with yields of >97% and a high specific activity of 700 GBq/ μ mol.

To investigate the uptake of [Lys⁴⁰(Ahx-DTPA-¹¹¹In)NH₂]-Exendin-4 into the tumor cells *in vivo*, varying concentrations of the radiopeptide were injected i.v. into Rip1Tag2 mice and the biodistribution after different time intervals was determined. Uptake of the radiopeptide was concentration-dependent, which is in accordance with similar experiments measuring the uptake of radio-labelled octreotide derivatives in a SSTR-2 expressing tumour model (Kolby et al., 2005). Injected peptide concentrations from 2 to 50 pmol yielded a tumor uptake of more than 200% IA/g, with the highest relative tumor uptake (307 ± 38% IA/g) after injection of 10 pmol (5.6 MBq) [Lys⁴⁰(Ahx-DTPA-¹¹¹In)NH₂]-Exendin-4 (Figure 7.5 **A**). However, a 25 times higher peptide concentration resulted in a tumor uptake of only 59% IA/g, whereas the kidney uptake was still 190% IA/g. Based on these results, a maximum dose of 40 pmol (28 MBq) [Lys⁴⁰(Ahx-DTPA-¹¹¹In)NH₂]-Exendin-4 was injected to assess the kinetics of its tumor-specific uptake. 84 hours after injection of the radiopeptide, tumor uptake was approximately 60% IA/g, while 168 hrs and 264 hrs after injection, tumor uptake was 180% ± 107% IA/g and 203 % ± 125% IA/g, respectively. At these later time points, all other organs showed a rapid decline in the levels of detectable radiopeptide (data not shown).

After a single injection of 28 MBq [Lys⁴⁰(Ahx-DTPA-¹¹¹In)NH₂]-Exendin-4, the highest dose deposition (3 Gy/MBq) was found in tumors of Rip1Tag2 mice. The absorbed dose per MBq in kidney, liver, spleen, bone marrow and blood as well as in GLP-1R positive organs, including lung, pancreas, small intestine and tumor is shown in Table 7.2.

Table 7.2: Absorbed dose per Megabecquerel (MBq) injected activity and tumor-to-normal tissue absorbed dose of [Lys⁴⁰(Ahx-DTPA-¹¹¹In)NH₂]-Exendin-4 in tumor bearing Rip1Tag2 mice.

Organ/tissue	Absorbed dose per MBq (Gy/MBq) ^a	Tumor-to-normal tissue absorbed dose ratio (TND _{tissue}) ^b
Lung	0.08	37
Pancreas	0.10	30
Small intestine	0.06	50
Tumor	3.0	-
Kidneys	2.0	1.5
Liver	0.01	300
Spleen	0.027	111
Bone marrow	0.013	230
Blood	0.003	1000

^a Peptide uptake was measured at 1h, 12h, 36h, 84h, 168h and 264h after injection. N = 5 per cohort. The absorbed dose was calculated from the serial biodistribution measurements using the algorithm described in the methods section.

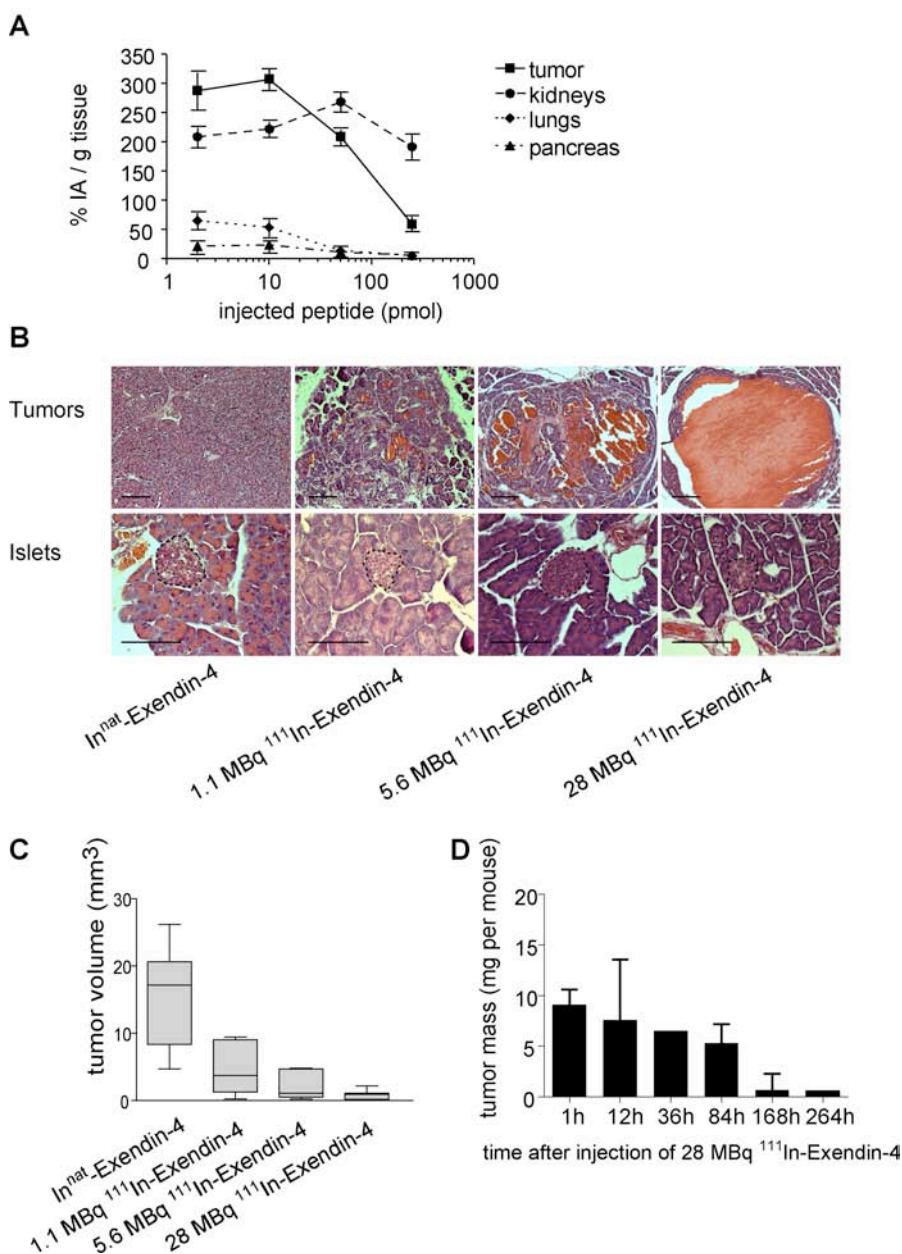
^b TND_{tissue} was calculated using the absorbed dose values.

The absorbed dose in kidney was 2 Gy/MBq resulting in a TND_{kidney} (tumor-to-kidney absorbed dose ratio) of 1.5. All other organs, including pancreas and blood, showed a TND_{tissue} ≥ 30. The high and specific uptake of [Lys⁴⁰(Ahx-DTPA-¹¹¹In)NH₂]-Exendin-4 into GLP-1R-expressing tumor cells as well as the observed high dose deposition into the tumor are critical for a therapeutic application of the radioligand. These dosimetry results indicate that the tumors of Rip1Tag2 transgenic mice can be specifically targeted with [Lys⁴⁰(Ahx-DTPA-¹¹¹In)NH₂]-Exendin-4 at high specific activities and that the kidney is expected to be the dose-limiting organ.

Reduced tumor volume

To investigate the therapeutic impact of [Lys⁴⁰(Ahx-DTPA-¹¹¹In)NH₂]-Exendin-4, cohorts of 7 Rip1Tag2 mice each were injected with single doses of 1.1, 5.6 and 28 MBq [Lys⁴⁰(Ahx-DTPA-¹¹¹In)NH₂]-Exendin-4. A control group of 8 Rip1Tag2 mice was injected with non-radioactive ^{nat}In-exendin-4. Mice were sacrificed eight days after the single injections. Histological analysis revealed dramatic morphological changes in tumor sections of radiopeptide-injected mice. With an increasing dose of radiopeptide, tumors appeared to disaggregate and to develop large hemorrhagic lacunae (Fig. 7.5 B).

Figure 7.5: Uptake and therapeutic effect of [Lys⁴⁰(Ahx-DTPA-¹¹¹In)NH₂]-Exendin-4



(A) Biodistribution four hours after injection of 2 pmol, 10 pmol, 50 pmol and 250 pmol [Lys⁴⁰(Ahx-DTPA-¹¹¹In)NH₂]-Exendin-4 in tumor bearing Rip1Tag2 mice. Values and standard deviations are the result of two independent experiments with a total of 6 animals in each group. (B) Analysis of H&E stainings of pancreas sections eight days after injection of [Lys⁴⁰(Ahx-DTPA-¹¹¹In)NH₂]-Exendin-4 and non-radioactive In^{nat}-Exendin-4. Tumor cell death and formation of hemorrhagic lacunae in the tumors of the interventional group (upper panels) are apparent, whereas morphologically normal islets are not affected by the treatment (lower panels). Size bars = 100 μ m. (C) Dose-dependent reduction of tumor volumes eight days after injection of [Lys⁴⁰(Ahx-DTPA-¹¹¹In)NH₂]-Exendin-4. The percentages of tumor volume reduction in treated compared to control mice (%T/C) are 27.9%, 13.7%, and 5.6% for the 1.1 Mbq, 5.6 Mbq and the 28 Mbq groups ($p = 0.0003$, Kruskal-Wallis test). (D) Kinetic of tumor mass reduction in the 28 MBq group. A first decrease in tumor mass is detectable 36 hrs after injection of the radiopeptide and a progressive reduction in tumor mass is apparent until 10 days after treatment.

In mice treated with a single injection of 28 MBq (equal to an average absorbed tumor dose of 84 Gy), approximately 50% of the tumors were completely dissolved with only cellular debris and hemorrhagic lacunae remaining. In the other 50% of

tumors, a thin tumor rim of morphologically intact cancer cells remained detectable (Fig. 7.5 B, top right panel). No morphological changes were evident in normal islets, indicating that exclusively cells of β adenoma or carcinoma were targeted, whereas untransformed islet cells were not significantly affected by the treatment (Fig. 7.5 B, bottom panels).

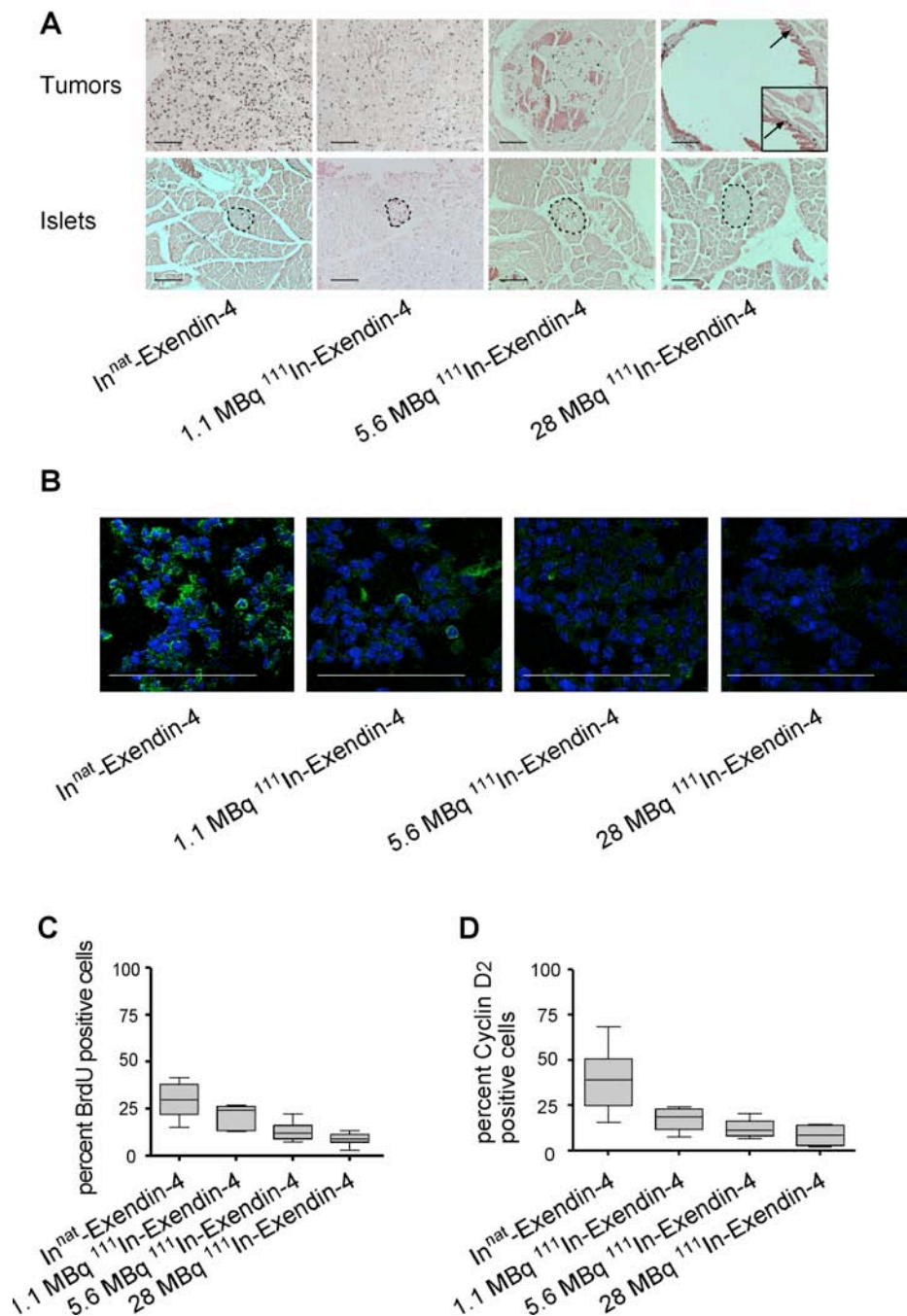
The observed reduction in tumor volumes was dependent on the dose of injected radiopeptide (Fig. 7.5 C). Eight days after injection of the radiopeptide, the percentage of tumor volumes in mice treated with 28 MBq compared to control mice (% T/C) were 5.6% ($p < 0.001$, Dunn's post-test). To investigate the kinetics of tumor growth and decrease, we also examined the total tumor mass per mouse at different time points after the injection of 28 MBq [Lys⁴⁰(Ahx-DTPA-¹¹¹In)NH₂]-Exendin-4 (Fig. 7.5 D). The first therapeutic effect was detectable as soon as 12 hrs after injection, and a continued decrease in tumor mass could be observed until 11 days after the single injection of the radiopeptide. In a cohort of untreated Rip1Tag2 mice ($n=4$), in the same timeframe the tumor volume increased by about 50% (data not shown). Taken together, these results show that a single injection of 28 MBq [Lys⁴⁰(Ahx-DTPA-¹¹¹In)NH₂]-Exendin-4 is sufficient to induce a dramatic and prolonged tumor response, i.e., a 94% decrease of tumor volume within eight days after application of the radiopeptide. At the same time, the residual haemorrhagic tumor mass still exhibited an uptake of 180 %I/g. This finding underlines the prolonged therapeutic effect of [Lys⁴⁰(Ahx-DTPA-¹¹¹In)NH₂]-Exendin-4, which is due to its persistence in GLP-1R-expressing cells.

Reduced tumor cell proliferation.

To determine the mechanistic basis of tumor regression exerted by [Lys⁴⁰(Ahx-DTPA-¹¹¹In)NH₂]-Exendin-4 in Rip1Tag2 mice, the rate of tumor cell proliferation was determined by labelling mice with BrdU two hours before sacrifice and visualizing cells in S-phase by immunohistochemical stainings of tumor sections with antibodies against BrdU. In radiopeptide-treated mice, the percentage of BrdU-positive tumor cells declined markedly with increasing radioactivity (Fig. 7.6 A, top panels). In cases where the tumor was not completely ablated, single proliferating tumor cells could still be detected in the tumor rim (Figure 7.6 A, top right panel). The reduction of proliferating tumor cells in treated compared to control mice (%T/C) was 29% for the 28 MBq group (Figure 7.6 C). Analysis of morphologically unaltered normal islets and small hyperplasias revealed few proliferating cells, independent from the injected activity (Figure 7.6 A, bottom panels). The reduction in the rate of BrdU-positive tumor cells argues in favour of a cell cycle arrest in the G1 to S phase. The transition of cells from the G1 to the S phase is dependent on the activity of specific cyclin-dependent kinases and their corresponding cyclins. In β tumor cells of Rip1Tag2 transgenic mice, cyclin D2 is a critical regulator of the G1 to S phase transition (Herzig et al., 2006). Injection of escalating doses of the radiopeptide revealed a significant, dose-dependent loss of cyclin D2 expression in the tumor cells (Fig. 7.6 B and D). These results indicate that treatment with [Lys⁴⁰(Ahx-DTPA-¹¹¹In)NH₂]-

Exendin-4 strongly represses insulinoma cell proliferation, mediated - at least in part - by a loss of cyclin D2 expression in tumor cells.

Figure 7.6: [Lys⁴⁰(Ahx-DTPA-¹¹¹In)NH₂]-Exendin-4 reduces tumor cell proliferation.

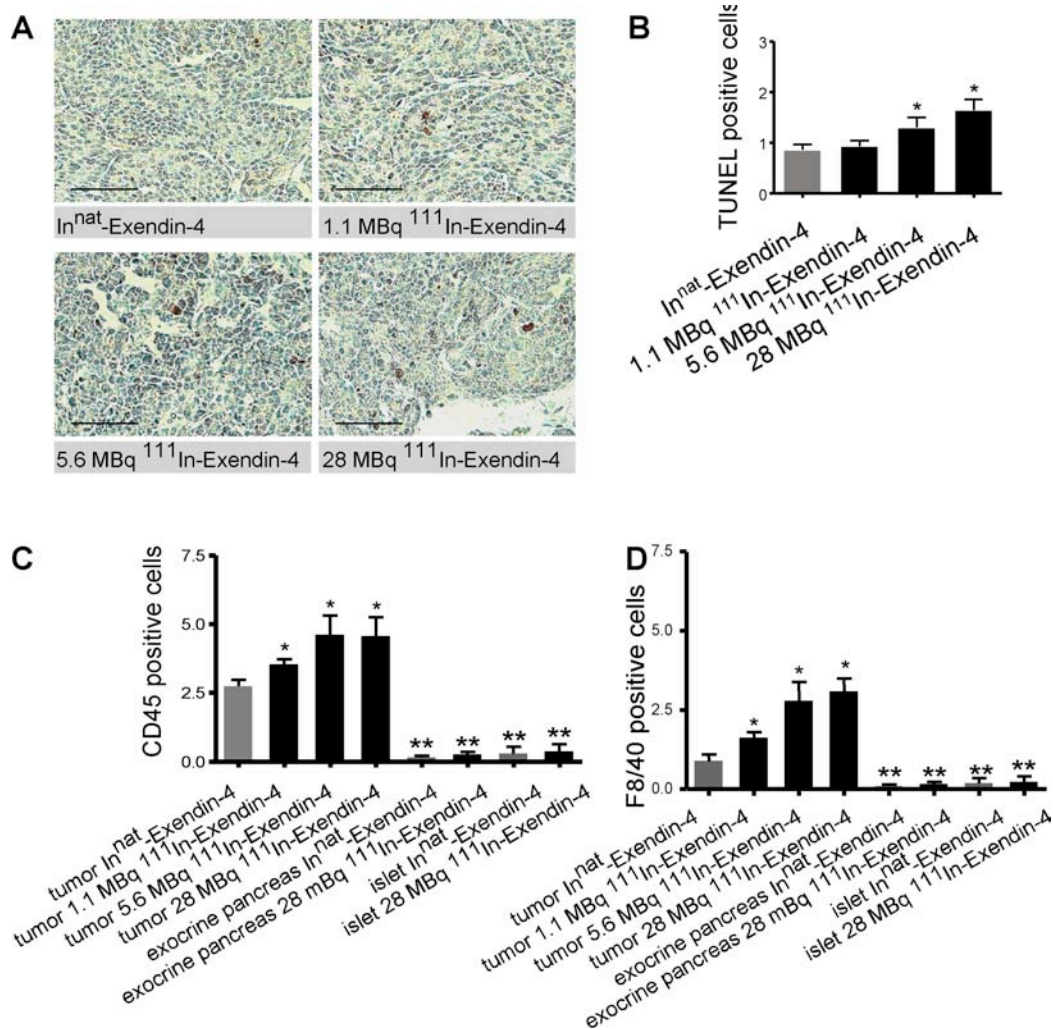


(A) Proliferation of tumor cells was assessed by BrdU staining of pancreas sections eight days after injection of the [Lys⁴⁰(Ahx-DTPA-¹¹¹In)NH₂]-Exendin-4. The staining reveals a dramatic reduction in tumor cell proliferation (top panels). Proliferating tumor cells in the tumor rim are indicated by arrows (inset = higher magnification of the tumor rim). The number of BrdU incorporating cells in normal islets is not affected by the treatment (bottom panels). Size bars = 100 μ m. (B) Immunofluorescence staining of tumor sections for cyclin D₂. The ratio of cyclin D₂ expressing tumor cells is reduced in a dose-dependent manner 8 days after injection of [Lys⁴⁰(Ahx-DTPA-¹¹¹In)NH₂]-Exendin-4. Green = cyclin D₂, blue = DAPI. Size bar = 50 μ m. (C) Quantitation of BrdU incorporation in tumor cells of treated and control mice, as indicated (percentage of total cells; $p < 0.0001$, one-way Anova). (D) Quantitation of cyclin D₂ expressing cells in tumor cells of treated and control mice, as indicated (percentage of total cells; $p = 0.0042$, one-way Anova).

Induction of necrosis and apoptosis

The reduced tumor volumes in Rip1Tag2 mice treated with [Lys⁴⁰(Ahx-DTPA-¹¹¹In)NH₂]-Exendin-4 may also be due to an increase in tumor cell apoptosis and/or necrosis. Quantification of tumor cell apoptosis by TUNEL assay on histological tumor sections revealed an increase of tumor cell apoptosis in a dose-dependent manner (Figure 7.7).

Figure 7.7: Tumor cell death induced by [Lys⁴⁰(Ahx-DTPA-¹¹¹In)NH₂]-Exendin-4 occurs by both apoptosis and necrosis.

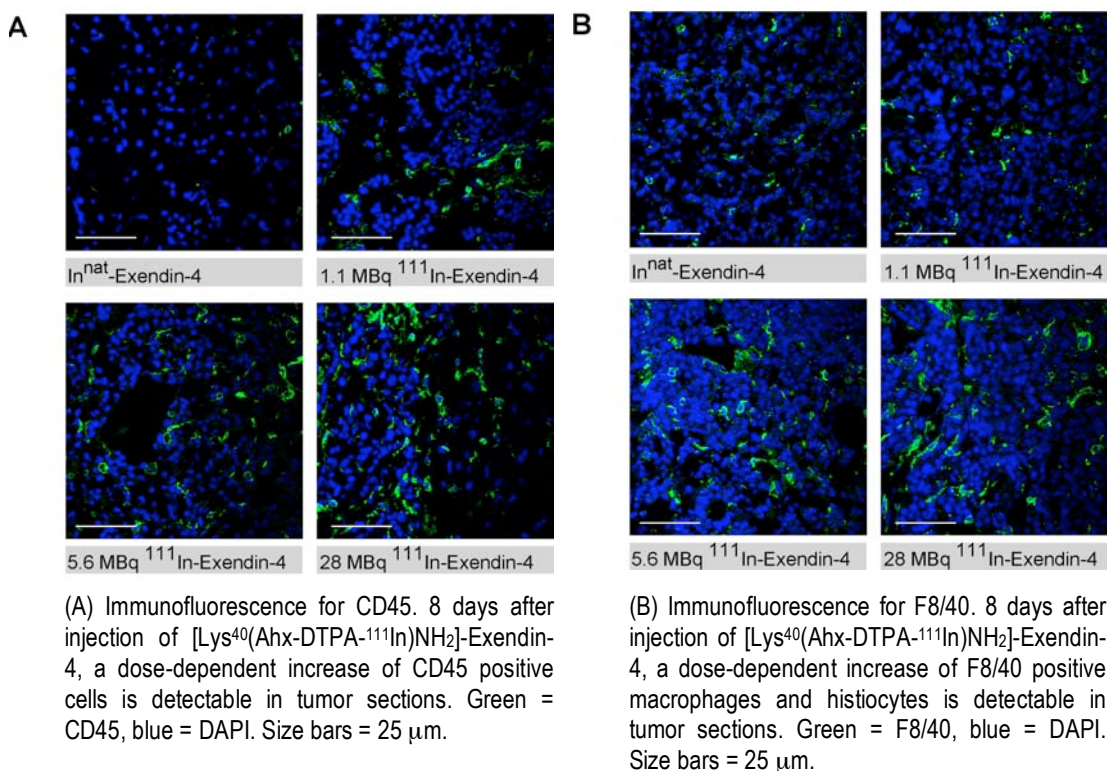


(A) TUNEL staining of tumor sections. More apoptotic cells are visible in the 5.6 and 28 MBq groups than in the In^{nat} and 1.1 MBq groups. Brown = TUNEL positive cells. Size bars = 50 μm. (B) Quantitation of TUNEL-positive cells in tumors of treated and control-treated Rip1Tag2 mice, as indicated. The number of apoptotic tumor cells per 0.1 mm² is 0.85 in the control group, 0.92 in the 1.1 MBq group, 1.30 in the 5.6 MBq group and 1.64 in the 28 MBq group ($p = 0.019$, one-way Anova; Newman-Keuls test: $*p < 0.05$ for the 5.6 and 28 MBq group, and $p > 0.05$ for the 1.1 MBq group). (C) Quantitation of infiltrating CD45-positive cells in tumors, normal islets and exocrine pancreas of control and treated mice, as indicated. In control mice, the number of CD45 positive cells per 0.05 mm² was 2.8, in the 1.1 MBq group 3.6, in the 5.6 MBq group 4.7 and in the 28 MBq group 4.6. No increase in CD45-positive cells could be detected in morphologically normal islets or exocrine pancreas ($p < 0.0001$, one-way anova; Newman-Keuls test: $*p < 0.05$, $**p < 0.01$). (D) Quantitation of F4/80-positive macrophages in tumors, normal islets and exocrine pancreas of Rip1Tag2 mice treated with [Lys⁴⁰(Ahx-DTPA-¹¹¹In)NH₂]-Exendin-4 or non-radioactive In^{nat}-Exendin-4. The increase of tumor-infiltrating immune cells was almost exclusively due to an increase in macrophages. No increase in macrophage numbers could be detected in morphologically normal islets or exocrine pancreas ($p < 0.0001$, one-way anova; Newman-Keuls test: $*p < 0.05$, $**p < 0.01$).

No significant difference could be detected when comparing the control and the 1.1 MBq group, whereas a significant increase of apoptotic cells was observed in the 5.6 MBq and the 28 MBq treatment groups (Figure 7.7 A and B). Quantification of microvessel density by staining of pancreatic sections of mice from all treatment groups with antibodies against CD31 did not reveal any significant differences, suggesting that tumor cell apoptosis was not due to a lack of tumor oxygenation and nutrition (data not shown).

The haemorrhagic and necrotic appearance of treated tumors (Fig. 7.5 B) led us to investigate whether the injection of [Lys⁴⁰(Ahx-DTPA-¹¹¹In)NH₂]-Exendin-4 induced an inflammatory response. Infiltration of leukocytes into tumors was analyzed by staining of pancreatic sections of mice from all study groups with anti-CD45 antibodies eight days after injection of the radiopeptide (Fig. 7.7 C and Fig. 7.8 A). The number of intra-tumoral CD45-positive cells significantly increased with treatment in a dose-dependent manner, whereas no change was evident in the exocrine pancreas or in small non-cancerous islets. Immunofluorescence stainings for different types of immune cells, including CD4, CD8, Gr-1 and F8/40 positive cells, revealed that the numbers of T cells or granulocytes did not change in the tumors of treated mice (data not shown). In contrast, the numbers of F8/40 positive cells increased significantly upon treatment in a dose-dependent manner (Fig. 7.7 D and 7.8 B). A concomitant increase of macrophages was not apparent in the surrounding exocrine tissue and in histologically normal islets.

Figure 7.8: Infiltration of tumors by immune cells after treatment of mice with [Lys⁴⁰(Ahx-DTPA-¹¹¹In)NH₂]-Exendin-4.



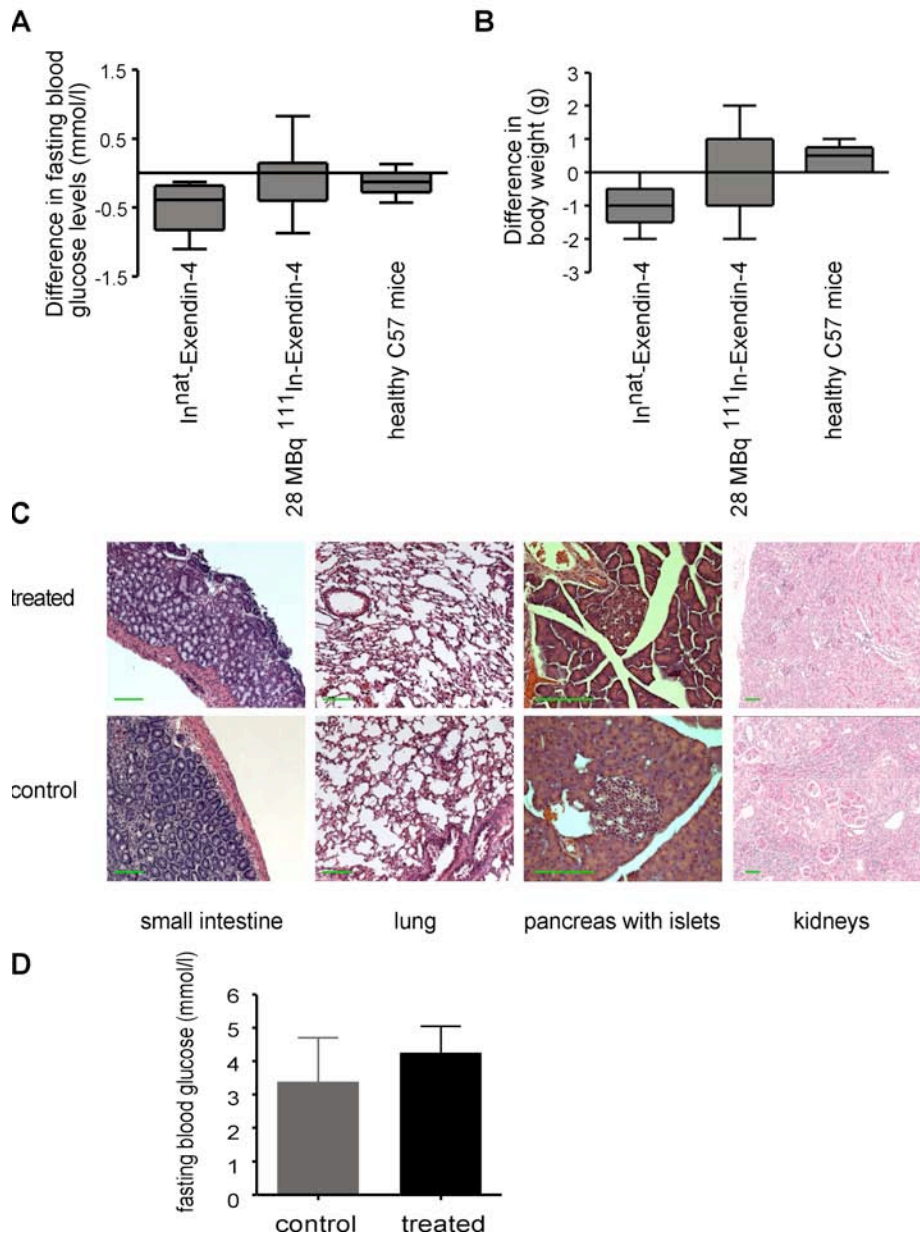
Restoration of glucose homeostasis and body weight

Clinically, human insulinomas present with the symptoms of hypoglycemia. Hence, blood glucose level is an important surrogate marker for the blood insulin concentration of insulinoma patients. A second, more general marker for health is body weight, which is reduced in patients with tumor cachexia. These two important functional readouts can be used to monitor the efficacy of therapies directed against insulinoma. Indeed, in mice treated with 28 MBq [Lys⁴⁰(Ahx-DTPA-¹¹¹In)NH₂]-Exendin-4, a stabilization of glucose levels was observed within eight days after treatment, whereas in the control group glucose levels significantly declined with insulinoma progression (Fig. 7.9 A). In addition, a significant decrease in body weight could be detected in mice of the control group, whereas the weight of animals treated with 28 MBq [Lys⁴⁰(Ahx-DTPA-¹¹¹In)NH₂]-Exendin-4 was stabilized (Fig. 7.9 B). These results show that the anti-tumoral therapy with [Lys⁴⁰(Ahx-DTPA-¹¹¹In)NH₂]-Exendin-4 also exerts a significant impact on both functional control of blood glucose levels and tumor cachexia.

Therapy toxicity

As demonstrated in the dosimetry experiments described above, a significant uptake of [Lys⁴⁰(Ahx-DTPA-¹¹¹In)NH₂]-Exendin-4 was observed in kidney, lung, bowel, total pancreas and tumor. All other organs did not significantly incorporate the radiopeptide. We therefore assessed the general toxicity of the therapy as well as the dose-limiting organ toxicity by investigating morphological changes in these organs following the injection of radiopeptide. To this end, Rip1Tag2 mice and healthy C57Bl/6 mice were injected with 1.1 MBq, 5.6 MBq or 28 MBq of [Lys⁴⁰(Ahx-DTPA-¹¹¹In)NH₂]-Exendin-4 and sacrificed after 3, 10 and 30 days. Due to the continuing expression of the transgenic SV40 large T oncogene, Rip1Tag2 mice start to form new tumors about two weeks after termination of the therapy, thus impeding further analysis of Rip1Tag2 mice at later time-points. Therefore, wildtype C57Bl/6 mice were employed for the analysis at 60 and 180 days, respectively, after injection of [Lys⁴⁰(Ahx-DTPA-¹¹¹In)NH₂]-Exendin-4. Control animals were injected with saline. All animals survived until their sacrifice and did not exhibit any apparent pathophysiological symptoms. Histopathological analysis of bowel, pancreas and lung did not reveal any apparent differences in morphology between control and treated mice, independently from the injected dose and the time point of sacrifice (Figure 7.9 C). In particular, the morphology of pancreatic islets was unaltered between treated and control mice, and no significant differences in blood glucose levels were found (Fig. 7.9 D). These results indicate the absence of any significant toxicity of [Lys⁴⁰(Ahx-DTPA-¹¹¹In)NH₂]-Exendin-4 on normal β -cells. We conclude that this is due to the lower GLP-1R density and thus a reduced uptake of the radiopeptide in normal pancreatic β cells compared to β tumor cells (Wild et al., 2006).

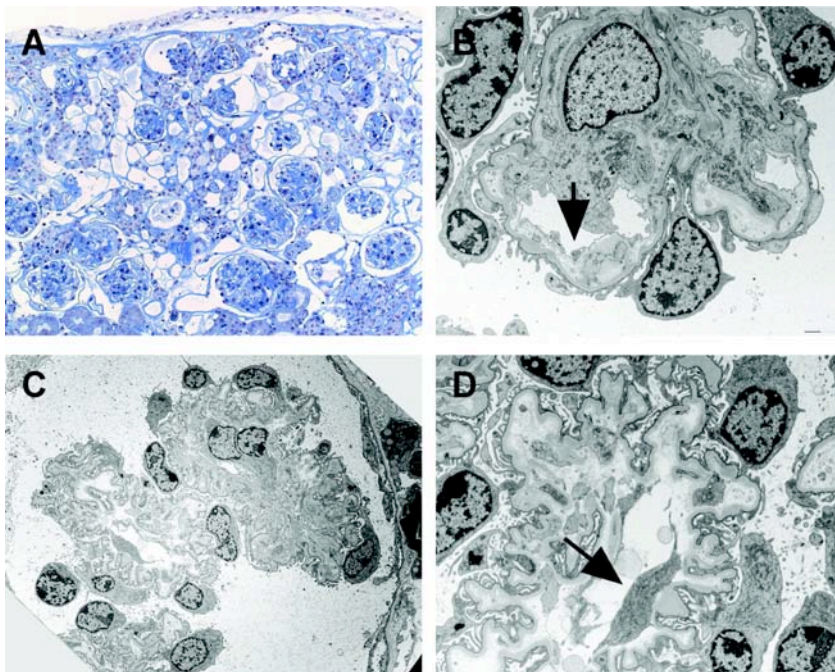
Figure 7.9: Blood glucose levels, body weight and organ toxicity after treatment with [Lys⁴⁰(Ahx-DTPA-¹¹¹In)NH₂]-Exendin-4.



(A) Blood glucose levels in Rip1Tag2 mice treated with [Lys⁴⁰(Ahx-DTPA-¹¹¹In)NH₂]-Exendin-4, non-radioactive In^{nat}-Exendin-4, or not treated at all. Blood glucose levels of the 28 MBq group were restored to normal and comparable to healthy control mice, while blood glucose levels of untreated control mice continued to deteriorate during an eight day observational period after injection of the radiopeptide ($p < 0.05$, Newman-Keuls post-test). (B) Body weights of Rip1Tag2 mice treated with [Lys⁴⁰(Ahx-DTPA-¹¹¹In)NH₂]-Exendin-4, non-radioactive ^{nat}In-Exendin-4, or not treated at all. In the control group, tumor cachexia led to a decrease in body weights during the observational period ($p < 0.05$, Newman-Keuls post-test). In contrast, body weights were stable in the animals treated with [Lys⁴⁰(Ahx-DTPA-¹¹¹In)NH₂]-Exendin-4 and slightly increased in healthy control animals. (C) Histopathological examination of various organs of C57Bl/6 mice, 6 months after injection of 28 MBq [Lys⁴⁰(Ahx-DTPA-¹¹¹In)NH₂]-Exendin-4 or saline (control), as indicated. Small intestine, lung and endo- as well as exocrine pancreas show no morphological signs of toxicity (H&E staining). In contrast, PAS staining of kidney sections reveals signs of chronic radiotoxicity, which manifests itself by glomerular shrinking and compensatory hypertrophy, tubular necrosis, interstitial fibrosis and narrowing of the cortex. Size bars = 100 μ m. (D) Fasting blood glucose levels of C57Bl/6 mice injected with either 28 MBq [Lys⁴⁰(Ahx-DTPA-¹¹¹In)NH₂]-Exendin-4 or saline are not significantly different indicating that treatment with [Lys⁴⁰(Ahx-DTPA-¹¹¹In)NH₂]-Exendin-4 does not affect normal islet physiology and function ($p = 0.21$, two-sided t-test).

However, consistent with the high uptake of radiopeptide in kidney, analysis of kidney sections 180 days after injection of 28 MBq [Lys⁴⁰(Ahx-DTPA-¹¹¹In)NH₂]-Exendin-4 revealed signs of radiation damage. In particular, tubular necrosis, glomerular sclerosis and minor interstitial fibrosis accompanied by an atrophy of the cortex of the kidneys were evident (Fig. 7.9 C). Electron microscopy imaging of these kidneys showed a marked enlargement of the glomerular mesangium, with concomitant signs of glomerular endothelial damage and regeneration. In glomerular capillaries, the lamina rara interna was enlarged considerably, although the other parts of the basal membrane were unaltered (Fig. 7.10 A-D). The tubular epithelium showed signs of cell death and partial denudation of some tubuli, while others were without pathological findings (Fig. 7.11 A-B). However, light microscopy of kidneys after 3, 10, 30 and 60 days and electron microscopy after 30 and 60 days did not reveal any signs of drug toxicity. These findings are therefore consistent with a chronic radiation damage of the kidneys after injection of 28 MBq [Lys⁴⁰(Ahx-DTPA-¹¹¹In)NH₂]-Exendin-4 with a total dose deposition of 56 Gy in the kidneys.

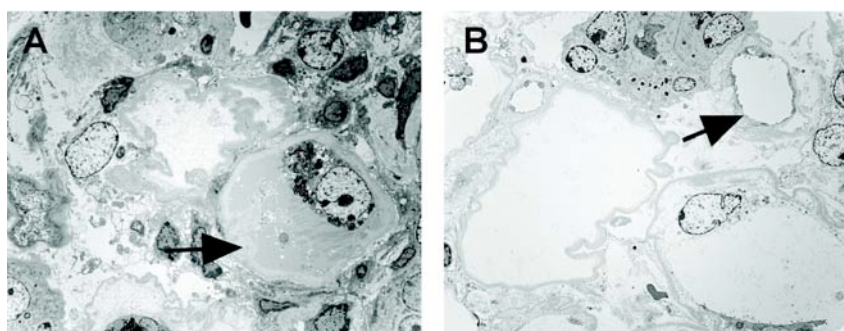
Figure 7.10: Light (LM) and Electron (EM) Microscopy images of mouse kidneys 180 days after injection of 28 MBq of [Lys⁴⁰(Ahx-DTPA-¹¹¹In)NH₂]-Exendin-4. Chronic radiation damage of the glomeruli.



(A) Light microscopic overview of the renal cortex: densely packed glomeruli with mesangial sclerosis, tubular atrophy, and extensive loss of the tubular epithelium (empty spaces). Toluidin blue stain, LM, 200x. **(B)** Glomerulus with prominent thickening of the lamina rara interna of the peripheral basement membrane (arrow). EM, 20'000x. **(C)** Collapsed glomerulus (wrinkling of the capillary basement membranes) and mesangiolytic changes. EM, 10'000x. **(D)** Mesangiolytic changes, i.e., loss of mesangial cells: massive thickening of the lamina rara interna of the basement membrane, basement membrane collapse, severe damage of the endothelium (arrow), resulting in an incomplete endothelial covering of the capillary loop lumen. EM, 20'000x.

Kidney sections of mice treated with 1.1 and 5.6 MBq (corresponding to a dose-deposition of 2.2 and 11.2 Gy, respectively) did not show signs of radiotoxicity at any time-points, although an efficient therapeutic effect on tumor growth was detectable. Together, the results indicate that [Lys⁴⁰(Ahx-DTPA-¹¹¹In)NH₂]-Exendin-4 has a favorable toxicity profile, which is mainly due to its highly specific internalization into tumor cells and its short range of action sparing the healthy tissue surrounding the tumor.

Figure 7.11: Electron (EM) Microscopy images of mouse kidneys 180 days after injection of 28 MBq of [Lys⁴⁰(Ahx-DTPA-¹¹¹In)NH₂]-Exendin-4. Chronic radiation damage of the tubuli.



(A) Massive tubular atrophy partially with tubular basement membrane thickening (arrow) or extensive loss of tubular epithelium. EM, 10'000x. (B) Dilatation of the peritubular capillaries (arrow). EM, 10'000x.

Discussion

Insulinoma, a hormone-active neuroendocrine tumor, is easily diagnosed by metabolic disturbances affecting patients. Yet, while benign insulinoma can be usually cured by surgical resection of the tumor mass, in many cases the usually small tumors are difficult to detect in the pancreas. Moreover, malignant insulinoma with metastatic spread is difficult to treat. The high and specific expression of the glucagon-like peptide-1 receptor (GLP-1R) on insulinoma cells make this surface molecule an attractive target for imaging of the tumors and for novel therapeutic approaches.

Here, we demonstrate that the radiopeptide, [Lys⁴⁰(Ahx-DTPA-¹¹¹In)NH₂]-Exendin-4, efficiently represses insulinoma growth in Rip1Tag2 mice. A single dose of [Lys⁴⁰(Ahx-DTPA-¹¹¹In)NH₂]-Exendin-4 results in a dramatic reduction of tumor burden within a few days without any apparent side effects. Of the many treatment regimen tested in Rip1Tag2 mice, including anti-angiogenic therapies, genetic ablation of tumor-promoting factors, and classical chemotherapy, the current treatment appears to be one of the most efficient, with up to 94% reduction in tumor volume, compared to 67-89% in other studies (Bergers et al., 1999; Parangi et al.,

1996; Christofori et al., 1994; Compagni et al., 2000; Pietras & Hanahan, 2005 and Casanovas et al., 2005).

Cell biological and biochemical analyses reveal that upon treatment tumor cells fail to enter the cell cycle and cease to proliferate. At the same time, tumor cells undergo massive apoptosis and inflammation-mediated necrosis. The development of an inflammatory reaction and subsequent migration of macrophages into the damaged tissue is a typical feature of tumor necrosis. The first cells to migrate in damaged tissue are granulocytes, which usually are the predominant cells during the first 3 days of tissue necrosis. Thereafter, they are replaced by macrophages, which dispose of the necrotic tissue. The marked increase in macrophage numbers observed in tumors of treated mice thus is consistent with tumor cell necrosis. Tumor regression after therapeutic intervention with [Lys⁴⁰(Ahx-DTPA-¹¹¹In)NH₂]-Exendin-4 enables the organism to regain control over the regulation of blood glucose and to normalize metabolism, also evidenced by stabilization of the treated mice's body weights.

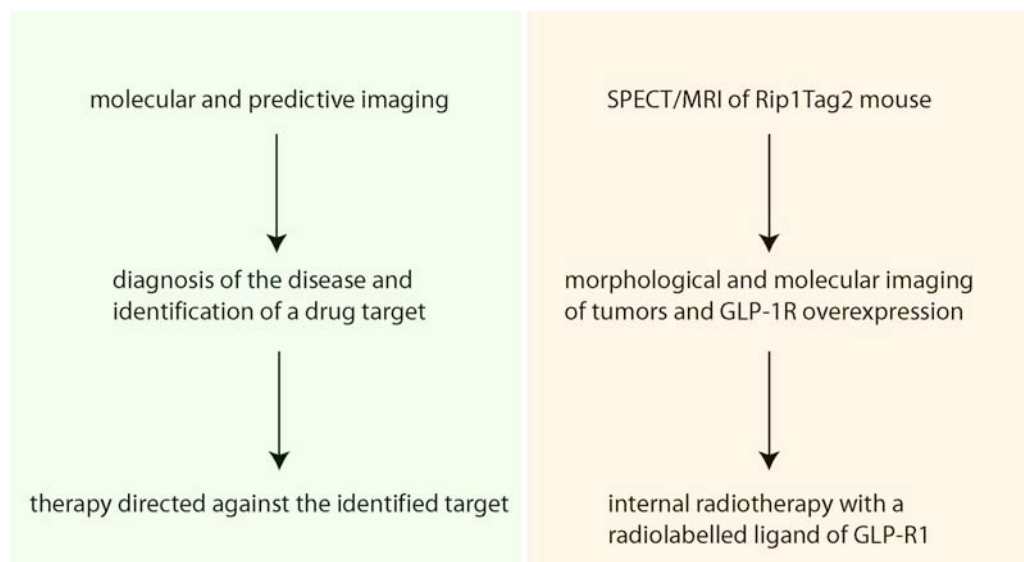
The high density and high specificity of GLP-1R expression in insulinoma cells of Rip1Tag2 mice allow an efficient and highly specific targeting of the tumor cells. The observed increased uptake of radiopeptide per tumor mass at later stages of treatment, when the radiopeptide has already been cleared from the circulation, can be explained by the significant reduction of the tumor volume and phagocytic uptake of apoptotic neighbouring cells, while no significant externalization of the peptide from GLP-1R-expressing tumor cells occurs during this time period (Wild et al., 2006). Other parameters that influence the uptake of the radiopeptide include the cell surface density of GLP-1R, radionuclide sequestration, and changes in tumor blood flow mediated by radiation. A similar phenomenon of tumor-specific uptake of a radiopeptide has been previously reported for a therapeutic dose of 30 MBq [¹⁷⁷Lu-DOTA⁰Tyr³Thr⁸]-octreotide in nude mice bearing a human midgut carcinoid GOT I xenograft (Kolby et al., 2005).

Treatment of mice with the highest dose of 28 MBq, corresponding to a dose deposition of 56 Gy, resulted in detectable morphological changes and in toxic side effects only in kidneys, but not in any other organ analyzed. However, at lower doses, where an efficient therapeutic effect is already apparent, no toxic effects on kidney morphology are detected. Hence, treatment with [Lys⁴⁰(Ahx-DTPA-¹¹¹In)NH₂]-Exendin-4 offers a useful therapeutic window for efficient treatment protocols. External radiation of the kidneys with 23-27 Gy results in kidney failure in 5-50% of treated patients (Emami et al., 1991). Our results are consistent with these findings and underline that kidney toxicity is the dose-limiting factor in the treatment of insulinomas with [Lys⁴⁰(Ahx-DTPA-¹¹¹In)NH₂]-Exendin-4.

8. Conclusions (part II): GLP-1R as a diagnostic and therapeutic target

Human insulinomas are rare tumors, but their diagnosis and treatment poses major clinical problems. Diagnosis is hampered by a lack of sensitivity of both computed tomography and ultrasonography. Therapy is characterized by the absence of a pharmacological alternative to surgery. The identification of the GLP-1R overexpression in human insulinoma opens new avenues towards early diagnosis and efficient treatment of insulinoma. In particular, we envisage the use of molecular and predictive imaging (Figure 8.1). Both molecular and predictive imaging are promising new concepts in the context of cancer diagnosis and therapy. Molecular imaging proves the presence of a molecular marker on the tissue of interest. If this marker has also a predictive value (i.e., it predicts the response to therapy), this modality is called predictive imaging.

Figure 8.1: Molecular imaging, predictive imaging and therapy of insulinoma



We have shown that the approach outlined in figure 8.1 is feasible in a mouse model of human insulinoma. GLP-1R is both a suitable target for molecular imaging as well as for insulinoma therapy. Thus, predictive imaging of insulinoma with [Lys⁴⁰(Ahx-DTPA-¹¹¹In)NH₂]-Exendin-4 reveals the presence of the drug target on the tumor cells, which then are attacked with a radio-labelled agonist of GLP-1R. Based on the high and specific expression of GLP-1R in human insulinoma, this hypothesis can now be tested in a clinical setting. Our findings also underline that Auger emitters, in particular ¹¹¹In, are potent therapeutic agents if an adequate delivery of the radiopeptide into cancer cells can be achieved. Moreover, targeting an Auger-emitter-tagged radiopeptide to cancer cells may contribute to implementing a therapy with a minimum of associated toxicity.

Outlook

Identification of new specific cell surface markers and intracellular signaling pathways is a promising strategy against cancer. Using molecular imaging, we can not only map cell surface molecules but also oncogenic pathways. In the future, the signature of oncogenic pathways in human cancers may also guide the choice of an appropriate targeted therapy (Bild et al., 2006). To achieve this goal, cancer must be diagnosed on the basis of the underlying etiology and pathogenesis, taking into account the interplay of different signaling pathways. A first step is the global analysis of cell signaling in cancer. Experiments in yeast demonstrate the feasibility of this approach, and – on a somewhat smaller scale - the profiling of phospho-protein networks in hematological malignancies is already possible (Ptacek et al., 2005 and Irish et al., 2004). In a second step, it should become possible to determine the global signaling profile of a tumor from a biopsy, while selected markers or pathways are visualized by molecular and predictive imaging *in vivo*. A diagnosis based on these foundations might then be followed by a very specific and adaptable targeted therapy.

References

- Ahlgren, U, J Jonsson, L Jonsson, K Simu, & H Edlund, 'beta-cell-specific inactivation of the mouse *Ipf1/Pdx1* gene results in loss of the beta-cell phenotype and maturity onset diabetes.', *Genes Dev* vol. 12, no. 12, 1998, pp. 1763-1768.
- Al-Hajj, M, MW Becker, M Wicha, I Weissman, & MF Clarke, 'Therapeutic implications of cancer stem cells.', *Curr Opin Genet Dev* vol. 14, no. 1, 2004, pp. 43-47.
- Angelini, L, M Bezzi, G Tucci, MM Lirici, F Candiani, L Rubaltelli, C Tremolada, G Tamburrano, & G Fegiz, 'The ultrasonic detection of insulinomas during surgical exploration of the pancreas.', *World J Surg* vol. 11, no. 5, 1987, pp. 642-647.
- Bartkova, J, Z Horejsi, K Koed, A Kramer, F Tort, K Zieger, P Guldborg, M Sehested, JM Nesland, C Lukas, T Orntoft, J Lukas, & J Bartek, 'DNA damage response as a candidate anti-cancer barrier in early human tumorigenesis.', *Nature* vol. 434, no. 7035, 2005, pp. 864-870.
- Behr, TM, M Behe, M Lohr, G Sgouros, C Angerstein, E Wehrmann, K Nebendahl, & W Becker, 'Therapeutic advantages of Auger electron- over beta-emitting radiometals or radioiodine when conjugated to internalizing antibodies.', *Eur J Nucl Med* vol. 27, no. 7, 2000, pp. 753-765.
- Behr, TM, & DM Goldenberg, 'Improved prospects for cancer therapy with radiolabeled antibody fragments and peptides?', *J Nucl Med* vol. 37, no. 5, 1996, pp. 834-836.
- Bell, CD, & E Waizbard, 'Variability of cell size in primary and metastatic human breast carcinoma.', *Invasion Metastasis* vol. 6, no. 1, 1986, pp. 11-20.
- Bergers, G, K Javaherian, KM Lo, J Folkman, & D Hanahan, 'Effects of angiogenesis inhibitors on multistage carcinogenesis in mice.', *Science* vol. 284, no. 5415, 1999, pp. 808-812.
- Bhowmick, NA, A Chytil, D Plieth, AE Gorska, N Dumont, S Shappell, MK Washington, EG Neilson, & HL Moses, 'TGF-beta signaling in fibroblasts modulates the oncogenic potential of adjacent epithelia.', *Science* vol. 303, no. 5659, 2004, pp. 848-851.
- Bild, AH, G Yao, JT Chang, Q Wang, A Potti, D Chasse, MB Joshi, D Harpole, JM Lancaster, A Berchuck, JAJ Olson, JR Marks, HK Dressman, M West, & JR Nevins, 'Oncogenic pathway signatures in human cancers as a guide to targeted therapies.', *Nature* vol. 439, no. 7074, 2006, pp. 353-357.
- Brabletz, T, A Jung, S Reu, M Porzner, F Hlubek, LA Kunz-Schughart, R Knuechel, & T Kirchner, 'Variable beta-catenin expression in colorectal cancers indicates tumor progression driven by the tumor environment.', *Proc Natl Acad Sci U S A* vol. 98, no. 18, 2001, pp. 10356-10361.
- Breiteneder-Geleff, S, A Soleiman, H Kowalski, R Horvat, G Amann, E Kriehuber, K Diem, W Weninger, E Tschachler, K Alitalo, & D Kerjaschki, 'Angiosarcomas express mixed endothelial phenotypes of blood and lymphatic capillaries: podoplanin as a specific marker for lymphatic endothelium.', *Am J Pathol* vol. 154, no. 2, 1999, pp. 385-394.
- Brodeur, GM, 'Neuroblastoma: biological insights into a clinical enigma.', *Nat Rev Cancer* vol. 3, no. 3, 2003, pp. 203-216.
- Brown, DM, & E Ruoslahti, 'Metadherin, a cell surface protein in breast tumors that mediates lung metastasis.', *Cancer Cell* vol. 5, no. 4, 2004, pp. 365-374.
- Calabrese, C, H Poppleton, M Kocak, TL Hogg, C Fuller, B Hamner, EY Oh, MW Gaber, D Finklestein, M Allen, A Frank, IT Bayazitov, SS Zakharenko, A Gajjar, A Davidoff, & RJ Gilbertson, 'A perivascular niche for brain tumor stem cells.', *Cancer Cell* vol. 11, no. 1, 2007, pp. 69-82.
- Casanovas, O, DJ Hicklin, G Bergers, & D Hanahan, 'Drug resistance by evasion of antiangiogenic targeting of VEGF signaling in late-stage pancreatic islet tumors.', *Cancer Cell* vol. 8, no. 4, 2005, pp. 299-309.
- Cavallaro, U, & G Christofori, 'Cell adhesion and signalling by cadherins and Ig-CAMs in cancer.', *Nat Rev Cancer* vol. 4, no. 2, 2004, pp. 118-132.
- Cavallaro, U, B Schaffhauser, & G Christofori, 'Cadherins and the tumour progression: is it all in a switch?', *Cancer Lett* vol. 176, no. 2, 2002, pp. 123-128.
- Chammas, NK, JD Teale, & JD Quin, 'Insulinoma: how reliable is the biochemical evidence?', *Ann Clin Biochem* vol. 40, no. Pt 6, 2003, pp. 689-693.
- Chen, P, J Wang, K Hope, L Jin, J Dick, R Cameron, J Brandwein, M Minden, & RM Reilly, 'Nuclear localizing sequences promote nuclear translocation and enhance the radiotoxicity of the anti-CD33 monoclonal antibody HuM195 labeled with ¹¹¹In in human

- myeloid leukemia cells.', *J Nucl Med* vol. 47, no. 5, 2006, pp. 827-836.
- Christofori, G, P Naik, & D Hanahan, 'A second signal supplied by insulin-like growth factor II in oncogene-induced tumorigenesis.', *Nature* vol. 369, no. 6479, 1994, pp. 414-418.
- Cianchi, F, L Messerini, A Palomba, V Boddi, G Perigli, F Pucciani, P Bechi, & C Cortesini, 'Character of the invasive margin in colorectal cancer: does it improve prognostic information of Dukes staging?', *Dis Colon Rectum* vol. 40, no. 10, 1997, pp. 1170-5; discussion 1175-6.
- Coiffier, B, E Lepage, J Briere, R Herbrecht, H Tilly, R Bouabdallah, P Morel, E Van Den Neste, G Salles, P Gaulard, F Reyes, P Lederlin, & C Gisselbrecht, 'CHOP chemotherapy plus rituximab compared with CHOP alone in elderly patients with diffuse large-B-cell lymphoma.', *N Engl J Med* vol. 346, no. 4, 2002, pp. 235-242.
- Compagni, A, P Wilgenbus, MA Impagnatiello, M Cotten, & G Christofori, 'Fibroblast growth factors are required for efficient tumor angiogenesis.', *Cancer Res* vol. 60, no. 24, 2000, pp. 7163-7169.
- Condeelis, J, & JW Pollard, 'Macrophages: obligate partners for tumor cell migration, invasion, and metastasis.', *Cell* vol. 124, no. 2, 2006, pp. 263-266.
- Condeelis, J, & JE Segall, 'Intravital imaging of cell movement in tumours.', *Nat Rev Cancer* vol. 3, no. 12, 2003, pp. 921-930.
- Criscuoli, ML, M Nguyen, & BP Eliceiri, 'Tumor metastasis but not tumor growth is dependent on Src-mediated vascular permeability.', *Blood* vol. 105, no. 4, 2005, pp. 1508-1514.
- Cutler, DM, AB Rosen, & S Vijan, 'The value of medical spending in the United States, 1960-2000.', *N Engl J Med* vol. 355, no. 9, 2006, pp. 920-927.
- Daniel, JM, & AB Reynolds, 'The catenin p120(ctn) interacts with Kaiso, a novel BTB/POZ domain zinc finger transcription factor.', *Mol Cell Biol* vol. 19, no. 5, 1999, pp. 3614-3623.
- d'Ortho, MP, H Stanton, M Butler, SJ Atkinson, G Murphy, & RM Hembry, 'MT1-MMP on the cell surface causes focal degradation of gelatin films.', *FEBS Lett* vol. 421, no. 2, 1998, pp. 159-164.
- de Visser, KE, A Eichten, & LM Coussens, 'Paradoxical roles of the immune system during cancer development.', *Nat Rev Cancer* vol. 6, no. 1, 2006, pp. 24-37.
- Derksen, PW, X Liu, F Saridin, H van der Gulden, J Zevenhoven, B Evers, JR van Beijnum, AW Griffioen, J Vink, P Krimpenfort, JL Peterse, RD Cardiff, A Berns, & J Jonkers, 'Somatic inactivation of E-cadherin and p53 in mice leads to metastatic lobular mammary carcinoma through induction of anoikis resistance and angiogenesis.', *Cancer Cell* vol. 10, no. 5, 2006, pp. 437-449.
- Dormond, O, A Foletti, C Paroz, & C Ruegg, 'NSAIDs inhibit alpha V beta 3 integrin-mediated and Cdc42/Rac-dependent endothelial-cell spreading, migration and angiogenesis.', *Nat Med* vol. 7, no. 9, 2001, pp. 1041-1047.
- Emami, B, J Lyman, A Brown, L Coia, M Goitein, JE Munzenrider, B Shank, LJ Solin, & M Wesson, 'Tolerance of normal tissue to therapeutic irradiation.', *Int J Radiat Oncol Biol Phys* vol. 21, no. 1, 1991, pp. 109-122.
- Farr, AG, ML Berry, A Kim, AJ Nelson, MP Welch, & A Aruffo, 'Characterization and cloning of a novel glycoprotein expressed by stromal cells in T-dependent areas of peripheral lymphoid tissues.', *J Exp Med* vol. 176, no. 5, 1992, pp. 1477-1482.
- Fedi P, Tronick SR, Aaronson SA, 'Growth factors' in BRC Holland JF, Morton DL, Frei E, Kufe DW, Weichselbaum RR (ed.), *Cancer Medicine*, Williams and Wilkins, Baltimore, 1997, pp. 41-64.
- Fidler, IJ, 'The pathogenesis of cancer metastasis: the 'seed and soil' hypothesis revisited.', *Nat Rev Cancer* vol. 3, no. 6, 2003, pp. 453-458.
- Firtel, RA, & R Meili, 'Dictyostelium: a model for regulated cell movement during morphogenesis.', *Curr Opin Genet Dev* vol. 10, no. 4, 2000, pp. 421-427.
- Friedl, P, S Borgmann, & EB Brouck, 'Amoeboid leukocyte crawling through extracellular matrix: lessons from the Dictyostelium paradigm of cell movement.', *J Leukoc Biol* vol. 70, no. 4, 2001, pp. 491-509.
- Friedl, P, Y Hegerfeldt, & M Tusch, 'Collective cell migration in morphogenesis and cancer.', *Int J Dev Biol* vol. 48, no. 5-6, 2004, pp. 441-449.
- Friedl, P, PB Noble, PA Walton, DW Laird, PJ Chauvin, RJ Tabah, M Black, & KS Zanker, 'Migration of coordinated cell clusters in mesenchymal and epithelial cancer explants in vitro.', *Cancer Res* vol. 55, no. 20, 1995, pp. 4557-4560.
- Friedl, P, & K Wolf, 'Tumour-cell invasion and migration: diversity and escape mechanisms.',

- Nat Rev Cancer* vol. 3, no. 5, 2003, pp. 362-374.
- Friedl, P, KS Zanker, & EB Brocker, 'Cell migration strategies in 3-D extracellular matrix: differences in morphology, cell matrix interactions, and integrin function.', *Microsc Res Tech* vol. 43, no. 5, 1998, pp. 369-378.
- Fukata, M, M Nakagawa, & K Kaibuchi, 'Roles of Rho-family GTPases in cell polarisation and directional migration.', *Curr Opin Cell Biol* vol. 15, no. 5, 2003, pp. 590-597.
- Gadea, G, L Lapasset, C Gauthier-Rouviere, & P Roux, 'Regulation of Cdc42-mediated morphological effects: a novel function for p53.', *EMBO J* vol. 21, no. 10, 2002, pp. 2373-2382.
- Gasic, GJ, TB Gasic, & S Murphy, 'Anti-metastatic effect of aspirin.', *Lancet* vol. 2, no. 7783, 1972, pp. 932-933.
- Gavert, N, M Conacci-Sorrell, D Gast, A Schneider, P Altevogt, T Brabletz, & A Ben-Ze'ev, 'L1, a novel target of beta-catenin signaling, transforms cells and is expressed at the invasive front of colon cancers.', *J Cell Biol* vol. 168, no. 4, 2005, pp. 633-642.
- Goddu, SM, RW Howell, & DV Rao, 'Cellular dosimetry: absorbed fractions for monoenergetic electron and alpha particle sources and S-values for radionuclides uniformly distributed in different cell compartments.', *J Nucl Med* vol. 35, no. 2, 1994, pp. 303-316.
- Gonzalez, RF, & LG Dobbs, 'Purification and analysis of RT140, a type I alveolar epithelial cell apical membrane protein.', *Biochim Biophys Acta* vol. 1429, no. 1, 1998, pp. 208-216.
- Gotthardt, M, M Fischer, I Naeher, JB Holz, H Jungclas, HW Fritsch, M Behe, B Goke, K Joseph, & TM Behr, 'Use of the incretin hormone glucagon-like peptide-1 (GLP-1) for the detection of insulinomas: initial experimental results.', *Eur J Nucl Med Mol Imaging* vol. 29, no. 5, 2002, pp. 597-606.
- Gouya, H, O Vignaux, J Augui, B Dousset, L Palazzo, A Louvel, S Chaussade, & P Legmann, 'CT, endoscopic sonography, and a combined protocol for preoperative evaluation of pancreatic insulinomas.', *AJR Am J Roentgenol* vol. 181, no. 4, 2003, pp. 987-992.
- Greenburg, G, & ED Hay, 'Epithelia suspended in collagen gels can lose polarity and express characteristics of migrating mesenchymal cells.', *J Cell Biol* vol. 95, no. 1, 1982, pp. 333-339.
- Grunert, S, M Jechlinger, & H Beug, 'Diverse cellular and molecular mechanisms contribute to epithelial plasticity and metastasis.', *Nat Rev Mol Cell Biol* vol. 4, no. 8, 2003, pp. 657-665.
- Gupta, GP, & J Massague, 'Cancer metastasis: building a framework.', *Cell* vol. 127, no. 4, 2006, pp. 679-695.
- Hanahan, D, 'Heritable formation of pancreatic beta-cell tumours in transgenic mice expressing recombinant insulin/simian virus 40 oncogenes.', *Nature* vol. 315, no. 6015, 1985, pp. 115-122.
- Hanahan, D, & RA Weinberg, 'The hallmarks of cancer.', *Cell* vol. 100, no. 1, 2000, pp. 57-70.
- Harris, AL, 'Hypoxia--a key regulatory factor in tumour growth.', *Nat Rev Cancer* vol. 2, no. 1, 2002, pp. 38-47.
- Hayflick, L, 'Mortality and immortality at the cellular level. A review.', *Biochemistry (Mosc)* vol. 62, no. 11, 1997, pp. 1180-1190.
- Hegerfeldt, Y, M Tusch, EB Brocker, & P Friedl, 'Collective cell movement in primary melanoma explants: plasticity of cell-cell interaction, beta1-integrin function, and migration strategies.', *Cancer Res* vol. 62, no. 7, 2002, pp. 2125-2130.
- Henderson, TO, J Whitton, M Stovall, AC Mertens, P Mitby, D Friedman, LC Strong, S Hammond, JP Neglia, AT Meadows, L Robison, & L Diller, 'Secondary sarcomas in childhood cancer survivors: a report from the Childhood Cancer Survivor Study.', *J Natl Cancer Inst* vol. 99, no. 4, 2007, pp. 300-308.
- Herzig, M, F Savarese, M Novatchkova, H Semb, & G Christofori, 'Tumor progression induced by the loss of E-cadherin independent of beta-catenin/Tcf-mediated Wnt signaling.', *Oncogene* 2006,
- Higgins, JM, DA Mandlebrot, SK Shaw, GJ Russell, EA Murphy, YT Chen, WJ Nelson, CM Parker, & MB Brenner, 'Direct and regulated interaction of integrin alphaEbeta7 with E-cadherin.', *J Cell Biol* vol. 140, no. 1, 1998, pp. 197-210.
- Hirohashi, S, & Y Kanai, 'Cell adhesion system and human cancer morphogenesis.', *Cancer Sci* vol. 94, no. 7, 2003, pp. 575-581.
- Hirshberg, B, C Cochran, MC Skarulis, SK Libutti, HR Alexander, BJ Wood, R Chang, DE Kleiner, & P Gorden, 'Malignant insulinoma: spectrum of unusual clinical features.', *Cancer* vol. 104, no. 2, 2005, pp. 264-272.

- Hsu, MY, MJ Wheelock, KR Johnson, & M Herlyn, 'Shifts in cadherin profiles between human normal melanocytes and melanomas.', *J Investig Dermatol Symp Proc* vol. 1, no. 2, 1996, pp. 188-194.
- Huber, MA, N Kraut, & H Beug, 'Molecular requirements for epithelial-mesenchymal transition during tumor progression.', *Curr Opin Cell Biol* vol. 17, no. 5, 2005, pp. 548-558.
- Hunter, KW, 'Ezrin, a key component in tumor metastasis.', *Trends Mol Med* vol. 10, no. 5, 2004, pp. 201-204.
- Imai, K, & A Takaoka, 'Comparing antibody and small-molecule therapies for cancer.', *Nat Rev Cancer* vol. 6, no. 9, 2006, pp. 714-727.
- Irish, JM, R Hovland, PO Krutzik, OD Perez, O Bruserud, BT Gjertsen, & GP Nolan, 'Single cell profiling of potentiated phospho-protein networks in cancer cells.', *Cell* vol. 118, no. 2, 2004, pp. 217-228.
- Ivetic, A, & AJ Ridley, 'Ezrin/radixin/moesin proteins and Rho GTPase signalling in leucocytes.', *Immunology* vol. 112, no. 2, 2004, pp. 165-176.
- Izawa, I, M Amano, K Chihara, T Yamamoto, & K Kaibuchi, 'Possible involvement of the inactivation of the Rho-Rho-kinase pathway in oncogenic Ras-induced transformation.', *Oncogene* vol. 17, no. 22, 1998, pp. 2863-2871.
- Jaaskela-Saari, HA, R Grenman, HA Ramsay, J Tarkkanen, T Paavonen, & KJ Kairemo, 'Indium-111-bleomycin complex in squamous cell cancer xenograft tumors of nude mice.', *Cancer Biother Radiopharm* vol. 20, no. 4, 2005, pp. 426-435.
- Kalluri, R, & M Zeisberg, 'Fibroblasts in cancer.', *Nat Rev Cancer* vol. 6, no. 5, 2006, pp. 392-401.
- Kaplan, RN, RD Riba, S Zacharoulis, AH Bramley, L Vincent, C Costa, DD MacDonald, DK Jin, K Shido, SA Kerns, Z Zhu, D Hicklin, Y Wu, JL Port, N Altorki, ER Port, D Ruggero, SV Shmelkov, KK Jensen, S Rafii, & D Lyden, 'VEGFR1-positive haematopoietic bone marrow progenitors initiate the pre-metastatic niche.', *Nature* vol. 438, no. 7069, 2005, pp. 820-827.
- Kassis AI, HRW, Sasry KSR, Adelstein SJ., 'Positional effects of Auger decays in mammalian cells in culture.' in CDE Baverstock KF (ed.), *DNA damage by Auger emitters*, Taylor & Francis, London, 1988, pp. 1-14.
- Kato, Y, M Kaneko, M Sata, N Fujita, T Tsuruo, & M Osawa, 'Enhanced expression of Aggrus (T1alpha/podoplanin), a platelet-aggregation-inducing factor in lung squamous cell carcinoma.', *Tumour Biol* vol. 26, no. 4, 2005, pp. 195-200.
- Kereiakes, JG, & DV Rao, 'Auger electron dosimetry: report of AAPM Nuclear Medicine Committee Task Group No. 6.', *Med Phys* vol. 19, no. 6, 1992, pp. 1359.
- Khanna, C, X Wan, S Bose, R Cassaday, O Olomu, A Mendoza, C Yeung, R Gorlick, SM Hewitt, & LJ Helman, 'The membrane-cytoskeleton linker ezrin is necessary for osteosarcoma metastasis.', *Nat Med* vol. 10, no. 2, 2004, pp. 182-186.
- Kimura, N, & I Kimura, 'Podoplanin as a marker for mesothelioma.', *Pathol Int* vol. 55, no. 2, 2005, pp. 83-86.
- Kolby, L, P Bernhardt, V Johanson, A Schmitt, H Ahlman, E Forssell-Aronsson, H Macke, & O Nilsson, 'Successful receptor-mediated radiation therapy of xenografted human midgut carcinoid tumour.', *Br J Cancer* vol. 93, no. 10, 2005, pp. 1144-1151.
- Krause, DS, & RA Van Etten, 'Tyrosine kinases as targets for cancer therapy.', *N Engl J Med* vol. 353, no. 2, 2005, pp. 172-187.
- Krenning, EP, DJ Kwekkeboom, WH Bakker, WA Breeman, PP Kooij, HY Oei, M van Hagen, PT Postema, M de Jong, JC Reubi, & a et, 'Somatostatin receptor scintigraphy with [¹¹¹In-DTPA-D-Phe1]- and [¹²³I-Tyr3]-octreotide: the Rotterdam experience with more than 1000 patients.', *Eur J Nucl Med* vol. 20, no. 8, 1993, pp. 716-731.
- Krenning, EP, DJ Kwekkeboom, JC Reubi, PM van Hagen, CH van Eijck, HY Oei, & SW Lamberts, '¹¹¹In-octreotide scintigraphy in oncology.', *Digestion* vol. 54 Suppl 1, 1993, pp. 84-87.
- Krenning, EP, DJ Kwekkeboom, R Valkema, S Pauwels, LK Kvols, & M De Jong, 'Peptide receptor radionuclide therapy.', *Ann N Y Acad Sci* vol. 1014, 2004, pp. 234-245.
- Kreymann, B, G Williams, MA Ghatei, & SR Bloom, 'Glucagon-like peptide-1 7-36: a physiological incretin in man.', *Lancet* vol. 2, no. 8571, 1987, pp. 1300-1304.
- Labosky, PA, DP Barlow, & BL Hogan, 'Embryonic germ cell lines and their derivation from mouse primordial germ cells.', *Ciba Found Symp* vol. 182, 1994, pp. 157-68; discussion 168-78.
- Lan, M, T Kojima, M Murata, M Osanai, K Takano, H Chiba, & N Sawada, 'Phosphorylation of

- ezrin enhances microvillus length via a p38 MAP-kinase pathway in an immortalized mouse hepatic cell line.', *Exp Cell Res* vol. 312, no. 2, 2006, pp. 111-120.
- Larue, L, M Ohsugi, J Hirchenhain, & R Kemler, 'E-cadherin null mutant embryos fail to form a trophectoderm epithelium.', *Proc Natl Acad Sci U S A* vol. 91, no. 17, 1994, pp. 8263-8267.
- Lauffenburger, DA, & AF Horwitz, 'Cell migration: a physically integrated molecular process.', *Cell* vol. 84, no. 3, 1996, pp. 359-369.
- Lee, JM, S Dedhar, R Kalluri, & EW Thompson, 'The epithelial-mesenchymal transition: new insights in signaling, development, and disease.', *J Cell Biol* vol. 172, no. 7, 2006, pp. 973-981.
- Li, G, & M Herlyn, 'Dynamics of intercellular communication during melanoma development.', *Mol Med Today* vol. 6, no. 4, 2000, pp. 163-169.
- Locascio, A, & MA Nieto, 'Cell movements during vertebrate development: integrated tissue behaviour versus individual cell migration.', *Curr Opin Genet Dev* vol. 11, no. 4, 2001, pp. 464-469.
- Loevinger, R, 'MIRD Primer for Absorbed Dose Calculations.', *Society of Nuclear Medicine*, 1988.
- Marambaud, P, PH Wen, A Dutt, J Shioi, A Takashima, R Siman, & NK Robakis, 'A CBP binding transcriptional repressor produced by the PS1/epsilon-cleavage of N-cadherin is inhibited by PS1 FAD mutations.', *Cell* vol. 114, no. 5, 2003, pp. 635-645.
- Martin-Villar, E, D Megias, S Castel, MM Yurrita, S Vilaro, & M Quintanilla, 'Podoplanin binds ERM proteins to activate RhoA and promote epithelial-mesenchymal transition.', *J Cell Sci* vol. 119, no. Pt 21, 2006, pp. 4541-4553.
- Martin-Villar, E, FG Scholl, C Gamallo, MM Yurrita, M Munoz-Guerra, J Cruces, & M Quintanilla, 'Characterization of human PA2.26 antigen (T1alpha-2, podoplanin), a small membrane mucin induced in oral squamous cell carcinomas.', *Int J Cancer* vol. 113, no. 6, 2005, pp. 899-910.
- Matsui, T, M Maeda, Y Doi, S Yonemura, M Amano, K Kaibuchi, S Tsukita, & S Tsukita, 'Rho-kinase phosphorylates COOH-terminal threonines of ezrin/radixin/moesin (ERM) proteins and regulates their head-to-tail association.', *J Cell Biol* vol. 140, no. 3, 1998, pp. 647-657.
- Mayo, KE, LJ Miller, D Bataille, S Dalle, B Goke, B Thorens, & DJ Drucker, 'International Union of Pharmacology. XXXV. The glucagon receptor family.', *Pharmacol Rev* vol. 55, no. 1, 2003, pp. 167-194.
- McClatchey, AI, 'Merlin and ERM proteins: unappreciated roles in cancer development?', *Nat Rev Cancer* vol. 3, no. 11, 2003, pp. 877-883.
- Mehlen, P, & A Puisieux, 'Metastasis: a question of life or death.', *Nat Rev Cancer* vol. 6, no. 6, 2006, pp. 449-458.
- Mehta, P, 'Potential role of platelets in the pathogenesis of tumor metastasis.', *Blood* vol. 63, no. 1, 1984, pp. 55-63.
- Michel, RB, PM Andrews, ME Castillo, & MJ Mattes, 'In vitro cytotoxicity of carcinoma cells with ¹¹¹In-labeled antibodies to HER-2.', *Mol Cancer Ther* vol. 4, no. 6, 2005, pp. 927-937.
- Minchinton, AI, & IF Tannock, 'Drug penetration in solid tumours.', *Nat Rev Cancer* vol. 6, no. 8, 2006, pp. 583-592.
- Modlin, IM, & LH Tang, 'Approaches to the diagnosis of gut neuroendocrine tumors: the last word (today).', *Gastroenterology* vol. 112, no. 2, 1997, pp. 583-590.
- Mohr, U, '*International Classification of Rodent Tumors: The Mouse*, Springer, Berlin, New York, 2001.
- Moré, JJ, 'The Levenberg-Marquardt Algorithm: Implementation and Theory.' in G Watson (ed.), *Lecture Notes in Mathematics*, 1978,
- Moré, JJ, Garbow BS, Hillstrom KE, 'Testing Unconstrained Optimization Software', *ACM Transactions and Mathematical Software* vol. Vol 7, No 1; 17-41, 1981,
- Nabeshima, K, T Inoue, Y Shimao, H Kataoka, & M Koono, 'Cohort migration of carcinoma cells: differentiated colorectal carcinoma cells move as coherent cell clusters or sheets.', *Histol Histopathol* vol. 14, no. 4, 1999, pp. 1183-1197.
- Nabeshima, K, T Inoue, Y Shimao, Y Okada, Y Itoh, M Seiki, & M Koono, 'Front-cell-specific expression of membrane-type 1 matrix metalloproteinase and gelatinase A during cohort migration of colon carcinoma cells induced by hepatocyte growth factor/scatter factor.', *Cancer Res* vol. 60, no. 13, 2000, pp. 3364-3369.

- Nabeshima, K, T Moriyama, Y Asada, N Komada, T Inoue, H Kataoka, A Sumiyoshi, & M Koono, 'Ultrastructural study of TPA-induced cell motility: human well-differentiated rectal adenocarcinoma cells move as coherent sheets via localized modulation of cell-cell adhesion.', *Clin Exp Metastasis* vol. 13, no. 6, 1995, pp. 499-508.
- Nash, GF, LF Turner, MF Scully, & AK Kakkar, 'Platelets and cancer.', *Lancet Oncol* vol. 3, no. 7, 2002, pp. 425-430.
- National Center for Health Statistics, '*Health, United States 2005*', Hyattsville, Maryland, 2005.
- Naumov, GN, E Bender, D Zurakowski, SY Kang, D Sampson, E Flynn, RS Watnick, O Straume, LA Aksten, J Folkman, & N Almog, 'A model of human tumor dormancy: an angiogenic switch from the nonangiogenic phenotype.', *J Natl Cancer Inst* vol. 98, no. 5, 2006, pp. 316-325.
- Noren, NK, BP Liu, K Burrige, & B Kreft, 'p120 catenin regulates the actin cytoskeleton via Rho family GTPases.', *J Cell Biol* vol. 150, no. 3, 2000, pp. 567-580.
- Nose, K, H Saito, & T Kuroki, 'Isolation of a gene sequence induced later by tumor-promoting 12-O-tetradecanoylphorbol-13-acetate in mouse osteoblastic cells (MC3T3-E1) and expressed constitutively in ras-transformed cells.', *Cell Growth Differ* vol. 1, no. 11, 1990, pp. 511-518.
- Ochakovskaya, R, L Osorio, DM Goldenberg, & MJ Mattes, 'Therapy of disseminated B-cell lymphoma xenografts in severe combined immunodeficient mice with an anti-CD74 antibody conjugated with (111)indium, (67)gallium, or (90)yttrium.', *Clin Cancer Res* vol. 7, no. 6, 2001, pp. 1505-1510.
- Oeffinger, KC, AC Mertens, CA Sklar, T Kawashima, MM Hudson, AT Meadows, DL Friedman, N Marina, W Hobbie, NS Kadan-Lottick, CL Schwartz, W Leisenring, & LL Robison, 'Chronic health conditions in adult survivors of childhood cancer.', *N Engl J Med* vol. 355, no. 15, 2006, pp. 1572-1582.
- Paget, S, 'The distribution of secondary growths in cancer of the breast', *Lancet* vol. 1, 1889, pp. 571-573.
- PANORAMA, '*Gesundheit*', Swiss Federal Statistical Office, Neuchâtel, 2006.
- Parangi, S, M O'Reilly, G Christofori, L Holmgren, J Grosfeld, J Folkman, & D Hanahan, 'Antiangiogenic therapy of transgenic mice impairs de novo tumor growth.', *Proc Natl Acad Sci U S A* vol. 93, no. 5, 1996, pp. 2002-2007.
- Perl, AK, P Wilgenbus, U Dahl, H Semb, & G Christofori, 'A causal role for E-cadherin in the transition from adenoma to carcinoma.', *Nature* vol. 392, no. 6672, 1998, pp. 190-193.
- Philippe, C, B Philippe, B Fouqueray, J Perez, M Lebreton, & L Baud, 'Protection from tumor necrosis factor-mediated cytolysis by platelets.', *Am J Pathol* vol. 143, no. 6, 1993, pp. 1713-1723.
- Pietras, K, & D Hanahan, 'A multitargeted, metronomic, and maximum-tolerated dose "chemo-switch" regimen is antiangiogenic, producing objective responses and survival benefit in a mouse model of cancer.', *J Clin Oncol* vol. 23, no. 5, 2005, pp. 939-952.
- Pitts, WC, VA Rojas, MJ Gaffey, RV Rouse, J Esteban, HF Frierson, RL Kempson, & LM Weiss, 'Carcinomas with metaplasia and sarcomas of the breast.', *Am J Clin Pathol* vol. 95, no. 5, 1991, pp. 623-632.
- Price, LS, J Leng, MA Schwartz, & GM Bokoch, 'Activation of Rac and Cdc42 by integrins mediates cell spreading.', *Mol Biol Cell* vol. 9, no. 7, 1998, pp. 1863-1871.
- Ptacek, J, G Devgan, G Michaud, H Zhu, X Zhu, J Fasolo, H Guo, G Jona, A Breitkreutz, R Sopko, RR McCartney, MC Schmidt, N Rachidi, SJ Lee, AS Mah, L Meng, MJ Stark, DF Stern, C De Virgilio, M Tyers, B Andrews, M Gerstein, B Schweitzer, PF Predki, & M Snyder, 'Global analysis of protein phosphorylation in yeast.', *Nature* vol. 438, no. 7068, 2005, pp. 679-684.
- Radisky, DC, DD Levy, LE Littlepage, H Liu, CM Nelson, JE Fata, D Leake, EL Godden, DG Albertson, MA Nieto, Z Werb, & MJ Bissell, 'Rac1b and reactive oxygen species mediate MMP-3-induced EMT and genomic instability.', *Nature* vol. 436, no. 7047, 2005, pp. 123-127.
- Rao, DV, VR Narra, RW Howell, GF Govelitz, & KS Sastry, 'In-vivo radiotoxicity of DNA-incorporated ¹²⁵I compared with that of densely ionising alpha-particles.', *Lancet* vol. 2, no. 8664, 1989, pp. 650-653.
- Reilly, RM, R Kiarash, RG Cameron, N Porlier, J Sandhu, RP Hill, K Vallis, A Hendler, & J Garipey, '¹¹¹In-labeled EGF is selectively radiotoxic to human breast cancer cells overexpressing EGFR.', *J Nucl Med* vol. 41, no. 3, 2000, pp. 429-438.

- Reubi, JC, 'Peptide receptors as molecular targets for cancer diagnosis and therapy.', *Endocr Rev* vol. 24, no. 4, 2003, pp. 389-427.
- Reubi, JC, M Gugger, B Waser, & JC Schaer, 'Y(1)-mediated effect of neuropeptide Y in cancer: breast carcinomas as targets.', *Cancer Res* vol. 61, no. 11, 2001, pp. 4636-4641.
- Reubi, JC, U Laderach, B Waser, JO Gebbers, P Robberecht, & JA Laissue, 'Vasoactive intestinal peptide/pituitary adenylate cyclase-activating peptide receptor subtypes in human tumors and their tissues of origin.', *Cancer Res* vol. 60, no. 11, 2000, pp. 3105-3112.
- Reubi, JC, & B Waser, 'Concomitant expression of several peptide receptors in neuroendocrine tumours: molecular basis for in vivo multireceptor tumour targeting.', *Eur J Nucl Med Mol Imaging* vol. 30, no. 5, 2003, pp. 781-793.
- Reya, T, SJ Morrison, MF Clarke, & IL Weissman, 'Stem cells, cancer, and cancer stem cells.', *Nature* vol. 414, no. 6859, 2001, pp. 105-111.
- Rishi, AK, M Joyce-Brady, J Fisher, LG Dobbs, J Floros, J VanderSpek, JS Brody, & MC Williams, 'Cloning, characterization, and development expression of a rat lung alveolar type I cell gene in embryonic endodermal and neural derivatives.', *Dev Biol* vol. 167, no. 1, 1995, pp. 294-306.
- Romond, EH, EA Perez, J Bryant, VJ Suman, CEJ Geyer, NE Davidson, E Tan-Chiu, S Martino, S Paik, PA Kaufman, SM Swain, TM Pisansky, L Fehrenbacher, LA Kutteh, VG Vogel, DW Visscher, G Yothers, RB Jenkins, AM Brown, SR Dakhil, EP Mamounas, WL Lingle, PM Klein, JN Ingle, & N Wolmark, 'Trastuzumab plus adjuvant chemotherapy for operable HER2-positive breast cancer.', *N Engl J Med* vol. 353, no. 16, 2005, pp. 1673-1684.
- Sahai, E, R Garcia-Medina, J Pouyssegur, & E Vial, 'Smurf1 regulates tumor cell plasticity and motility through degradation of RhoA leading to localized inhibition of contractility.', *J Cell Biol* vol. 176, no. 1, 2007, pp. 35-42.
- Sahai, E, & CJ Marshall, 'RHO-GTPases and cancer.', *Nat Rev Cancer* vol. 2, no. 2, 2002, pp. 133-142.
- Sameni, M, K Moin, & BF Sloane, 'Imaging proteolysis by living human breast cancer cells.', *Neoplasia* vol. 2, no. 6, 2000, pp. 496-504.
- Sander, EE, JP ten Klooster, S van Delft, RA van der Kammen, & JG Collard, 'Rac downregulates Rho activity: reciprocal balance between both GTPases determines cellular morphology and migratory behavior.', *J Cell Biol* vol. 147, no. 5, 1999, pp. 1009-1022.
- Schacht, V, SS Dadras, LA Johnson, DG Jackson, YK Hong, & M Detmar, 'Up-regulation of the lymphatic marker podoplanin, a mucin-type transmembrane glycoprotein, in human squamous cell carcinomas and germ cell tumors.', *Am J Pathol* vol. 166, no. 3, 2005, pp. 913-921.
- Schacht, V, MI Ramirez, YK Hong, S Hirakawa, D Feng, N Harvey, M Williams, AM Dvorak, HF Dvorak, G Oliver, & M Detmar, 'T1alpha/podoplanin deficiency disrupts normal lymphatic vasculature formation and causes lymphedema.', *EMBO J* vol. 22, no. 14, 2003, pp. 3546-3556.
- Sebolt-Leopold, JS, & JM English, 'Mechanisms of drug inhibition of signalling molecules.', *Nature* vol. 441, no. 7092, 2006, pp. 457-462.
- Seftor, EA, PS Meltzer, DA Kirschmann, J Pe'er, AJ Maniotis, JM Trent, R Folberg, & MJ Hendrix, 'Molecular determinants of human uveal melanoma invasion and metastasis.', *Clin Exp Metastasis* vol. 19, no. 3, 2002, pp. 233-246.
- Service, FJ, MM McMahon, PC O'Brien, & DJ Ballard, 'Functioning insulinoma--incidence, recurrence, and long-term survival of patients: a 60-year study.', *Mayo Clin Proc* vol. 66, no. 7, 1991, pp. 711-719.
- Shen, ZY, LY Xu, MH Chen, EM Li, JT Li, XY Wu, & Y Zeng, 'Upregulated expression of Ezrin and invasive phenotype in malignant transformed esophageal epithelial cells.', *World J Gastroenterol* vol. 9, no. 6, 2003, pp. 1182-1186.
- Sherwood, DR, 'Cell invasion through basement membranes: an anchor of understanding.', *Trends Cell Biol* vol. 16, no. 5, 2006, pp. 250-256.
- Siegel, PM, & J Massague, 'Cytostatic and apoptotic actions of TGF-beta in homeostasis and cancer.', *Nat Rev Cancer* vol. 3, no. 11, 2003, pp. 807-821.
- Smalley, KS, P Brafford, NK Haass, JM Brandner, E Brown, & M Herlyn, 'Up-regulated expression of zonula occludens protein-1 in human melanoma associates with N-

- cadherin and contributes to invasion and adhesion.', *Am J Pathol* vol. 166, no. 5, 2005, pp. 1541-1554.
- Sood, AK, EA Seftor, MS Fletcher, LM Gardner, PM Heidger, RE Buller, RE Seftor, & MJ Hendrix, 'Molecular determinants of ovarian cancer plasticity.', *Am J Pathol* vol. 158, no. 4, 2001, pp. 1279-1288.
- Stoker, M, & M Perryman, 'An epithelial scatter factor released by embryo fibroblasts.', *J Cell Sci* vol. 77, 1985, pp. 209-223.
- Tarin, D, JE Price, MG Kettlewell, RG Souter, AC Vass, & B Crossley, 'Mechanisms of human tumor metastasis studied in patients with peritoneovenous shunts.', *Cancer Res* vol. 44, no. 8, 1984, pp. 3584-3592.
- Thiery, JP, 'Epithelial-mesenchymal transitions in development and pathologies.', *Curr Opin Cell Biol* vol. 15, no. 6, 2003, pp. 740-746.
- Thiery, JP, 'Epithelial-mesenchymal transitions in tumour progression.', *Nat Rev Cancer* vol. 2, no. 6, 2002, pp. 442-454.
- Thorens, B, A Porret, L Buhler, SP Deng, P Morel, & C Widmann, 'Cloning and functional expression of the human islet GLP-1 receptor. Demonstration that exendin-4 is an agonist and exendin-(9-39) an antagonist of the receptor.', *Diabetes* vol. 42, no. 11, 1993, pp. 1678-1682.
- Ting, AH, KM McGarvey, & SB Baylin, 'The cancer epigenome--components and functional correlates.', *Genes Dev* vol. 20, no. 23, 2006, pp. 3215-3231.
- Valkema, R, M De Jong, WH Bakker, WA Breeman, PP Kooij, PJ Lugtenburg, FH De Jong, A Christiansen, BL Kam, WW De Herder, M Stridsberg, J Lindemans, G Ensing, & EP Krenning, 'Phase I study of peptide receptor radionuclide therapy with [¹¹¹In-DTPA]octreotide: the Rotterdam experience.', *Semin Nucl Med* vol. 32, no. 2, 2002, pp. 110-122.
- van den Brink, GR, & GJ Offerhaus, 'The Morphogenetic Code and Colon Cancer Development.', *Cancer Cell* vol. 11, no. 2, 2007, pp. 109-117.
- Vaughan, RB, & JP Trinkaus, 'Movements of epithelial cell sheets in vitro.', *J Cell Sci* vol. 1, no. 4, 1966, pp. 407-413.
- Vernon, AE, & C LaBonne, 'Tumor metastasis: a new twist on epithelial-mesenchymal transitions.', *Curr Biol* vol. 14, no. 17, 2004, pp. R719-21.
- Virchow, R, *Die krankhaften Geschwülste*, August Hirschwald, Berlin, 1863.
- Waldherr, C, M Pless, HR Maecke, T Schumacher, A Crazzolaro, EU Nitzsche, A Haldemann, & J Mueller-Brand, 'Tumor response and clinical benefit in neuroendocrine tumors after 7.4 GBq (90)Y-DOTATOC.', *J Nucl Med* vol. 43, no. 5, 2002, pp. 610-616.
- Wang, H, W Fu, JH Im, Z Zhou, SA Santoro, V Iyer, CM DiPersio, QC Yu, V Quaranta, A Al-Mehdi, & RJ Muschel, 'Tumor cell alpha3beta1 integrin and vascular laminin-5 mediate pulmonary arrest and metastasis.', *J Cell Biol* vol. 164, no. 6, 2004, pp. 935-941.
- Weinberg, RA, 'The retinoblastoma protein and cell cycle control.', *Cell* vol. 81, no. 3, 1995, pp. 323-330.
- Weis, SM, & DA Cheresh, 'Pathophysiological consequences of VEGF-induced vascular permeability.', *Nature* vol. 437, no. 7058, 2005, pp. 497-504.
- Wicki, A, & G Christofori, 'The potential role of podoplanin in tumour invasion.', *Br J Cancer* vol. 96, no. 1, 2007, pp. 1-5.
- Wicki, A, F Lehenbre, N Wick, B Hantusch, D Kerjaschki, & G Christofori, 'Tumor invasion in the absence of epithelial-mesenchymal transition: podoplanin-mediated remodeling of the actin cytoskeleton.', *Cancer Cell* vol. 9, no. 4, 2006, pp. 261-272.
- Wild, D, M Behe, A Wicki, D Storch, B Waser, M Gotthardt, B Keil, G Christofori, JC Reubi, & HR Macke, '[Lys⁴⁰(Ahx-DTPA-¹¹¹In)NH₂]exendin-4, a very promising ligand for glucagon-like peptide-1 (GLP-1) receptor targeting.', *J Nucl Med* vol. 47, no. 12, 2006, pp. 2025-2033.
- Wolf, K, I Mazo, H Leung, K Engelke, UH von Andrian, EI Deryugina, AY Strongin, EB Brouck, & P Friedl, 'Compensation mechanism in tumor cell migration: mesenchymal-amoeboid transition after blocking of pericellular proteolysis.', *J Cell Biol* vol. 160, no. 2, 2003, pp. 267-277.
- Yang, J, SA Mani, JL Donaher, S Ramaswamy, RA Itzykson, C Come, P Savagner, I Gitelman, A Richardson, & RA Weinberg, 'Twist, a master regulator of morphogenesis, plays an essential role in tumor metastasis.', *Cell* vol. 117, no. 7, 2004, pp. 927-939.
- Zimmer, G, F Lottspeich, A Maisner, HD Klenk, & G Herrler, 'Molecular characterization of gp40, a mucin-type glycoprotein from the apical plasma membrane of Madin-Darby

canine kidney cells (type I).', *Biochem J* vol. 326, no. Pt 1, 1997, pp. 99-108.
Zimmer, G, F Oeffner, V Von Messling, T Tschernig, HJ Groness, HD Klenk, & G Herrler,
'Cloning and characterization of gp36, a human mucin-type glycoprotein preferentially
expressed in vascular endothelium.', *Biochem J* vol. 341, no. Pt 2, 1999, pp. 277-284.

Acknowledgements

Such an endeavor cannot be completed without help. I want to thank the Swiss Academy of Medical Sciences, the Swiss National Science Foundation and the Roche Research Foundation for the logistical and financial support. Furthermore, I'd like to thank the members of the Christofori-lab for their help- and cheerful company. I could not have managed the practical work without advice from Dr. François Lehembre, whose practical skills and theoretical knowledge are unequalled. I am also grateful to the group of Prof. Helmut Mäcke at the University Hospital of Basel. They provided the know-how for the synthesis and radiolabelling of Exendin, as well as for the HPLC analysis and the SPECT/CT imaging. Thanks also to the groups of Prof. Donscho Kerjaschki, Vienna, and Prof. Michael Mihatsch, Basel, for the analysis of the biopsy samples and the EM images. The group of Dr. Martin Behé, Marburg, performed the SPECT/MR imaging, and Prof. Jean-Claude Reubi, Berne, the tissue autoradiography. Special thanks go to my boss, Prof. Gerhard Christofori, a true polymath who gave me the opportunity to work in a fabulous lab and to learn a lot about science. It was a great time, these three years in your lab. Finally, I owe thanks to Sibyl and my parents, for their love and continuing support. I could never have done this work without you.

Publication list

Original articles (peer-reviewed):

1. Wicki A, Malik N, Gratwohl A, Tichelli A, Meyer-Monard S, Muller H (2002) Determination of the donor:host blood cell ratio after haematological stem cell transplant by means of semiquantitative detection of short tandem repeat polymorphisms. **Swiss Med Wkly**, 132(21-22):288-95
2. Wicki A, Lehembre F, Wick N, Hantusch B, Kerjaschki D, Christofori G (2006) Tumor invasion in the absence of epithelial-mesenchymal transition: Podoplanin-mediated remodeling of the actin cytoskeleton. **Cancer Cell**, 9(4): 261-72
3. Wild D, Béhé M, Wicki A, Storch D, Waser B, Gotthard M, Christofori G, Reubi JC, Mäcke HR (2006) Preclinical Evaluation of [Lys⁴⁰(Ahx-DTPA-¹¹¹In)NH₂]-Exendin-4, a very promising ligand for glucagon-like-peptide-1 (GLP-1) receptor targeting. **J Nucl Med**, 47(12):2025-2033
4. Wicki A, Wild D, Storch D, Seemayer C, Béhé M, Gotthard M, Kneifel S, Mihatsch M, Reubi JC, Mäcke HR, Christofori G (2007) [Lys⁴⁰(Ahx-DTPA-¹¹¹In)NH₂]-Exendin-4 is a highly efficient radiotherapeutic for glucagon-like-peptide-1 receptor targeted therapy for insulinoma. **Clin Cancer Res**, 13(12):3696-3705

Invited Reviews and Book Chapters:

1. Wicki A, Christofori G (2007) The Potential Role of Podoplanin in Tumour Invasion. **Br J Cancer** 96(1):1-5
2. Wicki A, Christofori G (2007) The Angiogenic Switch in Tumorigenesis. In: Tumor Angiogenesis: Basic Mechanisms and Cancer Therapy (Marmé D and Fusenig N, Eds.). **Springer Verlag**, Heidelberg, Germany; pp 67-88. In press.